# UNDERSTANDING THE BIOLOGICAL FUNCTION OF PHOSPHATASES OF REGENERATING LIVER, FROM BIOCHEMISTRY TO PHYSIOLOGY

Yunpeng Bai

Submitted to the faculty of the University Graduate School
in partial fulfillment of the requirements
for the degree
Doctor of Philosophy
in the Department of Biochemistry and Molecular Biology,
Indiana University

July 2014

Accepted by the Graduate Faculty, of Indiana University, in partial fulfillment of the requirements for the degree of Doctor of Philosophy.

Zhong-Yin Zhang, Ph.D., Chair

Lawrence Quilliam, Ph.D.

Doctoral Committee

Weinian Shou, Ph.D.

April 30, 2014

X. Charlie Dong, Ph.D.

ACKNOWLEDGEMENTS

Six years ago, when I stepped on the land of America for the first time in my life to pursue my Ph.D, I never realized how fast time flies. However, the time I spent at Indiana University School of Medicine has been the most joyful but also challenging time of my life. This dissertation has witnessed all my success and most of the time, failure. It would not have been possible to finish this work without the advice and support of many people. I would like to take this opportunity to express my sincere gratitude to everyone.

First and foremost, I want to thank my advisor, Dr. Zhong-Yin Zhang, who has been my mentor not only in my research, but also in my life. I knew him when I was an undergraduate student in Nankai University, where he gave a presentation about chemical genomics. I was impressed by his presentation and scientific achievements, and encouraged to pursue science and research as my career goal. Later I came to US by myself, with nothing but suitcases. It was Dr. Zhang who helped me in the beginning of my life in a completely different place. Dr. Zhang's academic success is coming from his open-minded vision, continuous passion, scientific intelligence and persistent effort to research. His dedication and attitude always inspires me to overcome any obstacles in my research. The scientific abilities that I have acquired are a direct reflection of his mentorship and support.

I would also like to thank my research committee members: Dr. Lawrence Quilliam, Dr. Weinian Shou and Dr. X. Charlie Dong for their generous support. They provided valuable time and resources, constructive suggestions and criticisms to help me finish this dissertation. I also want to thank Dr. Clark Wells for confocal microscope

support. I am also very grateful to the graduate advisor Dr. Mark Goebl for supervising my graduate study and research.

I appreciate all the former and present lab members, especially Dr. David Liu, Dr. Zhihong Yu, Dr. Yuanshu Dong, Dr. Hongming Zhou, Dr. Chad Walls and Dr. Yong Luo who directly contributed to this dissertation. I also acknowledge Lily Wu for organizing the whole lab and taking care of all the orders. I am also grateful to other colleagues in the Zhang lab for their help and support. It was a great pleasure to work with all of them every day.

I would like to express my sincere gratitude to Dr. Weinian Shou and his lab members Dr. Hanying Chen, Dr. Xiaoxin Sun, Dr. Wei Li, Dr. Weidong Yong and Dr. Wenjun Zhang for helping me generate knockout mice. It is also my pleasure to collaborate with Dr. Yan Liu's lab and work with Dr. Michihiro Kobayashi for the hematopoiesis projects, and I learned a lot about hematopoietic stem cells from them.

I will give special thanks to the administrative staffs of the departmental office, Sandy McClain, Melissa Tarrh, Jack Arthur, Patty Dilworth, Sheila Reynolds and Darlene Lambert for taking care of all the paperwork, organizing the conference room, maintaining the equipment, placing all the orders and providing the computer support.

Finally, I would like to express my deepest love and thanks to my parents and my family. My parents gave me their love and trust to support my Ph.D study throughout the years. I'm so grateful for everything that they have done for me and I couldn't go this far without their support. Most importantly, I would like to thank my wife Lujuan Zhang for her unconditional love, support and encouragement. Thank you for giving me a beautiful baby girl, Katherine Bai, and a chance to be a father, which is the best thing that ever happened.

Yunpeng Bai

# UNDERSTANDING THE BIOLOGICAL FUNCTION OF PHOSPHATASES OF REGENERATING LIVER, FROM BIOCHEMISTRY TO PHYSIOLOGY

Phosphatases of regenerating liver, consisting of PRL-1, PRL-2 and PRL-3, belong to a novel protein tyrosine phosphatases subfamily, whose overexpression promotes cell proliferation, migration and invasion and contributes to tumorigenesis and metastasis. However, although great efforts have been made to uncover the biological function of PRLs, limited knowledge is available on the underlying mechanism of PRLs' actions, therapeutic value by targeting PRLs, as well as the physiological function of PRLs *in vivo*.

To answer these questions, we first screened a phage display library and identified p115 RhoGAP as a novel PRL-1 binding partner. Mechanistically, we demonstrated that PRL-1 activates RhoA and ERK1/2 by decreasing the association between active RhoA with GAP domain of p115 RhoGAP, and displacing MEKK1 from the SH3 domain of p115 RhoGAP, respectively, leading to enhanced cell proliferation and migration.

Secondly, structure-based virtual screening was employed to discover small molecule inhibitors blocking PRL-1 trimer formation which has been suggested to play an important role for PRL-1 mediated oncogenesis. We identified Cmpd-43 as a novel PRL-1 trimer disruptor. Structural study demonstrated the binding mode of PRL-1 with the trimer disruptor. Most importantly, cellular data revealed that Cmpd-43 inhibited

PRL-1 induced cell proliferation and migration in breast cancer cell line MDA-MB-231 and lung cancer cell line H1299.

Finally, in order to investigate the physiological function of PRLs, we generated mouse knockout models for *Prl-1*, *Prl-2* and *Prl-3*. Although mice deficient for *Prl-1* and *Prl-3* were normally developed, *Prl-2*-null mice displayed growth retardation, impaired male reproductive ability and insufficient hematopoiesis. To further investigate the *in vivo* function of *Prl-1*, we generated *Prl-1*$^{-/-}$/*Prl-2*$^{+/-}$ and *Prl-1*$^{+/-}$/*Prl-2*$^{-/-}$ mice. Similar to *Prl-2* deficient male mice, *Prl-1*$^{-/-}$/*Prl-2*$^{+/-}$ males also have impaired spermatogenesis and reproductivity. More strikingly, *Prl-1*$^{+/-}$/*Prl-2*$^{-/-}$ mice are completely infertile, suggesting that, in addition to PRL-2, PRL-1 also plays an important role in maintaining normal testis function.

In summary, these studies demonstrated for the first time that PRL-1 activates ERK1/2 and RhoA through the novel interaction with p115 RhoGAP, targeting PRL-1 trimer interface is a novel anti-cancer therapeutic treatment and both PRL-1 and PRL-2 contribute to spermatogenesis and male mice reproductivity.

Zhong-Yin Zhang, Ph.D., Chair

## TABLE OF CONTENTS

## LIST OF TABLES

## LIST OF FIGURES

## LIST OF ABBREVIATIONS

| | |
|---|---|
| BAC | Bacterial artificial chromosome |
| BMMC | Bone marrow mononuclear cells |
| CHO | Chinese hamster ovary |
| CHX | Cycloheximide |
| CRC | Colorectal carcinoma |
| CSK | C-terminal Src kinase |
| DMEM | Dulbecco’s modified Eagle’s medium |
| DSS | Disease-specific survival |
| DTA | Diphtheria Toxin A-chain gene |
| ECM | Extracellular matrix |
| EMT | Epithelial-mesenchymal transition |
| ERK | Extracellular signal-regulated kinase |
| FBS | Fetal bovine serum |
| GAP | GTPase activating proteins |
| GDP | Guanosine diphosphate |
| GEF | Guanine nucleotide exchange factors |
| GTP | Guanosine triphosphate |
| GST | Glutathione S-transferase |
| HA | Hemaglutinin epitope |
| HEK | Human embryonic kidney |
| HMVEC | Human dermal microvascular endothelial cells |
| HSC | Hematopoietic stem cell |
| HSPC | Hematopoietic stem and progenitor cells |

| | |
|---|---|
| LGALS | Lamarckian genetic algorithm with local search |
| MAPK | Mitogen activated protein kinase |
| MEF | Murine embryonic fibroblast |
| MEKK1 | MAP/ERK kinase kinase 1 |
| MPP | Multipotent progenitor cells |
| NRPTP | Non-receptor protein tyrosine phosphatase |
| PBS | Phosphate buffered saline |
| PARP | Poly ADP-ribose polymerase |
| PCNA | Proliferating cell nuclear antigen |
| PI3K | Phosphatidylinositol 3-kinase |
| PIP3 | Phosphatidylinositol (3,4,5)-trisphosphate |
| PRL | Phosphatase of regenerating liver |
| PTEN | Phosphatase and tensin homologue |
| PTK | Protein tyrosine kinase |
| PTP | Protein tyrosine phosphatase |
| RTK | Receptor tyrosine kinase |
| ROCK | Rho-associated protein kinase |
| RPTP | Receptor protein tyrosine phosphatase |
| RT-PCR | Reverse transcription polymerase chain reaction |
| SDS | Sodium dodecyl sulfate |
| siRNA | Short interference RNAs |

# CHAPTER 1: INTRODUCTION

## 1.1 Protein Tyrosine Phosphatases

Protein tyrosine phosphorylation is a key mechanism in signal transduction controlling many cellular events, including cell proliferation, migration, differentiation, survival, as well as apoptosis (1,2). Protein tyrosine kinases (PTKs) and protein tyrosine phosphatases (PTPs) regulate these reversible phosphorylation events by adding and removing phosphate, respectively. The equilibrium of kinase-phosphatase activity is important to maintain normal homeostasis in a resting state and to respond to various extracellular stimuli.

In humans, 107 genes have been identified as PTP superfamily members (2). These PTPs are classified into four groups based on the amino acid sequences of catalytic domains (Figure 1). The first group is Class I cysteine-based PTPs which consists of 99 members. This group can be further classified into two subgroups, classical PTPs, which contain 38 well-known tyrosine-specific PTPs members, and VH1-like or "dual-specific" PTPs, which consist of 61 members. Classical PTPs can be divided into receptor PTPs (RPTPs) and non-receptor PTPs (NRPTPs). The transmembrane RPTPs are represented by 21 members, such as RPTPα, RPTPβ and CD45, while the intracellular NRPTPs consist of 17 phosphatases, such as PTP1B, PTP-MEG2 and SHP2. The VH1-like PTPs can be divided into several diverse groups including MKPs, atypical DSPs, Slingshots, PRLs, CDC14s, PTENs and Myotubularins. The second group is Class II cysteine-based PTPs which constitute of one member, low-molecular-weight PTP. Class III cysteine-based PTPs are tyrosine/threonine specific phosphatases containing three members of Cdc25 cell cycle regulators. These three groups share similar active site structure and catalytic mechanism with an active site

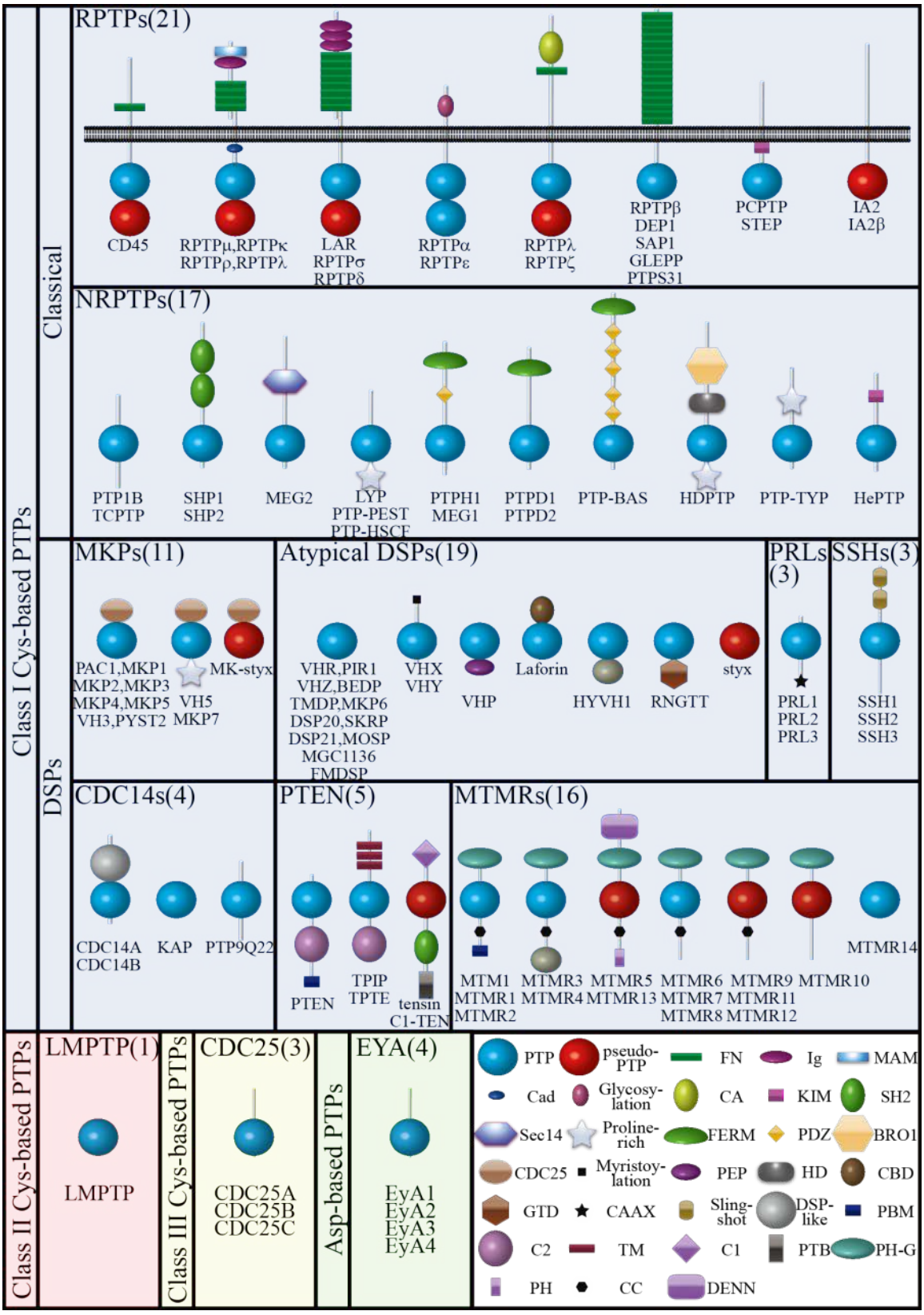


**Figure 1. Classification of PTP superfamily.**

Protein tyrosine phosphatase superfamily, consisting of 107 members, is divided into four classes based on the amino acid sequence of the catalytic domain. The class I cysteine-based PTPs have 99 members that are divided into two subfamilies: tyrosine-specific classical PTPs (38 members) and VH1-like or dual specificity phosphatases (DSPs, 61 members). Classical PTP subfamily is further divided into two groups: receptor PTPs (RPTPs, 21 members) and non-receptor PTPs (NRPTPs, 17 members). The DSP subfamily is divided into seven different groups: MAPK phosphatases (MKPs, 11 members), atypical DSPs (19 members), phosphatases of regenerating liver (PRLs, 3 members), slingshot phosphatases (SSHs, 3 members), cell division cycle 14 phosphatases (CDC14s, 4 members), PTEN phosphatases (5 members) and myotubularin-related phosphatases (MTMRs, 16). The class II cysteine-based PTPs has only one member which is low-molecular-weight PTP (LMW-PTP). The class III cysteine-based PTP family comprises three members in Cdc25 family. The class IV aspartic acid-based PTP family members are encoded by the four eyes absent homologue (EYA) genes. BRO1, baculovirus BRO1 homology; C1, protein kinase C conserved region 1; C2, protein kinase C conserved region 2; CA, carbonic anhydrase-like domain; CAAX, farnesylation signal; Cad, cadherin-like juxtamembrane sequence; CBD, carbohydrate-binding module; CC, coiled-coil domain; CDC25, CDC25-homology domain; DENN, DENN domain; FERM, band 4.1/ezrin/radixin/moesin homology; FN, fibronectin-like domain; GTD, guanylyltransferase domain; HD, histidine domain; Ig, immunoglobulin-like domain; KIM, kinase interaction motif; MAM, Meprin/A2/PTPRM homology domain; PBM, PDZ binding motif; PDZ, postsynaptic density-95/discs large/ZO1 homology; PEP, N-terminal peptidase-like domain; PH, pleckstrin homology domain; PH-G, pleckstrin homology-“GRAM” domain; PTB, phosphotyrosine-binding domain; Sec14, Sec14p homology; SH2, Src homology 2 domain; TM, putative transmembrane segment.

cysteine as the nucleophile. In stark contrast, the last group of PTPs, Class IV Asp-based PTPs, utilized a different catalytic mechanism with a key aspartic acid. Four members of EYA proteins were discovered recently and classified into this family. Altogether, PTP superfamily consists of various genes that work together to regulate cellular tyrosine phosphorylation levels in many physiological processes.

The balance of cellular tyrosine phosphorylation is essential for normal cell processes, whereas the disruption of equilibrium of kinase-phosphatase activity can ultimately results in various diseases including cancer. It is well documented that many PTKs, such as receptor tyrosine kinases (RTKs), are considered as oncogenes. Aberrant activation of PTKs will cause deleterious cell proliferation, leading to cancer development. PTPs conventionally are thought to be tumor suppressors by counteracting PTKs activity and attenuating signals for cell proliferation. However, recent studies have shown that 22 PTPs may also have oncogenic properties by mutation, overexpression or amplification (3). For examples, the Src homology-2 domain-containing phosphatase SHP2, encoded by *PTPN11*, is the first identified proto-oncogene in the PTP superfamily. While germline mutations in *PTPN11* cause Noonan syndrome and LEOPARD syndrome, somatic gain-of-function *PTPN11* mutations were observed in juvenile myelomonocytic leukemia, and rarely in adult leukemias and solid tumors (4,5). Even though the detailed mechanisms need to be elucidated, increasing evidence has suggested that PTP1B, encoded by *PTPN1* gene, plays an oncogenic role in breast cancer, ovarian cancer, gastric cancer, pancreatic cancer and prostate cancer by overexpression and amplification (6-10). Other PTP family members are also implicated in cancer progression including PRLs (3). All these results demonstrated that PTPs are potential therapeutic targets in cancer treatment and inhibition of these PTPs may provide medical benefits.

**1.2 Phosphatases of Regenerating Liver**

Phosphatases of the Regenerating Liver (PRLs) represent a unique subfamily of PTPs with three members (PRL-1, 2 and 3), sharing a high degree (>75%) of amino acid sequence identity (11-13). PRL-1 was the first identified member of PRL family that

showed increased expression in regenerating liver (11). Later on, two other members, PRL-2 and PRL-3, were found by sequence homology searches (14). Amino acid sequences of human and mouse PRL-1 or PRL-2 are 100% identical, while PRL-3 sequences from mouse and human are slightly different (Figure 2). Like other PTPs, PRLs contain the canonical phosphatase motif $C(X)_5R$. The unique feature of PRL phosphatases is that they possess a C-terminal prenylation motif CAAX (Where C is cysteine that could be prenylated, A is an aliphatic amino acid). Once prenylated, they will localize to the plasma membrane and early endosomal compartments (15). Mutation of the CAAX box or treatment with farnesyl transferase inhibitors will re-localize PRLs to the nucleus, suggesting the translocation of PRLs from plasma membrane to nucleus depends on the removal of prenylation signal (15-17). PRLs also share an adjacent polybasic region with a cluster of positive charges, which facilitates the membrane binding. Both the prenylation group and the polybasic residues are required for their proper localization and full biological activity (17). It is noteworthy that PRLs may be susceptible to redox regulation and their activity could be inhibited by the formation of a disulfide bond at their active sites (18-20).

Several PRL structures have been reported (17,21-23). The structures of PRL-1 and PRL-3 revealed that the active sites are shallow and wide, indicating that both shorter side-chains of phospho-Ser and phospho-Thr and longer side- chain of phospho-Tyr can be dephosphorylated. This feature of PRLs allows its access to a broad range of substrates, and classifies PRLs into the subfamily of dual specificity phosphatases (DSP) (21). In addition, the structures of PRL-1 solved by us and others also revealed a trimeric

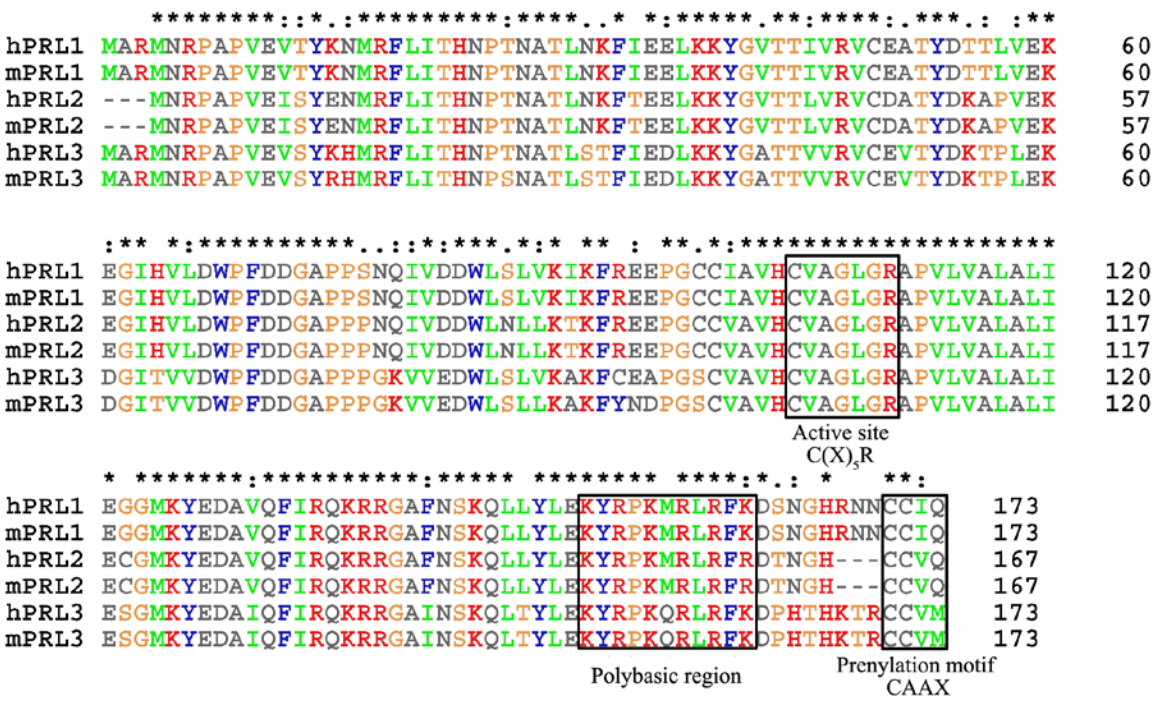


**Figure 2. Amino acid sequence alignment of human and mouse PRLs.**

The amino acids sequence alignment was generated by ClustalX. The active site $C(X)_5R$ motif, polybasic region and the prenylation motif CAAX are boxed.

arrangement (Figure 3A & 3B, created by Sijiu Liu). The trimerization of PRL-1 provides a membrane-binding surface with polybasic residues and the adjacent C-terminal prenylation motif to anchor PRL-1 on the inner plasma membrane (17,23) (Figure 3B). Furthermore, residues involved in the trimer interface are identical or similar among all PRLs, suggesting that trimerization is a general property for all PRL enzymes. This is supported by the evidence that PRL-3 can also form trimers both *in vitro* and *in vivo* (17). Since PRLs are all implicated as oncogenes, targeting the trimer interface by small molecule inhibitors may provide a novel approach to develop anti-cancer therapeutics (see details in Chapter 3).

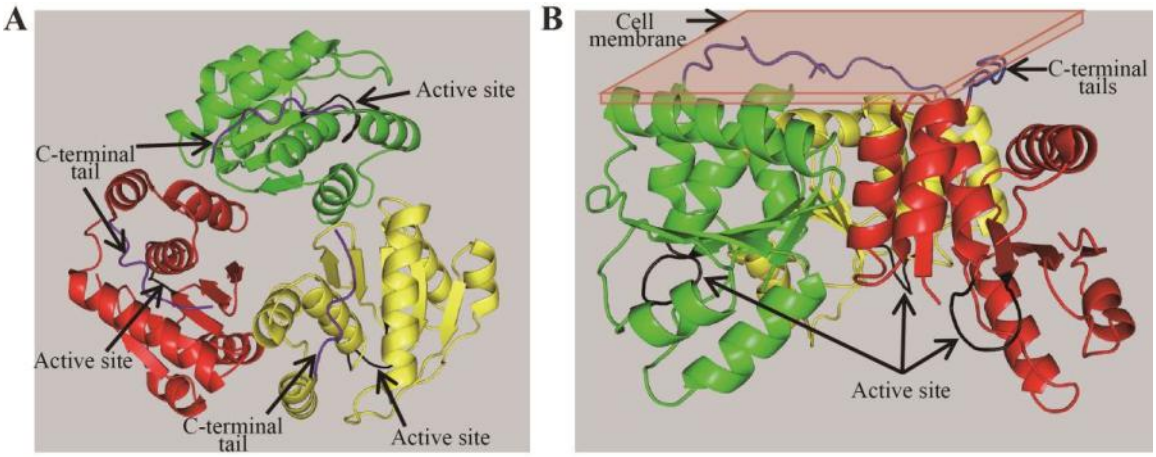


**Figure 3. Crystal structure of PRL-1 trimer.**

**A.** Vertical view of PRL-1 trimer. **B.** Horizontal view of PRL-1 trimer attached to inner plasma membrane. All figures were created with PyMol (DeLano Scientific; http:/www.pymol.org) by Sijiu Liu. Each monomer is labeled as different color (green, red and yellow). Active site is black, and C-terminal tail is blue.

The expression patterns of PRL-1, -2 and -3 transcripts in human and mouse have been well-studied (14,24,25). Both PRL-1 and PRL-2 were found to be expressed in almost all organs by *in situ* hybridization (24). Interestingly, PRL-1 expression level was relatively lower than PRL-2. The broad expression pattern of PRL-1 and PRL-2 indicates that they function in basic cell signaling that exists in most tissues. In contrast, PRL-3 is primarily expressed in heart and skeletal muscle (14). However, a recent study revealed a more ubiquitous but low level expression of PRL-3 protein in a number of other tissues such as spleen, pancreas, brain, lung, thymus, colon, and small intestine, but not in liver and kidney (26). These organs that have low levels of PRL-3 or even no PRL-3 expression will be susceptible to the oncogenic effect due to elevated PRL-3, which may explain why overexpression of PRL-3 will lead to enhanced tumorigenesis and metastasis in so many tissues.

### 1.3 PRLs and Cancer

As mentioned previously, cellular protein tyrosine phosphorylation level is balanced by the actions of PTKs and PTPs. Dysregulation of PTK and PTP activity results in aberrant tyrosine phosphorylation, which contributes to the development of many human diseases, including cancer (27,28). Because many PTKs have been implicated in oncogenesis, people may believe that PTPs should act as tumor suppressors because of their counteractive action on PTKs. However, accumulating evidence suggested that some of the PTPs may also function as oncogenes. To date, about 22 human PTPs have been reported in human cancers with potential oncogenic function (3).

Overexpression of PRLs has been found in a variety of late-stage tumors and their distant metastatic sites, which makes PRLs intriguing biomarkers and attractive targets in cancer (Table 1). In 2001, it was reported that PRL-3 expression was dramatically up-regulated in liver metastases of colorectal cancer (CRC) compared to its expression in primary tumors and normal colorectal epithelium (29). Since then, a number of studies have focused on the association between PRL-3 overexpression and CRC progression. For examples, further investigations have revealed that PRL-3 expression is also elevated in primary CRC tumors compared to normal tissues (30-34). PRL-3 overexpression was found not only in liver metastasis of CRC, but also other organs including lung, brain, ovary, peritoneum and lymph nodes (30,31,33,34). Most importantly, PRL-3 expression level in primary CRC is correlated with its progression to liver and lung metastasis as well as venous invasion (30). Clinically, high level of PRL-3 expression in primary CRC has significance in predicting reduced survival rate (30,33). Thus, PRL-3 is an ideal prognostic marker for cancer progression and outcome in patients with CRC.

**Table 1. The implication of PRLs in human malignancy**

| Cancer type | PRL-1 | PRL-2 | PRL-3 |
|---|---|---|---|
| Colorectal | (34) | (34) | (29-34) |
| Breast | | (35) | (36-39) |
| Gastric | (40) | | (41-48) |
| Ovarian | | | (49,50) |
| Liver | (40,51) | (40) | (52,53) |
| Oral | | | (54) |
| Nasopharyngeal | | | (55) |
| Uvea | | | (56) |
| Cervical | | | (57) |
| Esophageal | (58) | | (58) |
| Lung | (59) | (60) | (61) |
| Brain | | | (62) |
| Multiple Myeloma | | | (63,64) |
| Acute Myeloid Leukemia | | (65) | (66-68) |
| Prostate | | (69) | |
| Pancreas | (70) | (70) | |

The expression of PRL-3 has been widely investigated in other cancer types after the initial investigation in CRC by Saha *et al.* To date, up-regulation of PRL-3 has been found in a variety of late-stage neoplasms and/or metastases (Table 1). For examples, Radke *et al.* reported that mRNA expression of PRL-3, but not PRL-1 or PRL-2, was significantly higher in malignant breast cancer compared to benign breast tissue (36). At the same time, Wang *et al.* investigated 382 breast cancer patients and found that breast cancer patients with high PRL-3 expression in the tumor had a worse disease-specific survival (DSS) rate than those with low PRL-3 expression, and PRL-3 showed a significant correlation with DSS in node-negative patients (37). Miskad found that, compared to primary gastric cancer, the incidence of PRL-3 expression was significantly

higher in lymph node metastasis (41). Similarly, it was also reported that PRL-3 expression is significantly higher in peritoneal metastasis than primary gastric cancers (42). Wu *et al.* demonstrated that PRL-3 expression was enhanced in human liver carcinoma compared with normal liver tissue (71). In ovarian cancers, there was a significant correlation between PRL-3 expression and disease progression (49). Ming *et al.* also reported that PRL-3 expression is correlated with cancer progression and poor post-operative survival in non-small cell lung cancer (72).

PRL-1 and PRL-2 phosphatases are also implicated in many types of cancers (Table 1). However, the expression of PRL-1 and PRL-2 in human malignancy has not been extensively studied. Wang *et al.* determined the expression of PRL-1 and PRL-2 in colorectal carcinoma samples and found that both PRL-1 and PRL-2 are highly expressed in lymph node metastases (34). In addition, PRL-2 overexpression in prostate carcinoma was reported by Wang *et al.* (69). PRL-2 expression was also significantly elevated in primary breast tumors compared to corresponding normal tissue, and was also increased in metastatic lymph nodes compared to primary tumors (35). Recently, PRL-1 and PRL-2 expression in 285 normal, benign, and malignant human tissues of diverse origin was determined. Both PRL-1 and PRL-2 were significantly overexpressed in hepatocellular carcinomas, while PRL-1 was also strongly expressed in gastric carcinomas (40).

In conclusion, all these studies demonstrate that elevated PRLs expression is associated with the progression of different types of human malignancies, and PRLs are potential biomarkers and therapeutic targets for cancer treatment.

### 1.4 The Function of PRLs in Cell Culture

It is clear that elevated PRLs expression is correlated with tumor progression and metastasis. To further investigate the function of PRLs, many studies have focused on cell culture systems, either by overexpression or ablation of PRL expression, then observing the consequence of this alteration on cancer-related cell properties, such as cell proliferation, migration or invasion.

Zeng *et al.* demonstrated that overexpression of PRL-1 and PRL-3 promoted cell migration in wound healing and Trans-well assays, and increased cell invasion by Matrigel assay in Chinese hamster ovary (CHO) cell line (13). In addition, PRL-1 and PRL-3 overexpressing cells strongly induced lung and liver metastases after injection of cells into mouse tail veins (13). The key conclusion from this study is that PRL overexpression observed in human tumors possibly plays a causal role in tumorigenesis and metastasis but not simply a biomarker in the tumor progression. Similar results were reported by using a soft agar assay (73). High level of PRL-3 expression was also reported in the highly metastatic melanoma cell line B16-BL6 compared to the parental B16 cell line (71). Additionally, overexpression of PRL-3 in parental B16 cell line increases the migration and invasion rate to the level comparable to that in B16-BL6 cells. Injection of PRL-3 overexpressing B16 cells to mouse model also results in increased tumor growth and metastases in the liver and lung. Furthermore, PRL-3-induced oncogenic property could be reversed by treating B16-BL6 cells with PRL-3 specific siRNA to knock down endogenous PRL-3 expression (74). Finally, it is also suggested that PRL-3 overexpression promotes angiogenesis during tumor development. Up-regulation of PRL-3 expression was observed in tumor vasculature (31,75). Injection of PRL-3 expressing cells into nude mice increased the development of highly

vascularized tumors (30,73,76). PRL-3 overexpression is able to induce tube formation in human dermal microvascular endothelial cells (HMVEC) (77).

In addition to PRL-1 and PRL-3, overexpression of PRL-2 in D27 hamster pancreatic ductal epithelial cells also increased proliferation and tumor formation (12). Knocking down PRL-2 in metastatic breast cancer cells MDA-MB-231 decreased anchorage-independent growth and cell migration (35). Moreover, PRL-2 knockdown by siRNA markedly inhibited cell migration and invasion in lung cancer cell line A549 (78). However, only limited information about PRL-2 actions is current available, and further investigation is required.

Therefore, mounting evidence suggests that cancer-associated phenotypes in many different types of cancer cells are sensitively altered in response to PRLs' level change. Either overexpression or reduction of PRLs leads to dramatic phenotypic changes, suggesting that endogenous PRLs expression is critical for basic cellular events.

**1.5 Signaling Mediated by PRLs**

Excess of PRLs contributes to the acquisition of tumor-associated phenotypes. In order to obtain the detailed mechanism about PRLs, many studies have also focused on the cell signaling pathways that are regulated by PRLs. Overall, PRLs promote cell proliferation and migration through a number of signaling pathways, including the PI3K/Akt, Src, Rho family of small GTPases and p53 signaling.

It is reported that PRL-2 and PRL-3 positively regulate PI3K/Akt signaling by down-regulating the expression of tumor suppressor PTEN (79-81). PTEN is a dual specificity phosphatase that can dephosphorylate D3 position of the lipid second messenger phosphatidylinositol 3, 4, 5-trisphosphate (PIP3), through which PTEN reverses the activity of PI3K (82). In DLD-1 human colorectal cancer cells stably

expressing PRL-3, the serine/threonine protein kinase Akt was activated, and its substrate GSK-3β was inactivated by phosphorylation. Overexpression of PRL-3 but not its phosphatase-dead mutant PRL-3 (C104S) down-regulates PTEN protein level in DLD-1 cells. RT-PCR examination indicates that mRNA levels of PTEN were not changed, implying that PTEN down-regulation by PRL-3 is a post-transcriptional event (79). Recently, we have generated *Prl-2* deficient mice (see details in Chapter 4) and demonstrated that ablation of *Prl-2* up-regulates PTEN and thereby inactivates Akt in the placenta, resulting in decreased proliferation of glycogen cells, which are potential energy source in placenta, and impaired placenta function. Conversely, overexpression of PRL-2 in HEK293 cells promotes Akt activation by down-regulating PTEN through the proteasome pathway (80). Similarly, *Prl-2* deficiency also results in elevated PTEN level in the testis, which attenuates the PI3K/Akt pathway, leading to increased germ cell apoptosis and decreased male mouse reproductive capacity. In contrast, increasing PRL-2 expression in GC-1 mouse spermatogonia cells reduces PTEN and promotes Akt activation. PRL-2-mediated PTEN reduction is through enhanced PTEN degradation as assessed by a cycloheximide chase experiment. (81). Most recently, we also found an up-regulation of PTEN and inactivation of PI3K/Akt signaling in hematopoietic stem and progenitor cells (HSPCs) from *Prl-2*-null mice (83). These studies demonstrate that both PRL-2 and PRL-3 activate PI3K/Akt signaling pathway by down-regulation tumor suppressor PTEN. Notably, PTEN loss-of-function and PI3K/Akt pathway activation are frequently observed in human cancers, indicating a potential mechanism underlying PRL-mediated tumorigenesis.

In addition, PRL-3 also promotes epithelial-mesenchymal transition (EMT), a process during which epithelial cells lose cell-cell adherens and convert to migratory and

invasive cells. EMT is characterized by loss of adherens junctions and desmosomes (cell-cell interaction) with the acquisition of focal adhesions (cell-matrix interaction). PRL-3 overexpression in DLD-1 cells reduced the expression of epithelial markers E-Cadherin and γ-Catenin, and enhanced the expression of mesenchymal markers Snail and Fibronectin (79). Interestingly, PRL-3-mediated disassembly of adherens junction complex may contribute to PTEN degradation, because PTEN stability is controlled by Vinculin through the interaction of the adherens junction protein β-Catenin with the scaffold protein MAGI-2 (84). In line with this notion, PRL-2 overexpression also down-regulates both Vinculin and β-Catenin, two major components of adherens junction complexes (80,81). Similar to PRL-2, PRL-3 overexpression also results in reduction of Vinculin expression in HeLa and CHO cells (79), suggesting that PRLs may share a common mechanism in regulating adherens junctions components and PTEN stability. In addition to adherens junctions, Integrin-centered focal adhesions are also regulated by PRLs. It has been proposed that Integrin α1 is an interacting protein of PRL-3, and PRL-3 promotes the dephosphorylation of Integrin β1 (85), suggested that PRL-3 is involved in both adherens junctions and focal adhesions.

Src kinase is also activated upon PRL-1 and PRL-3 overexpression (86-88). In line with this, several Src downstream effectors including STAT3 and ERK1/2 are also activated following PRL-1 and PRL-3 overexpression (86-88). Src tyrosine kinase is implicated as an oncogene that works under multiple receptor-mediated signaling pathways. Aberrant Src activation hijacks these signaling networks to facilitate the PRL-3 induced tumorigenesis and metastasis in PRL-3 overexpression HEK293 cells (87). Src is auto-inhibited by the internal interaction between SH2 domain and phosphorylated $Tyr^{527}$ in its C-terminal tail. Once $Tyr^{527}$ is phosphorylated by C-terminal Src Kinase

(CSK), Src activity is inhibited (89). It is suggested that the negative regulator Csk is down-regulated in PRL-3 overexpressing cells to induce Src activation (86). Moreover, PRL-3-mediated Src activation is attributable to translational control of Csk expression (90). Activation of Src will result in the tyrosine phosphorylation of the adaptor protein $p130^{Cas}$, which is a key player in focal adhesion formation (91). Consistent with the elevated Src activity observed in PRL-3 overexpression cells, $p130^{Cas}$ phosphorylation as well as the interaction between $p130^{Cas}$ and Vinculin was increased (86). Interestingly, a recent report suggested that PRL-2 suppression by siRNA in A549 cells also down-regulates $p130^{Cas}$ expression (78), which is consistent with a previous observation that $p130^{Cas}$ was also decreased in PRL-1-silencing A549 cells (59), implying that all PRLs are able to regulate $p130^{Cas}$ in the focal adhesion complex. Together with the function of PRLs in adherens junctions, all these data indicate that PRLs definitely modulate the turnover and function of adherens junctions and focal adhesions to facilitate cell migration and invasion.

Rho family of small GTPases (Rho, Rac and Cdc42) regulates actin cytoskeleton dynamics through modulating actin polymerization, focal adhesion formation and cell motility. The first evidence that put PRLs into Rho GTPases signaling is reported by Fiordalisi *et al.* (16). They found that PRL-1 and PRL-3 overexpression in SW480 colorectal carcinoma cells significantly increased active RhoA and RhoC level. In contrast, active Rac level was significantly reduced by PRL overexpression, whereas Cdc42 activity was unaffected. Treatment with specific inhibitor for Rho kinase ROCK, a key Rho effector, attenuated the PRL-dependent motility and invasion, suggesting that PRLs acts upstream of Rho and ROCK signaling to promote cell migration and motility. Recently, the same proup further demonstrated that Src-mediated PRL-3

phosphorylation is required for PRL-3-induced Rho activation, motility and invasion, indicating that Src not only is a key effector downstream of PRL-3, but also may act as a switch on PRL-3 to initiate the migration and invasion (92).

A recent phage display screening by us identified p115 RhoGAP, also known as ARHGAP4, as a PRL-1 binding protein (93). Like other RhoGAPs, p115 RhoGAP plays a negative role in RhoA activation by increasing the intrinsic GTPases activity which converts GTP-bound active RhoA to GDP-bound inactive RhoA. In addition, p115 RhoGAP also inhibited MAP/ERK pathways through interaction with and inhibition of MAP/ERK kinase kinase 1 (MEKK1) (94). It is worthy to test the possibility that PRL-1 activates RhoA and ERK1/2 by inhibiting p115 RhoGAP function, and thereby promotes cell migration and proliferation (see details in Chapter 2).

PRLs are also possibly involved in cell cycle regulation. The localization of PRL-1 in HeLa cells is controlled in a cell cycle dependent manner (95). PRL-1 localized to the endoplasmic reticulum (ER) in non-mitotic cells, while it moved to centrosomes and spindle apparatus in mitotic cells, suggesting that PRL-1 plays a role in spindle dynamics. Overexpression of PRL-1 and PRL-2 in D27 cells enhanced cell cycle progression possibly through down regulation of p21, a cyclin-dependent kinase inhibitor (96). Recently, it is reported that PRL-1 and PRL-3 are new p53 transcriptional target genes, and also down-regulates p53 through Mdm2 and Pirh2 (97-99). p53 is a well-characterized tumor suppressor that is the most commonly inactivated in numerous tumors (100-102). It is widely accepted that p53 inhibits tumor formation through activation of cell cycle arrest, apoptosis and senescence. Reducing PRL-3 expression levels in MEF cells led to cell cycle arrest through increased p53 expression, while overexpression of PRL-3 also resulted in G1 arrest, indicating that basal expression of

PRL-3 in MEF cells seems to be critical to ensure cell cycle progression via facilitating G1/S transition (97). In accord with the results shown in MEF cells, up-regulation of PRL-3 in HCT116 colorectal cancer cells decreased p53 expression. However, it inhibited p53-mediated apoptosis rather than cell cycle arrest (99).

Overall, all those studies on the PRLs-mediated signaling pathways suggested that PRLs are multifunctional proteins that involved in four signaling pathways, PI3K/Akt pathway, Src pathway, Rho family pathway and p53 pathway. All those signaling pathways mainly control two cell functions, EMT and cell cycle regulation, both of which contribute to PRLs' oncogenic function.

**1.6 Therapeutic targeting of PRLs**

Pharmacological inhibition of PRLs has gained widespread attention since the identification of PRLs as potential therapeutic targets in cancer treatment. Several PRLs inhibitors have been discovered to date (Figure 4).

Pentamidine [1,5-di(4-amidinophenoxy)pentane], a drug clinically used for treatment of leishmaniasis, has been identified as a pan inhibitor for all PRLs with anti-cancer potential in a melanoma xenograft mouse model (103). However, pentamidine inhibits not only PRLs but also other PTPs including PTP1B, suggesting the real *in vivo* target and mechanism are still not clear. In a high throughput screening using chemical library of Korea Chemical Bank, BR-1, one of the rhodanine derivatives, was discovered as PRL-3 inhibitor with $IC_{50}$ value of 0.9 μM and reduced invasion of B16F10 cells, which have high levels of endogenous PRL-3 expression compared to the parental cell line B16F0 (104), and strongly inhibited migration and invasion of PRL-3 overexpressing DLD-1 cells (105). Daouti *et al.* reported the first selective PRLs

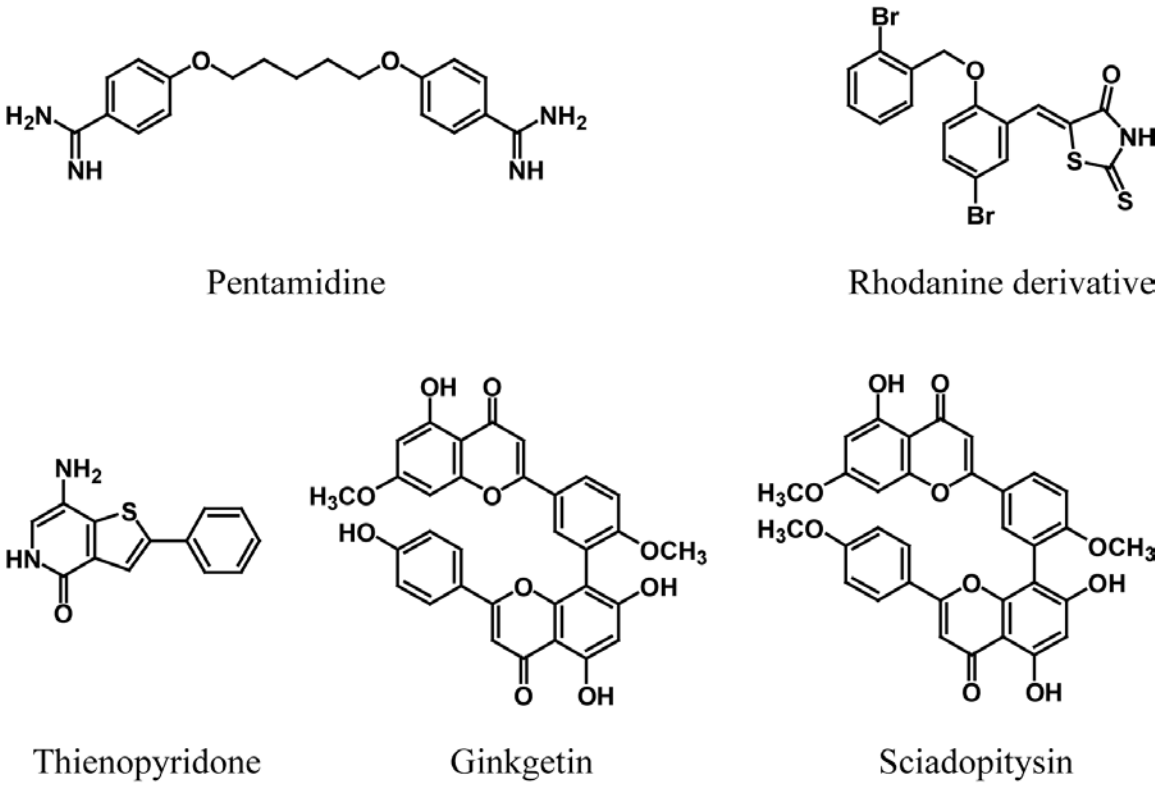


**Figure 4. Chemical structure of small molecule inhibitors for PRLs.**

Pentamidine is a pan inhibitor for all PRLs with low potency. The Rhodanine derivative is a PRL-3 inhibitor with $IC_{50}$ value of 0.9 μM. Thienopyridone is another potent and specific pan PRLs inhibitor with $IC_{50}$ values of 173, 277 and 128 nM for PRL-1, PRL-2 and PRL-3, respectively. Natural products ginkgetin and sciadopitysin inhibited PRL-3 with $IC_{50}$ values of 25.8 and 46.2 μM, respectively.

inhibitor, thienopyridone, which suppresses tumor cell anchorage-independent growth in soft agar (106). Thienopyridone potently and selectively inhibited all three PRLs *in vitro* with $IC_{50}$ values of 173, 277 and 128 nM for PRL-1, PRL-2 and PRL-3, respectively. Thienopyridone reduced tumor cell three-dimensional growth by a novel mechanism involving $p130^{Cas}$ cleavage and anoikis, a form of programmed cell death induced by anchorage-dependent cells detaching from the surrounding extracellular matrix (ECM). Ginkgetin and sciadopitysin, two biflavonoids isolated from the MeOH extract of the young branches of *Taxus cuspidata*, inhibited PRL-3 with $IC_{50}$ values of 25.8 and 46.2

μM, respectively (107). These are the first report of natural products that inhibit PRL-3. Park *et al*. reported that 12 novel PRL-3 inhibitors with diverse structures and $IC_{50}$ values ranging from 10 to 50 μM were identified by virtual screening (108). Recently, curcumin, the natural product from spice turmeric, has been shown to prevent B16BL6 cells from invading by selectively down-regulating PRL-3 but not PRL-1 and PRL-2 mRNA expression (109). However, this inhibition of PRL-3 transcription is possibly through other targets in cancer cells. Antibody-based cancer therapies have better specificity and thus improved efficacy compared to standard small molecule inhibitors. Most recently, Guo *et al.* identified a novel PRL-3 antibody that effectively retarded metastatic tumors that express endogenous PRL-3 (110). However, the mechanism by which this antibody can target intracellular PRL-3 is still not understood.

Collectively, many efforts have been made to establish novel therapeutic tools by targeting PRLs. However, none of those have been tested in clinical trials due to low specificity or limited information on mechanisms of action. Developing better PRLs inhibitors with higher specificity are still required for anti-cancer therapeutics.

**1.7 Genetic models for PRLs**

Despite numerous studies having been performed to understand PRLs action, they all used cultured cells aberrantly or ectopically expressing PRLs. Thus the exact biological function of PRLs remains unknown. Recently, several studies with *Prl*-null mice were reported. Our group published the first study on *Prl-2* knockout mice (see details in Chapter 4) and demonstrated that deletion of *Prl-2*, the most ubiquitously expressed *Prl* family member, impaired placental development and growth in both embryos and adult mice (80). At the molecular level, PRL-2 activated the anti-apoptotic kinase Akt by down-regulating the tumor suppressor PTEN through degradation in the

proteasome, which is consistent with cell based studies where PRL-2 elicited oncogenic activity by negatively regulating PTEN, thereby activating the PI3K-Akt pathway (79). This study provided the first evidence that PRL-2 is required for extra-embryonic development. Following this discovery, we also found a similar functional role for PRL-2 in spermatogenesis. *Prl-2* deficient mice exhibited testis hypotrophy, reduced sperm production and impaired reproductive ability (81). Mechanistically, *Prl-2* deficiency results in elevated PTEN level in the testis, which attenuates the Kit-PI3K-Akt pathway, resulting in ectopic germ cell apoptosis. Collaborating with Dr. Michihiro Kobayashi in Dr. Yan Liu's lab, we also found that *Prl-2* deficiency results in ineffective hematopoiesis and impaired long-term repopulating ability of hematopoietic stem cells (HSCs) (83). Biochemical data demonstrated that *Prl-2* deletion impairs the activation of SCF/KIT signaling via down-regulating PTEN in hematopoietic stem and progenitor cells (HSPCs), leading to reduced HSPCs proliferation. All these data support the conclusion that PRL-2 plays a pro-proliferative and pro-survival role in different tissues through down-regulation of PTEN and subsequent activation of PI3K/Akt signaling.

The first gene-targeted murine knockout for *Prl-3*, the most widely studied *Prl* family member, was reported by Zimmerman *et al.* (26,111). Mice deficient for *Prl-3* have no obvious phenotype except that fewer homozygous-null males were observed at weaning. Similar to *Prl-2* null mice, *Prl-3* deficient mice also exhibited an approximate 10% decrease in body mass. *Prl-3*-null mice treated with carcinogen azoxymethane and dextran sodium sulfate developed 50% fewer colon tumors than wild-type mice, highlighting the potential value of this phosphatase as a therapeutic target in colon cancer (26). Following this study, Zimmerman *et al.* further demonstrated that colon tumor tissue developed in *Prl-3*-null mice had less tumor microvessel density

compared to wild-type controls, and endothelial cells derived from *Prl-3* deficient mice displayed significantly reduced migration *in vitro*, suggesting that PRL-3 is involved in VEGF signaling and contributes to pathological angiogenesis (111).

At the same time, we also independently generated *Prl-3*-null mice (see details in Chapter 4). We also found a significant decrease of *Prl-3*$^{-/-}$ birth rate, suggesting indeed loss of PRL-3 leads to survival disadvantage. However, we did not observe any significant reduction in body mass in *Prl-3*-null males, which may be due to difference in genetic background of animals used in the experiments. While Zimmerman *et al.* used C57BL/6J strain with 5 generations of backcrossing, our results were derived from a C57BL6/129P2 mixed genetic background. Further investigations were required to establish the physiological role of PRL-3 *in vivo*.

In addition to mouse knockout models, several groups are also working on PRLs transgenic mice. Hardy et al. reported the first PRL-2 transgenic mouse model by co-expressing both activated ErbB2 and PRL-2 in the mammary epithelium (35). Mammary-targeted overexpression of PRL-2 did not exhibit spontaneous tumorigenesis, but they accelerated development of mammary tumors initiated by introduction of an activated ErbB2 transgene. However, the effects of PRL-2 overexpression in other tumor models, as well as the oncogenic potential of transgenic mice with two other PRL family members, PRL-1 and PRL-3, require further investigation.

Most recently, Pagarigan *et al.* reported the first study of PRL overexpression in *Drosophila*, another genetically controlled organismal model (112). The *Drosophila* genome encodes a single PRL protein (dPRL-1), which is highly similar (74-76%) to all three human PRLs. Strikingly, they found that overexpression of dPRL-1 broadly resulted in growth inhibition, suggesting that *Drosophila* PRL performs as a tumor

suppressor. Further evaluations are needed to explain the opposing outcomes observed in different genetic organisms.

All together, the studies in mice not only revealed the oncogenic role of PRLs by *in vivo* carcinogenesis models, but also demonstrated the important physiological function of PRLs in normal development. However, the physiological role of PRL-1 is still unclear due to the lack of *Prl-1* deficient mice (see details in Chapter 4). In addition, due to the high homology of PRLs, it is possible that two other PRLs may compensate for the loss of a single isoform. Thus, to establish the complete physiological functions of PRLs, it is necessary to generate double or even triple knockout mice for *Prls* (see details in Chapter 5).

**1.8 Research gaps and thesis objectives**

Since the discovery of PRL phosphatases, an intense interest has been focused on PRLs' role in promoting cancer. Numerous studies support their strong implication in biological process during tumorigenesis and metastasis. However, there still exist unanswered questions regarding the mechanisms, therapeutic values and physiological functions of PRLs. First of all, PRLs have been implicated as oncogenes that alter signaling pathways affecting basic cell processes. However, little is known about the detailed mechanisms underlying PRLs actions. Secondly, given their pathogenic role in tumorigenesis and metastasis, PRL phosphatases are attractive therapeutic targets to develop anti-cancer agents. However, very few effective PRLs inhibitors have been developed. Finally, while PRLs have been widely studied in cell culture systems, the real physiological role of PRLs *in vivo* is still unknown. The work described in this dissertation will cover three projects: 1) Phage display was used to identify PRL-1 binding partners; 2) Virtual screening was utilized to develop small molecule inhibitors

targeting PRL-1 trimer interface; and 3) Mice that are deficient for PRL-1, PRL-2 or PRL-3 were generated to investigate the *in vivo* functions of PRLs. Identification of PRL-1 interacting proteins will benefit our understanding on the molecular mechanism by which PRL-1 promotes cell migration and proliferation. Development of small molecule inhibitors that interfer with the PRL-1 trimer interface may provide novel agents for anti-cancer treatment. Generation of knockout mice for individual *Prl* genes will contribute to the understanding of the physiological functions of PRLs *in vivo*.

# CHAPTER 2: PRL-1 PROMOTES ERK1/2 AND RHOA ACTIVATION THROUGH A NOVEL INTERACTION WITH P115 RHOGAP

## 2.1 Overview

Among all PRLs, PRL-1 was the first identified member, whose expression was induced during liver regeneration after partial hepatectomy (11). Subsequently, PRL-1 expression was found to be elevated in many tumor cell lines, and cells expressing high levels of PRL-1 exhibited enhanced proliferation and anchorage-independent growth (11,12,95,96). PRL-1 also promotes cell invasion and tumor metastasis. For example, overexpression of PRL-1 in CHO or HEK293 cells displays enhanced cell motility and invasiveness (13,17). CHO cells with elevated PRL-1 also preferentially form metastatic tumors in nude mice (13). Furthermore, an increase in PRL-1 expression enhances motility and invasion of SW480 colon adenocarcinoma cells (16), while knockdown of endogenous PRL-1 inhibits human A549 lung cancer cell invasion (59). These results suggest an oncogenic role for PRL-1 in cancer development and metastatic progression. However, less knowledge is available with respect to the underlying mechanisms.

## 2.2 Hypothesis and Specific Aims

Recently, biochemical studies revealed that PRL-1 promotes cell proliferation and invasion by up-regulating both ERK1/2 and RhoA (16,17,88,113). ERK1/2 are serine/threonine kinases that are required for many fundamental cellular processes including cell proliferation, survival and motility (114), while the Rho family of GTPases are mainly recognized as key regulators of actin cytoskeletal dynamics and cell migration (115,116). However, the underlying mechanism by which PRL-1 activates ERK1/2 and RhoA remains to be established. Through a phage display library screening, I identified a novel PRL-1 binding peptide, corresponding to a sequence motif located in

the SH3 domain of p115 Rho GTPase-activating protein. Like other RhoGAPs, p115 RhoGAP lowers the active RhoA level by accelerating the cycling between the biologically active GTP-bound form and inactive GDP-bound form. In addition, p115 RhoGAP also inhibits the MAP/ERK pathways through interaction with and inhibition of MAP/ERK kinase kinase 1 (MEKK1) (94). Given the inhibitory role of p115 RhoGAP in ERK1/2 and RhoA activation, I hypothesized that **PRL-1 promotes ERK1/2 and RhoA activation through the novel interaction with p115 RhoGAP**. To test this hypothesis, I developed two specific aims: 1) to validate the interaction between PRL-1 and p115 RhoGAP via biochemical, cellular and structural studies; and 2) to determine the mechanism of PRL-1 mediated ERK1/2 and RhoA activation through the interaction with p115 RhoGAP. The work described here will contribute to the understanding of the molecular mechanism by which PRL-1 promotes cell proliferation and migration and the overall biological functions of PRLs in tumorigenesis and metastasis.

## 2.3 Materials and Methods

### 2.3.1 Materials

Anti-HA, anti-His, anti-GST, anti-RhoA, anti-Actin and anti-MEKK1 antibodies were purchased from Santa Cruz Biotechnology. Anti-Flag and anti-p115 RhoGAP antibodies were from Sigma. Polyclonal anti-ERK1/2, anti-pERK1/2 (Thr-202/Tyr-204) and anti-Myc antibodies were obtained from Cell Signaling (Beverly, MA). Dulbecco's modified Eagle's medium (DMEM), fetal bovine serum, penicillin, and streptomycin were from Invitrogen.

### 2.3.2 Phage display

The PH.D.-12 phage display peptide library kit (New England Biolabs) was used to screen PRL-1 binding peptides according to manufacturer's instructions. On day 1, 3 μg of recombinant PRL-1 was coated in a well of 96-well plate at 4°C overnight. On day 2, 200 μL MPBS (2% (v/v) non-fat milk in PBS (137 mM NaCl, 2.7 mM KCl, 10 mM $NaH_2PO_4$, 1.4 mM $KH_2PO_4$, pH 7.4)) was added to the well with shaking for 1 hr at room temperature to block non-specific binding. During this time, the input phage was mixed in 100 μL MPBS and incubated for 1 hr at room temperature in an empty well to allow any "sticky" phage to adhere to the plastic. Then the protein/MPBS solution was discarded and the well was washed five times with 200 μL PBST [0.1% (v/v) Tween in PBS]. The phage/MPBS solution was transferred from the pre-clearing well to the PRL-1-coated well incubating for 2 hrs at RT on the shaker. After washing away unbound phage with 200 μL PBST for five times, the bound phage was eluted by adding 100 μL 0.1 M HCI for 10 min at room temperature on the shaker. Eluted phage was transferred to a tube and immediately neutralized by adding 50 μL 1 M Tris-HCI buffer (pH 7.4). A small part of this output phage was used for titration and the rest was amplified to get an input titer of $10^{13}$ phage for the following panning. A total of four rounds of panning were performed to obtain PRL-1 specific phages. Individual phage clones were amplified and single strand DNA was isolated according to the manufacturer's instruction. The sequence of the 12 amino acid PRL-1 binding peptide was obtained by DNA sequencing.

### 2.3.3 Cell culture and transfection

HEK293 cells and mouse embryonic fibroblast cells were grown in DMEM supplemented with 10% fetal bovine serum, penicillin (50 units/mL), and streptomycin

(50 μg/mL) under a humidified atmosphere containing 5% $CO_2$. HEK293 cells were seeded at 40% confluency in antibiotic-free medium and grown overnight. Transfection was performed using Fugene 6 (Roche, Indianapolis, IN) according to the manufacturer's recommendations.

### 2.3.4 Immunoblotting and immunoprecipitation

Cells were grown to 70% confluency, washed with ice-cold phosphate-buffered saline, and lysed on ice for 30 min in lysis buffer (50 mM Tris-HCl [pH 7.4], 150 mM NaCl, 1% Triton X-100, 10% glycerol) supplemented with a complete protease inhibitor tablet (Roche). Cell lysates were cleared by centrifugation at 15000 rpm for 10 min. The lysate protein concentration was estimated using a BCA protein assay kit (Pierce). For immunoprecipitation, 3 μg of antibody was added to 1 mg of cell lysate and incubated at 4 °C for 4 hrs with protein A/G-agarose beads. After being extensively washed, the protein complex was boiled with sample buffer, separated by SDS-PAGE, transferred electrophoretically to a nitrocellulose membrane, and immunoblotted with appropriate antibodies followed by incubation with horseradish peroxidase-conjugated secondary antibodies. The blots were developed by the enhanced chemiluminescence technique (ECL kit, GE Biosciences). Representative results from at least two independent experiments are shown.

### 2.3.5 GST pull-down assay

Pull-down assays were performed with GST, GST fusion Peptide **1**, or GST-SrGAP-SH3 bound to reduced glutathione agarose after washing 3 times in Tris-buffered saline. Purified His-PRL-1 proteins or cell lysates containing HA-PRL-1 were added to immobilized GST fusions in binding buffer (50 mM Tris-HCl, pH 7.5, 150 mM NaCl, 10% glycerol 0.5% Triton X-100, 5 mM EDTA and proteinase inhibitors cocktail) and

incubated for 2 hrs at 4°C in a tube rotator. After centrifugation, the beads were kept on ice and washed 3 times for 5 min each in washing buffer (50 mM Tris-HCl, pH 7.5, 150 mM NaCl, 10% glycerol, 0.1% Triton X-100, 5mM EDTA and proteinase inhibitors cocktail). The washed beads were boiled in loading buffer for 5 min and separated in SDS-PAGE gel. Proteins were transferred to PVDF and immunostained with anti-His, anti-HA and anti-GST antibodies.

**2.3.6 Effector pull-down assay**

Effector pull-down assay was performed to monitor RhoA activity. Cells were lysed in a buffer containing 20 mM Tris-HCl, pH 7.6, 100 mM NaCl, 1% Triton X-100, 10 mM $MgCl_2$, 2 mM NaF, and protease inhibitors cocktail for 30 min at 4 °C. Cell lysate was incubated with the GST-RBD domain of Rhotekin immobilized on reduced glutathione agarose for 2hr at 4°C in a tube rotator. The level of active RhoA was detected by Western blotting with anti-RhoA antibody.

**2.3.7 GAP activity assay**

Immunoprecipitated p115 RhoGAP activity was measured by analyzing the ratio of GTP and GDP bound to RhoA as described (117). Recombinant human RhoA protein was purified as described (118) and was loaded with [$\alpha$-$^{32}$P] GTP by incubation 10 min at 30 °C, in 50 mM Tris HCl, pH 7.4, 150 mM NaCl, 5 mM EDTA, 1 mg/mL BSA, 6 μM GTP, 5 μCi [a-$^{32}$P]GTP, 1 mM dithiothreitol. $MgCl_2$ was added to 10 mM and free nucleotide removed by washing beads 3X with the loading buffer minus GTP. Proteins were then eluted by incubating beads with 100 μL of 100 mM Tris HCl, pH 8.0, 10 mM $MgCl_2$ and 20 mM glutathione on ice for 20 min. GTP loaded RhoA was then incubated with Flag-p115 RhoGAP produced by transient transfection in 293 cells and immunoprecipitation with anti-Flag antibody in a 50 μL final reaction volume containing

25 mM Tris HCl (pH7.5), 1.5 mg/mL BSA, 7.5 mM $MgCl_2$, 2 mM dithiothreitol at room temperature for 1 hr. The reaction was stopped by addition of 4 μL 0.5 M EDTA and 1 μL 10% SDS and RhoA protein denatured by incubation at 68°C, 5 min and guanine nucleotides separated by thin layer chromatography on polyethyleneimine cellulose plates TLC plate (J. T. Baker, Inc., Phillipsburg, NJ) using 0.75 M $KH_2PO_4$/HCl, pH 3.4 as solvent. Chromatograms were dried and Ras-bound GDP and GTP were visualized by autoradiography.

**2.3.8 Immunofluorescence and confocal microscopy**

Mouse Embryo Fibroblast (MEF) cells were cultured directly on glass coverslips in 6-well plates. Twenty-four hours later, cells were transfected with the indicated constructs. After an additional 24 h, cells were fixed with 4% paraformaldehyde in phosphate-buffered saline (PBS) for 10 min at room temperature, permeabilized with 0.2% Triton X-100 in PBS for 10 min, and blocked with BSA. Monoclonal antibody to Flag (M2) was applied for 1 h, followed by 1h incubation with Texas Red-conjugated anti-mouse immunoglobulin G (Jackson ImmunoResearch Laboratories). DNA staining (0.5 μg of Hoechst no. 33258/mL; Sigma) was used to identify cell nuclei. After washing with PBS, the coverslips were mounted with anti-fade mounting solution. Confocal microscope images were obtained with a Zeiss AxioObserverZ1 microscope with a Plan Apochromat ×63 oil immersion objective and processed with Zeiss Axiovision 4.7.

**2.3.9 Cell migration assay**

Cell migration was assessed as described previously (88) with some modifications. The assay was performed with Transwells (6.5 mM diameter; 8 μM pore size polycarbonate membrane) obtained from Corning (Costar, Acton, MA). Cells ($3.75 \times 10^5$) in 1.5 mL of serum-free medium were placed in the upper chamber, whereas the

lower chamber was loaded with 2.6 mL of medium containing 10% FBS. After incubation at 37 °C with 5% $CO_2$ for 24 h, the total numbers of cells that migrated into the lower chamber was counted with a hemacytometer.

### 2.3.10 siRNA knockdown

Duplex siRNAs were provided by Proligo at a concentration of 50 μM. The siRNA sequences were as follows: human p115 RhoGAP-1, 5′-CUGAGGUGCCGCUGCUGGAdTdT (sense), 5′-UCCAGCAGCGGCACCUCAGdTdT (antisense), target position 2880; p115 RhoGAP-2, 5′- GCGUGAAUGCCGAGGCCAAdTdT (sense), 5′-UUGGCCUCGGCAUUCACGCdTdT (antisense), target position 575. siRNAs were transfected by RNAiFect (Qiagen), and the knockdown of targeted genes was verified after 72 hrs by Western blotting analysis.

### 2.3.11 Luciferase assay

Luciferase assays were modified as previously described (88). Cells were transfected with SRE.L triple repeat promoter-luciferase construct (119). Cells were harvested and lysed 48 hrs after transfection. Luciferase activities were determined using the luciferase assay system (Promega, Madison, WI) according to the manufacturer's specifications. Individual assays were normalized by internal Renilla luciferase activity. Experiments were performed in triplicate and repeated three times with similar results. The statistics were done using a Student's *t*-test, with a $P$ of $<0.05$ considered significant.

### 2.3.12 Protein purification, crystallization and data collection

PRL-1 without tag (residues 4-160) was sub-cloned into pET21a, and the vector was transformed into *Escherichia coli* BL21-(DE3). Transformed cells were grown at 37°C in Luria broth (LB) containing 100 mg/mL ampicillin for 4 hrs until the OD600

reached 0.6, and then induced for overnight at room temperature with 0.4 mM IPTG. Cells were harvested by centrifugation (6000 rpm for 15 min at 4 °C), and the cell pellets from 1.5 L of LB medium were suspended in 30 mL of ice-cold buffer A consisting of 50 mM NaCl, 20 mM MES (pH 5.8), and 1 mM EDTA. In this stage, trypsin inhibitor and PMSF were also added to buffer A to final concentration of 0.05 mg/mL and 0.1 mM, respectively. The suspensions were passed twice through a French Press at 1000 psi, and the cell lysates were centrifuged at 4 °C for 30 min at 15000 rpm. The supernatants were mixed with 0.5 g beads of CM Sephadex C50 (Sigma-Aldrich) at 4 °C for 1 h, and then the mixture was transferred to an empty column. The column was washed by 200 mL of buffer A, and then eluted with 20 mL of buffer B (500 mM NaCl, 20 mM MES (pH 5.8), 5 mM DTT). The elution was dialyzed for 6 hrs at 4 °C against 1 L buffer A, and then loaded onto a Mono S column equilibrated at 4 °C with buffer A. The column was washed with 10 mL of buffer A and then eluted with a 40 mL of linear gradient of 0 to 1 M NaCl in buffer A. The column fractions were analyzed by measuring the absorbance at 280 nm and by carrying out SDS-PAGE analysis. The fractions were combined and concentrated at 4 °C to ≤ 1 mL using an Amicon concentrator and then loaded onto a gel filtration column Superdex 75. The column was eluted with buffer A, and fractions which contain protein were combined and concentrated to 7 mg/mL and stored at −80 °C. The sample PRL-1 was shown to be homogeneous by SDS-PAGE analysis.

PRL-1 (7 mg/mL) was mixed with Peptide **1** with a molar ratio of 1:2, and PRL-1•Peptide **1** were co-crystallized by vapor diffusion in hanging drops at 4 °C. Drops containing 1:1 volumes of the protein in stock buffer (20 mM Tris-HCl, pH 7.5) and reservoir solution A (20% PEG 3350, 0.1 M NaCl, 0.1 M Bis-Tris pH 6.4) were

equilibrated against reservoir solution A. The crystal was transferred into reservoir solution B (28% PEG 3350, 0.1 M NaCl, 0.1 M Bis-Tris pH 6.4, 0.2 mM Peptide **1**), soaked for 5 hours, and flash-cooled in liquid nitrogen. X-ray data were collected at 100 K at SBC-CAT beamline 19-BM at the Advanced Photon Source (Argonne, IL) equipped with a mosaic CCD detector. All data were processed with HKL3000 (120).

### 2.3.13 Structural determination and refinement

The structure of PRL-1•Peptide **1** was solved by molecular replacement using program AMoRe (121). The structure of PRL-1 (PDB entry code 2ZCK) (23), without the solvent molecules, was used as the search model. The structure was refined to 2.8 Å resolution with the program CNS1.1 (122). The progress of the refinement was evaluated by the improvement in the quality of the electron density maps, and the reduced values of the conventional *R* factor and the free *R* factor (123) (3.3% of the reflections omitted from the refinement). Electron density maps were inspected and the model was modified on an interactive graphics workstation with the program O (124). Finally, water molecules were added gradually as the refinement progressed. They were assigned in the $F_o$ - $F_c$ difference Fourier maps with a 3σ cutoff for inclusion in the model.

## 2.4 Results

### 2.4.1 Identification and characterization of a PRL-1 binding peptide

In order to discover new PRL-1 binding proteins and get new insight into the mechanism that accounts for PRL-1 mediated ERK1/2 and RhoA, I screened a 12-mer phage display peptide library against $(His)_6$-tagged recombinant PRL-1 and identified Peptide **1** (GWWSLIPPKYIT) as a putative PRL-1 binding peptide. Consistent with this peptide interacting with PRL-1, purified GST-Peptide **1** fusion protein, but not GST, was capable of precipitating $(His)_6$-tagged recombinant PRL-1 from solution (Figure 5A,

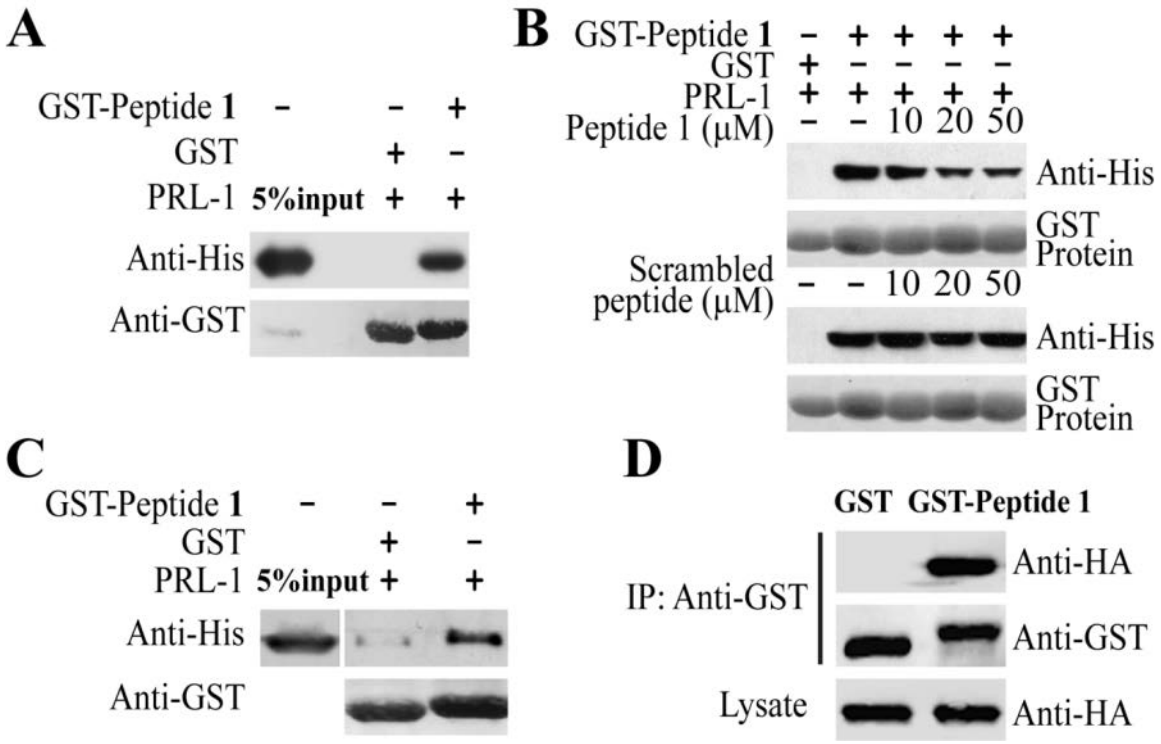


**Figure 5. Identification and characterization of a PRL-1-binding Peptide 1.**

**A.** *In vitro* GST pulldown assay verified the interaction between His6-tagged PRL-1 and GST-Peptide 1. **B.** Synthetic Peptide 1 blocks binding between PRL-1 and GST-Peptide 1. **C.** GST-Peptide 1 pulls down HA-tagged PRL-1 from HEK293 cell lysate. **D.** GST-Peptide 1 co-immunoprecipitates (IP) HA-PRL-1 from HEK293 cells. Data shown are representative of triplicate experiments with similar results. Panel A, C and D were generated by Yong Luo.

created by Yong Luo). The concentration dependent displacement of PRL-1 from GST-Peptide **1** fusion protein by synthetic Peptide **1** but not by a scrambled peptide indicates the specificity of this interaction (Figure 5B). In addition, GST-Peptide **1** pulled down HA-PRL-1 from HEK293 cell lysate (Figure 5C, created by Yong Luo), and GST-Peptide **1** readily co-immunoprecipitated with HA-PRL-1 when both were expressed in HEK293 cells (Figure 5D, created by Yong Luo). Collectively, these results indicate that Peptide **1** directly binds PRL-1 both in solution and in mammalian cells.

### 2.4.2 Identification of p115 RhoGAP as a PRL-1 binding protein

Then we launched a BLAST search using Peptide **1** as a query to identify PRL-1 binding proteins. The top hit was the human protein p115 RhoGAP (125), a member of the Slit-Robo (Sr) GAP family of proteins that have attributed roles in axon guidance and cell migration (93,126). All members of the SrGAP family (SrGAP1, 2, 3 and p115 RhoGAP) contain an N-terminal Fes/CIP4 (Cdc42-interacting protein 4) homology (FCH) domain, a central RhoGAP domain and a C-terminal SH3 domain (125,127). Because Peptide **1** shares strong sequence identity with contiguous residues in the SH3 domains of all srGAP proteins (Figure 6A), we compared their relative association with PRL-1 by co-immunoprecipitation. For this purpose, Flag-tagged p115 RhoGAP, SrGAP1, 2, and 3 were transfected into HEK293 cells stably expressing HA-PRL-1. Protein complexes were immuno-isolated from cell lysates using anti-HA antibody and immunoblotted with antibodies against Flag or HA. The result revealed that PRL-1 co-immunoprecipitates with all SrGAP family members (Figure 6B, generated by Yong Luo). Consistently, GST pulldown assays demonstrated that PRL-1 directly binds the SH3 domains of each SrGAP (Figure 6C, generated by Yong Luo), but not to a truncated p115 RhoGAP lacking its SH3 domain nor to ArhGAP9, an SH3 domain containing RhoGAP that is not in the SrGAP family (Figure 6D). Further, GST-Peptide **1** disrupts the intracellular association between PRL-1 and p115 RhoGAP (Figure 6E). These findings suggest that PRL-1 binds p115 RhoGAP through a short motif in its SH3 domain.

We next examined the subcellular co-distribution of PRL-1 and p115 RhoGAP. Flag-tagged p115 RhoGAP and GFP-tagged PRL-1 were co-expressed in mouse embryonic fibroblast cells and their cellular localization was visualized by confocal

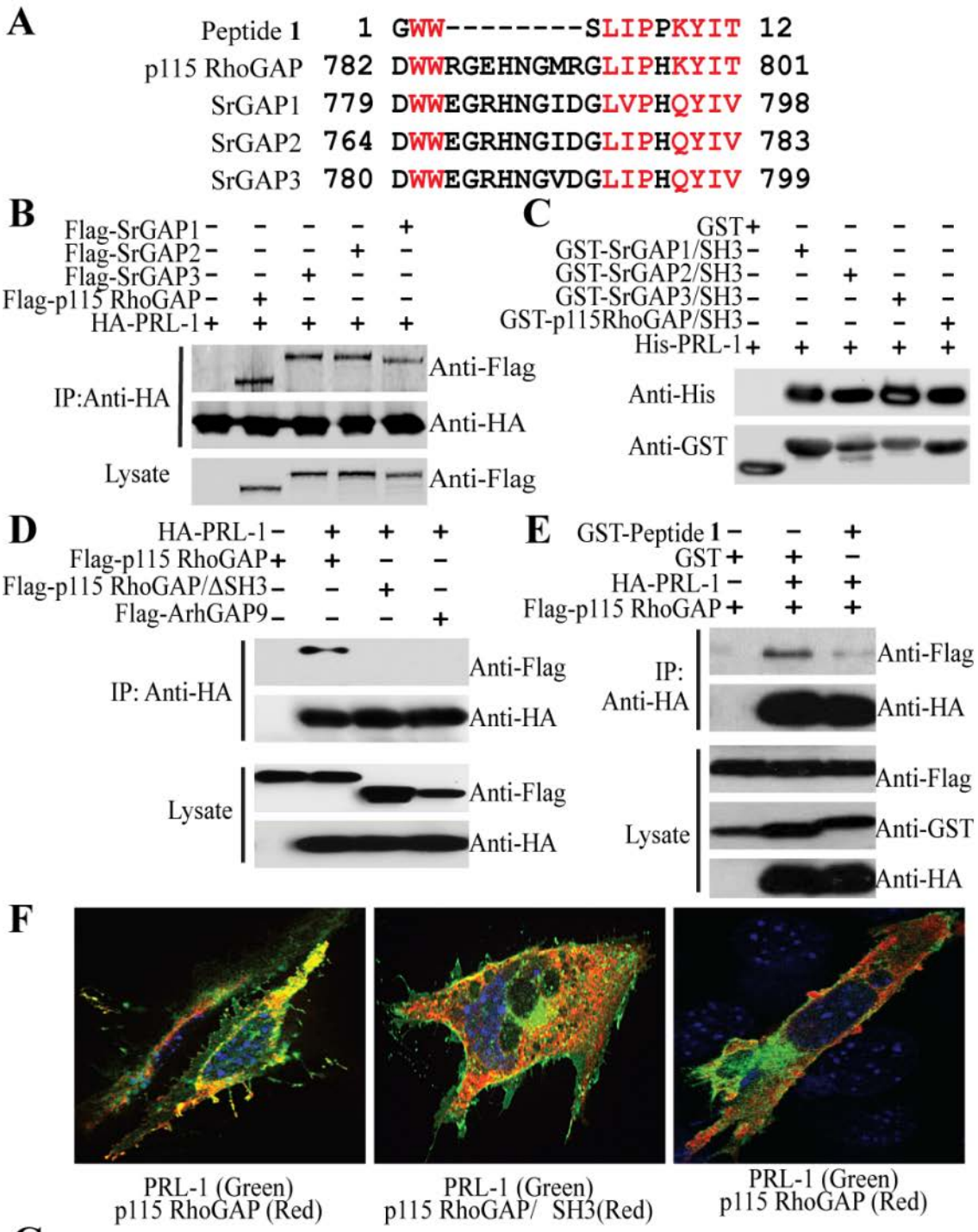
A
Peptide 1 1 GWW--------SLIPPKYIT 12
p115 RhoGAP 782 DWWRGEHNGMRGLIPHKYIT 801
SrGAP1 779 DWWEGRHNGIDGLVPHQYIV 798
SrGAP2 764 DWWEGRHNGIDGLIPHQYIV 783
SrGAP3 780 DWWEGRHNGVDGLIPHQYIV 799
B
Flag-SrGAP1
Flag-SrGAP2
Flag-SrGAP3
Flag-p115 RhoGAP
HA-PRL-1
IP:Anti-HA
Anti-Flag
Anti-HA
Lysate
Anti-Flag
C
GST
GST-SrGAP1/SH3
GST-SrGAP2/SH3
GST-SrGAP3/SH3
GST-p115RhoGAP/SH3
His-PRL-1
Anti-His
Anti-GST
D
HA-PRL-1
Flag-p115 RhoGAP
Flag-p115 RhoGAP/ΔSH3
Flag-ArhGAP9
IP: Anti-HA
Anti-Flag
Anti-HA
Lysate
Anti-Flag
Anti-HA
E
GST-Peptide 1
GST
HA-PRL-1
Flag-p115 RhoGAP
IP: Anti-HA
Anti-Flag
Anti-HA
Lysate
Anti-Flag
Anti-GST
Anti-HA
F
PRL-1 (Green)
p115 RhoGAP (Red)
PRL-1 (Green)
p115 RhoGAP/ SH3(Red)
PRL-1 (Green)
p115 RhoGAP (Red)
G
IP
Lysate
IgG
Anti-PRL-1
Anti-p115 RhoGAP
Anti-PRL-1

**Figure 6. Identification of p115 RhoGAP as a PRL-1-binding protein.**

**A.** Sequence alignment between Peptide 1 and p115 RhoGAP, SrGAP1, SrGAP2, and SrGAP3. **B.** HA-tagged PRL-1 immunoprecipitates (IP) p115 RhoGAP, SrGAP1, SrGAP2, and SrGAP3 from HEK293 cells. **C.** Recombinant His6-tagged PRL-1 binds the SH3 domains of p115 RhoGAP, SrGAP1, SrGAP2, and SrGAP3 in a GST pulldown assay. **D.** The interaction between PRL-1 and p115 RhoGAP depends on the SH3 domain of p115 RhoGAP. **E.** GST-Peptide 1 disrupts the interaction between HA-PRL-1 and FLAG-p115 RhoGAP inside HEK293 cells. **F.** Subcellular co-localization of PRL-1 and p115 RhoGAP in mouse embryonic fibroblast cells. Cells were processed for imaging within 24 hours after transfection with GFP-PRL-1, Flag-p115 RhoGAP, Flag-p115 RhoGAPΔSH3, or GST-Peptide **1**. p115 RhoGAP or p115 RhoGAPΔSH3 was detected by indirect immunostaining for the flag epitope (Red), Nuclei were stained with Hoechst no. 33258 dye (Blue) while GFP-PRL-1 (Green) was directly visualized. The images from merging the three confocal fluorescence channels are depicted where co-localization between red and green is seen as yellow. **G.** Endogenous PRL-1 immunoprecipitates endogenous p115 RhoGAP in H1299 cells. The Western blot shown is representative of triplicate experiments with similar results. Panel B and C were generated by Yong Luo.

observations (15), PRL-1 was associated with plasma membrane as well as intracellular punctate structures dispersed throughout the cytoplasm. Similar to earlier finding that p115 RhoGAP localizes to the leading edges of cells via the FCH domain (93), we observed that p115 RhoGAP resides primarily at the cell periphery and this pattern of localization is independent of the SH3 domain. In agreement with our findings that p115 RhoGAP biochemically associates with PRL-1, these two proteins highly co-localized at the plasma membrane and at the leading edges of cells. However, a mutant of p115 RhoGAP lacking the SH3 domain showed no co-localization with PRL-1. In addition, co-transfection of GST-Peptide **1** abrogated the co-localization of p115 RhoGAP and PRL-1. Taken together, these results support the conclusion that p115 RhoGAP is a specific PRL-1 binding protein and that a motif within the SH3 domain of p115 RhoGAP is required for binding PRL-1. We further suggest that Peptide **1** and a region

within the SH3 domain of p115 RhoGAP bind a common site in PRL-1. Finally, we determined whether PRL-1 can bind p115 RhoGAP under endogenous conditions. PRL-1 is overexpressed in many lung cancer cell lines, including H1299 cells (95). Knockdown of PRL-1 in H1299 cells significantly decreases cell proliferation and migration (88). To demonstrate direct association of PRL-1 and p115 RhoGAP in H1299 cells, we used anti-PRL-1 antibodies to immunoprecipitate endogenous PRL-1. As shown in Figure 6G, we detected p115 RhoGAP in the PRL-1 immunoprecipitates, indicating endogenous association between PRL-1 and p115 RhoGAP.

### 2.4.3 Structural basis of PRL-1 interaction with Peptide 1/SH3 domain of p115 RhoGAP

To elucidate the molecular basis by which PRL-1 recognizes Peptide **1** and most likely the SH3 domain of p115 RhoGAP, we solved the crystal structure of PRL-1 in complex with Peptide **1** at 2.8 Å resolution. Data collection and structural refinement statistics are summarized in Table 2 (Generated by Sijiu Liu). The final atomic model encompasses residues 9-160 of PRL-1 in a complex with residues 4-12 of Peptide **1**, as revealed by the unbiased $F_o$-$F_c$ omit density map (Figure 7A, generated by Sijiu Liu). Peptide **1** binds PRL-1 in an extended $\beta$-strand conformation that lies 18 Å away from the PRL-1 active site (defined by the P-loop ($H^{103}CVAGLGR^{110}$)) and 20 Å from the C-terminus of PRL-1 (Figure 7B, generated by Sijiu Liu). Complex formation between PRL-1 and Peptide **1** buries a contiguous surface area of 1,140 $Å^2$ in PRL-1.

The structure of the PRL-1•Peptide **1** complex defines a novel protein-protein interaction site in PRL-1 through an unexpected mode of interaction with the SH3 domain of p115 RhoGAP. The first three residues in Peptide **1** are invisible in the structure, and Ser4 is exposed to solvent. Thus interactions between PRL-1 and these

**Table 2. Data collection and refinement statistics for PRL-1•Peptide 1 complex**

| | |
|---|---|
| Space group | $I\,2_13$ |
| Cell dimensions | a=146.5, b=146.5, c=146.5 Å |
| Data collection | |
| Resolution range (Å) | 50.0 – 2.5 |
| No. of unique reflections | 18,287 |
| Completeness (%) | 99.9 (99.8)[a] |
| Redundancy | 24.9 |
| $R_{merge}$[b] | 0.150 (0.872)[a] |
| Refinement | |
| Resolution range (Å) | 50.0 – 2.8 |
| No. of reflections used ($F \geq 1.5\delta(F)$) | 12,045 |
| No. of protein atoms | 2,280 |
| No. of peptides | 2 |
| No. of waters | 38 |
| $R_{work}$[c]/$R_{free}$[d] | 18.0/20.1 |
| r.m.s.d.[e] from ideal geometry | |
| Bond length (Å) | 0.008 |
| Bond angle | 1.33° |
| Average *B*-factors (Å$^2$) | |
| Overall | 65.80 |
| Protein | 65.45 |
| Peptide **1** | 72.16 |
| Waters | 61.56 |

[a]The values in parentheses correspond to the highest resolution shell (2.54 – 2.50 Å)

[b]$R_{merge} = \Sigma_h\Sigma_i|I(h)_i - \langle I(h)\rangle|/\Sigma_h\Sigma_i I(h)_i$.

[c]$R_{work} = \Sigma_h|F(h)_{calcd} - F(h)_{obsd}|/\Sigma F(h)_{obsd}$, where $F(h)_{calcd}$ and $F(h)_{obsd}$ were the refined calculated and observed structure factors, respectively.

[d]$R_{free}$ was calculated for a randomly selected 3.3% of the reflections that were omitted from refinement.

[e]r.m.s.d., root mean square deviation.

residues, if present, are likely to be weak. Detailed interactions between PRL-1 and the rest of Peptide **1** are shown in Figure 7C (Generated by Sijiu Liu). Leu5 in Peptide **1** is engaged in hydrophobic interactions with residues Asp54 and Thr56 in PRL-1. Ile6 is within Van der Waals contacts with residue Asp54 and forms two weak polar interactions with the side-chains of Asp54 and Thr55. Hydrophobic interactions are observed between

Pro7 of Peptide **1** and the side-chain of Thr55 and the phenyl ring of Try53 in PRL-1. Pro8 is also within Van der Waals contacts with Thr55. Both Lys9 and Tyr10 contact PRL-1 residue His64. In addition, hydrophobic interactions exist between Tyr10 and the side-chains of Asp67 and Trp68, and Ile11 may interact with residues Leu66 and Trp68. Finally, Thr12 may form weak interactions with PRL-1 residues Trp68 and Gln79.

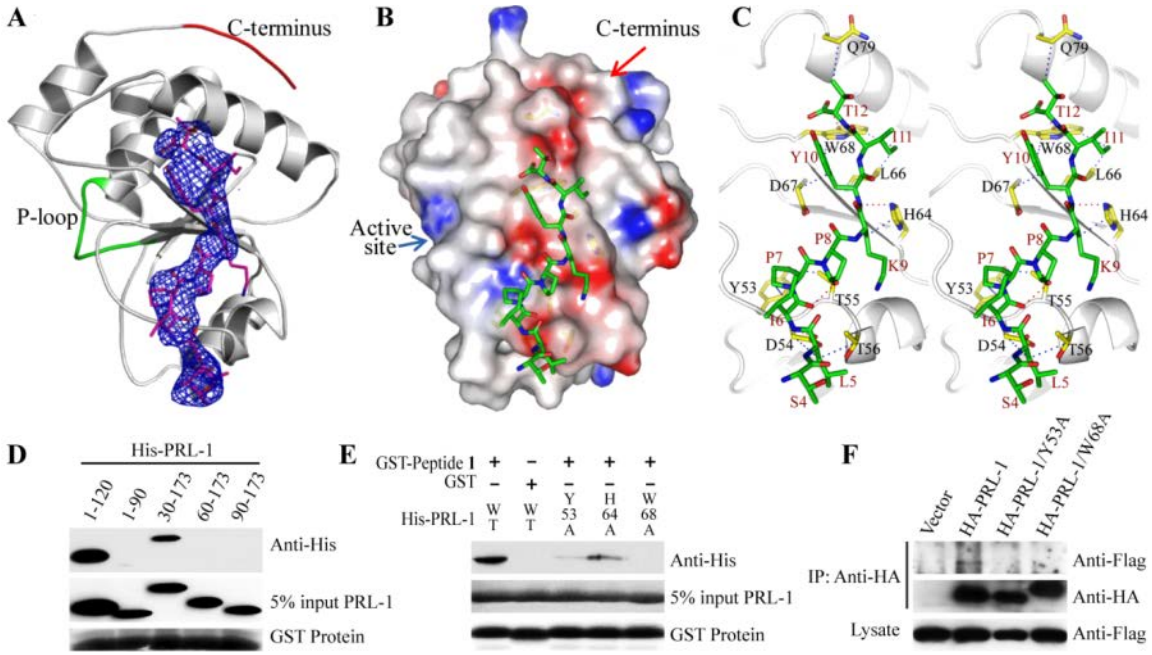


**Figure 7. Structural basis of PRL-1 interaction with Peptide 1.**

**A.** Overall structure of PRL-1 in complex with Peptide **1**. The peptide is shown in stick model with the unbiased omit *Fo-Fc* density map contoured at 3.0σ. The P-loop and C terminus are shown in green and red, respectively. **B.** Surface representation of PRL-1 in complex with Peptide **1**, colored by electrostatic potential calculated by DelPhi. **C.** Stereo diagram of the interactions between residues in PRL-1 (yellow) and Peptide **1** (green). **D.** Identification of the region in PRL-1 responsible for binding p115 RhoGAP by GST pulldown assay. **E.** Substitution of PRL-1 Tyr-53, His-64, and Trp-68 impairs its ability to bind GST-Peptide **1**. **F.** Substitution of PRL-1 Tyr-53 and Trp-68 abrogates its ability to bind p115 RhoGAP in HEK293 cells. Western blots are representative of triplicate experiments with similar results. Panel A, B and C were generated with PyMol (DeLano Scientific; http:/www.pymol.org) by Sijiu Liu.

The residues within PRL-1 that are predicted to contact Peptide **1** from our structural data were probed for their requirement for interaction with both Peptide **1** and p115 RhoGAP. Serial truncations from either the N- or C-terminus of PRL-1 (full length 1-173) indicated that residues 1-120 and 30-173 can still bind GST-Peptide **1**, whereas fragments containing 1-90, 60-173, and 90-173 displayed no detectable binding (Figure 7D). The results suggest that Peptide **1** likely binds within residues 30-120 in PRL-1. Additionally, the binding affinity of PRL-1 for Peptide **1** was significantly diminished when His64 was replaced by an Ala, and completely abolished when Tyr53 or Trp68 were changed to an Ala (Figure 7E). Importantly, the latter two mutants also lacked the ability to immunoprecipitate p115 RhoGAP in HEK293 cells (Figure 7F). These results are in complete agreement with the structural observations that residues from Tyr53 to Gln79 in PRL-1 are involved in binding Peptide **1**. Importantly, residues within Peptide **1** binding site are most likely also required for binding the analogous region within the SH3 domain of p115 RhoGAP.

Taken together, these results reveal a novel mode of interaction between an SH3 domain and its binding partner where PRL-1 serves as the receptor for recognizing a sequence motif (corresponding to Peptide **1** residues Leu5-Thr12) within the SH3 domain of p115 RhoGAP. As shown in the crystal structure of SrGAP1 SH3 domain (128), Pro793 and Tyr796 (Pro7 and Tyr10 in Peptide **1**) form ligand binding pocket 2 and Leu791 (Leu5 in Peptide **1**) lines ligand binding pocket 3. Since there is no PxxP sequence in PRL-1 and residues involved in binding Peptide **1** are non-contiguous (Figure 7C), the recognition of Peptide **1**/p115 RhoGAP SH3 domain by PRL-1 represents a novel protein-protein interaction, which differs from the canonical SH3 domain/PxxP binding mode.

### 2.4.4 p115 RhoGAP negatively regulates PRL-1 mediated cell migration and ERK1/2 and RhoA activation

It is well documented that PRL-1 promotes cell migration through activation of ERK1/2 and RhoA pathways (16,17,88,113). It is also reported that p115 RhoGAP inhibits cell motility through its GAP domain and the C-terminal SH3 domain (93). To understand the functional significance of the novel PRL-1/p115 RhoGAP interaction, we evaluated the effect of modulating expression of p115 RhoGAP on PRL-1 mediated cell migration as well as on ERK1/2 and RhoA activity. We found that overexpression of p115 RhoGAP in cells stably transfected with PRL-1 diminished PRL-1 induced cell migration (Figure 8A), whereas p115 RhoGAP knock-down by siRNA enhanced PRL-1 induced cell migration (Figure 8B). Moreover, overexpression of p115 RhoGAP also reduced PRL-1 mediated ERK1/2 and RhoA activation (Figure 8C). The negative effect of p115 RhoGAP on RhoA signaling was further confirmed by a 40% decrease in the transcriptional activity of the RhoA specific reporter SRE.L (Figure 8D, generated by Yong Luo). We conclude that p115 RhoGAP plays a negative role in PRL-1 mediated cell migration by down-regulating both ERK1/2 and RhoA activity.

### 2.4.5 Mechanism of PRL-1 mediated ERK1/2 and RhoA activation

p115 RhoGAP has been previously found to associate with and inhibit MAP/ERK kinase kinase 1 (MEKK1) through its SH3 domain (94). MEKK1 is the essential upstream kinase that phosphorylates and activates ERK1/2 and is required for cell motility. Because the region in the SH3 domain of p115 RhoGAP that corresponds to residues Leu5-Thr12 in Peptide **1** makes up the center of the PxxP ligand binding site, PRL-1 binding to this site was predicted to block canonical interactions by this domain. We further speculated that one consequence of such displacement of MEKK1 from p115

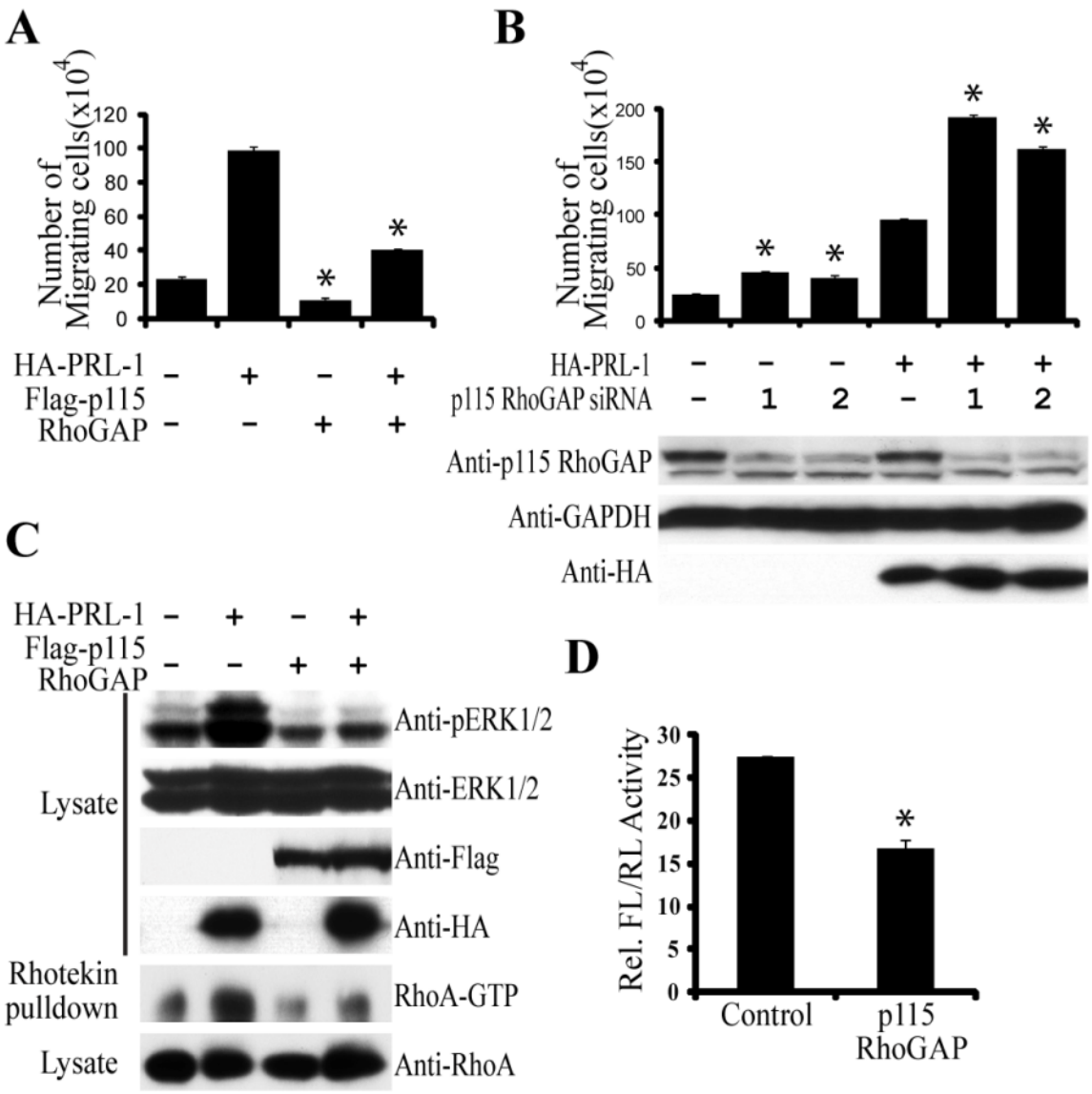


**Figure 8. p115 RhoGAP negatively regulates cell migration and ERK and RhoA activation.**

**A.** Overexpression of p115 RhoGAP inhibits cell migration in both control HEK293 cells and PRL-1-expressing HEK293 cells. **B.** Knockdown of p115 RhoGAP enhances cell migration in both control HEK293 cells and PRL-1-expressing HEK293 cells. **C.** Overexpression of p115 RhoGAP reduces ERK1/2 and RhoA activation in both control HEK293 cells and PRL-1-expressing HEK293 cells. **D.** p115 RhoGAP decreases RhoA-specific reporter activity. Results shown are representative of triplicate experiments with similar results. Results are presented as means ± S.D. *, $P<0.01$. Rel. FL/RL, relative fluorescence/Renilla luciferase. Panel D was generated by Yong Luo.

RhoGAP by PRL-1 would be the activation of ERK1/2. To test this hypothesis, control and cells expressing PRL-1 were transfected with Flag-tagged p115 RhoGAP and the amount of p115 RhoGAP associated with MEKK1 as well as the phosphorylation status of ERK1/2 were measured. Compared to control cells, the fraction of p115 RhoGAP associated with MEKK1 was reduced and the ratio of phosphorylated ERK1/2 was increased in PRL-1 cells (Figure 9A). This effect is likely specific, as expression of GST-peptide **1** restored the level of p115 RhoGAP associated with MEKK1 and concordantly reduced ERK1/2 phosphorylation (Figure 9A). Thus, PRL-1 interaction with p115 RhoGAP likely mitigates the inhibitory effect of p115 RhoGAP on MEKK1, resulting in ERK1/2 activation.

Given that p115 RhoGAP inhibits RhoA by accelerating its catalysis of GTP hydrolysis to GDP (94,125), we investigated whether PRL-1 binding to p115 RhoGAP could modulate its ability to regulate RhoA activity. To this end, immunoprecipitated Flag-tagged p115 RhoGAP or p115 RhoGAP/ΔSH3 from either control or PRL-1 cells was incubated with purified GST-RhoA loaded with a-$^{32}$P-labeled GTP. The data revealed that p115 RhoGAP from PRL-1 cells showed significantly lower GAP activity than that from the control cells (Figure 9B, generated by Yong Luo). This inhibitory effect of PRL-1 on p115 RhoGAP activity likely occurs via interaction with the SH3 domain as p115 RhoGAP/ΔSH3 exhibited equal GAP activity in PRL-1 expressing or control cells (Figure 9B). To further define the mechanism by which PRL-1 inhibits the GAP activity of p115 RhoGAP, we measured the effect of PRL-1 on the binding of p115 RhoGAP to RhoA/G14V, a constitutively active form of RhoA that stably associates with the GAPs due to resisting GTP hydrolysis. Control and PRL-1 expressing cells were transfected with Myc-RhoA/G14V and Flag-tagged p115 RhoGAP or p115

RhoGAP/ΔSH3. The amount of RhoA/G14V associated with p115 RhoGAP or p115 RhoGAP/ΔSH3 was visualized by Western blot. The observation that both the full length and the SH3 domain deleted p115 RhoGAP bound RhoA/G14V indicates that recognition of RhoA by p115RhoGAP does not require its SH3 domain. In stark contrast, the ability of PRL-1 to block the interaction between RhoA/G14V and p115 RhoGAP strongly depended on the presence of the SH3 domain (Figure 9C). Apparently, association of PRL-1 with the SH3 domain of p115 RhoGAP prevents p115 RhoGAP from binding RhoA, which results in increased levels of GTP bound RhoA. Finally, PRL-1 mutants (PRL-1/Y53A and PRL-1/W68A), which are defective in binding p115 RhoGAP, were unable to activate ERK1/2 or RhoA (Figure 9D). This indicates that physical interaction between PRL-1 and p115RhoGAP is a prerequisite for PRL-1 mediated ERK1/2 and RhoA activation.

**2.5 Discussion**

PRLs are implicated in tumorigenesis and metastasis, but the underlying mechanism is still elusive. Even if increasing amount of effort has been put into the establishment of PRLs-mediated signaling pathways, little study is focused on the discovery of natural substrates or binding partners of PRLs. To date, only a limited number of proteins have been suggested as substrates or interaction proteins: Ezrin (129), Keratin 8 (130), Integrin β1 (131), and Stathmin (132). Unfortunately, those molecules have so far not been placed into direct context with the pathways affected by PRLs. Thus, the identification of substrate(s) and binding partners of PRLs is the first step to have a better understanding on the mechanisms of PRLs action.

To this end, we utilized phage display method and tried to identify potential PRL-1 binding partners. Phage display is a technique designed to study protein-peptide interactions, in which bacteriophage particles are bioengineered to express a peptide

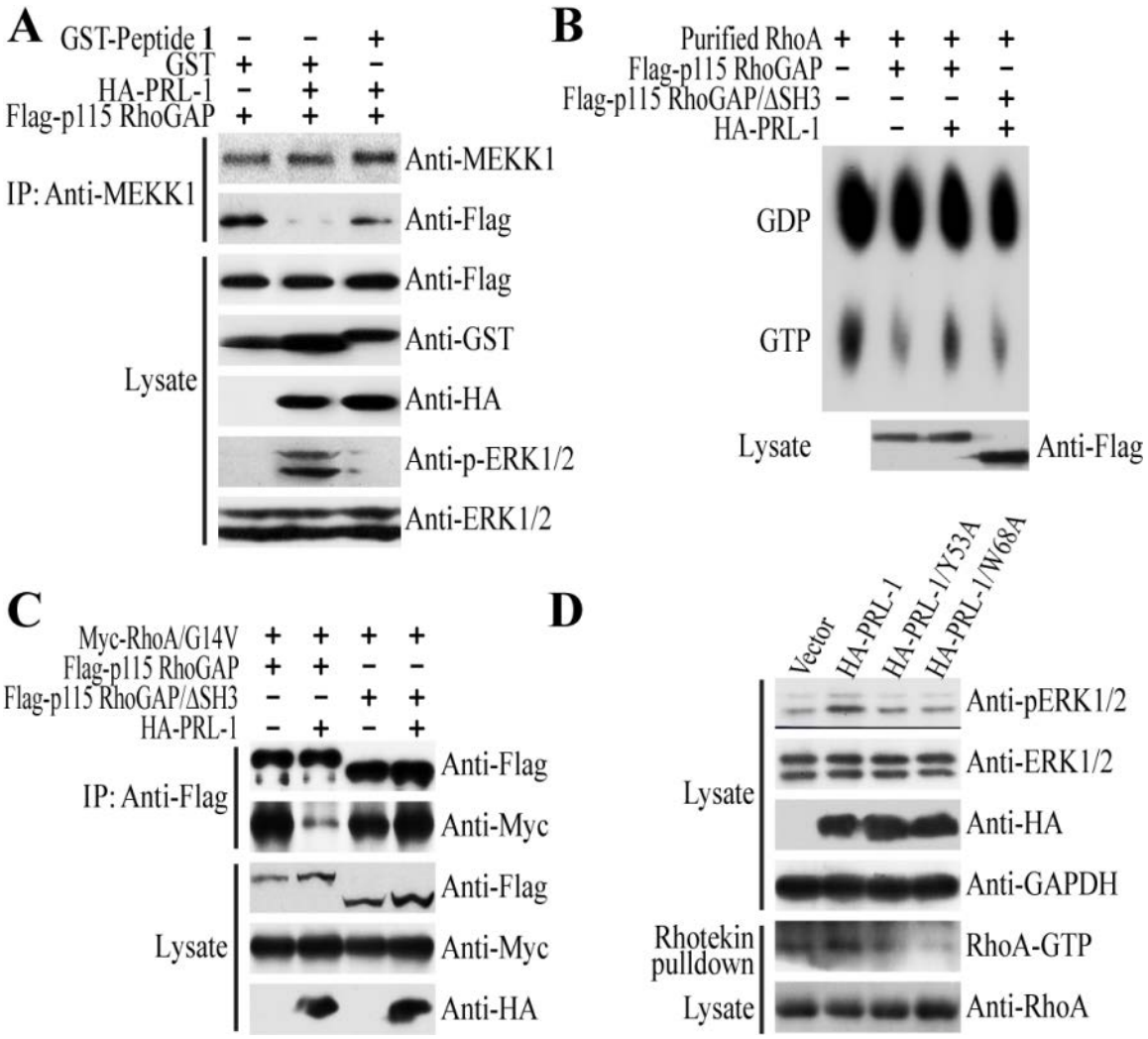


**Figure 9. Molecular mechanisms of PRL-1-mediated ERK1/2 and RhoA activation.**

**A.** PRL-1 activates ERK1/2 by displacing MEKK1 from p115 RhoGAP. **B.** PRL-1 inhibits the GAP activity of p115 RhoGAP through its interaction with the SH3 domain of p115 RhoGAP. **C.** PRL-1 directly blocks the interaction between p115 RhoGAP and RhoA (G14V) in an SH3 domain-dependent manner. **D.** PRL-1-mediated ERK1/2 and RhoA activation requires physical interaction between PRL-1 and p115 RhoGAP. Results shown are representative of triplicate experiments with similar results. Panel B was generated by Yong Luo.

library of interest fused to coat protein. In this dissertation, I used PH.D.-12 phage display peptide library kit from New England Biolabs. This phage display kit contains combinatorial library of random 12-mer peptides fused to a minor coat protein (PIII) of M13 phage. The titer of the library is $1.5\times10^{13}$ pfu. The library contains a complexity of $2.7\times10^{9}$ sequences. After four rounds of screening, several 12-mer peptides have been identified as PRL-1 binding peptides. By performing a BLAST search, Peptide **1** (GWWSLIPPKYIT) matched a sequence motif in the SH3 domain of p115 RhoGAP.

p115 RhoGAP is a member of the Slit-Robo (Sr) GAP family (SrGAP1, 2, 3 and p115 RhoGAP) that are implicated in axon guidance and cell migration through inactivation of Rho GTPases (93,126). The Rho family small GTPases act as molecular switches involved in fundamental cellular process. Three widely expressed members, RhoA, Rac1 and Cdc42 are the best characterized family members. This family of proteins has intrinsic GTPase activity and cycle between an active GTP-bound form and an inactive GDP-bound form. Guanine nucleotide exchange factors (GEFs) and GTPase activating proteins (GAPs) are two major classes of regulators that modulate the activation of GTPases. GEFs activate Rho GTPases by accelerating the release of guanosine diphosphate (GDP) to allow binding of new guanosine triphosphate (GTP). GAPs enhanced the intrinsic GTPase activity of Rho, leading to their inactivation (133,134). Given the role of PRL-1 in activating RhoA, we tested the hypothesis that PRL-1 binds to and inhibits p115 RhoGAP to turn on RhoA activation. This notion is supported by the data that PRL-1disrupted the interaction between p115 RhoGAP and RhoA/G14V, a constitutively activated RhoA.

p115 RhoGAP has been implicated in MAP kinase pathway by the discovery of its interacting protein MEKK1 (94). MEKK1 is a MAP kinase kinase kinase linked to

ERK1/2 and JNK MAP kinase cascades (135,136). *Mekk1*-null cells are defective in cell migration, suggesting that MEKK1 is required for cell motility. The interaction between p115 RhoGAP and MEKK1 may prevent the association between MEKK1 with other components in MAP kinase pathways, leading to ERK1/2 inactivation (94). Given the positive role of PRL-1 in activating MAP kinase pathway and that PRL-1 shares the same binding site on p115 RhoGAP with MEKK1, we might expect that PRL-1 association with p115 RhoGAP might block the interaction between p115 RhoGAP and MEKK1 and release MEKK1 from the inhibitory effect of p115 RhoGAP. Our data support this possibility, because PRL-1 overexpression reduced the interaction between p115 RhoGAP and MEKK1 by co-IP experiment.

In summary, starting from an unbiased screen for PRL-1 effectors, we have identified p115 RhoGAP as a *bona fide* PRL-1 binding protein. Biochemical and cellular studies suggest that the SH3 domain of p115RhoGAP is required for its interaction with PRL-1. Structural analyses reveal that this interaction occurs via a novel protein-protein interaction whereby PRL-1 recognizes a conserved sequence motif in the canonical PxxP ligand binding site of the SH3 domain in p115 RhoGAP. The interaction between PRL-1 and p115 RhoGAP coordinately activates the ERK1/2 pathway by displacing MEKK1 from p115 RhoGAP and it activates RhoA by preventing its interaction with p115 RhoGAP. Our study not only offers a mechanistic explanation for ERK1/2 and RhoA activation by PRL-1, but also identifies a novel p115 RhoGAP binding site in PRL-1 for the development of anticancer therapeutics by blocking the interaction between PRL-1 and p115 RhoGAP.

# CHAPTER 3: TARGETING PRL-1 TRIMER INTERFACE FOR NOVEL ANTICANCER AGENT

## 3.1 Overview

The PRL phosphatases belong to a novel PTP subfamily that has three members (PRL-1, 2 and 3), sharing a high degree (>75%) of amino acid sequence identity (11-13). PRL-1 expression was found to be elevated in many tumor cell lines, and cells expressing high levels of PRL-1 exhibited enhanced proliferation and anchorage-independent growth (11,12,95,96). PRL-2 level is also elevated in different cancers, such as prostate cancer (69). Overexpression of PRL-3 in HEK293 cells also leads to higher growth rates (25). In addition, expression of PRL-3 was found to be highly increased in colon cancer liver metastasis but not in non-metastatic tumors or in normal colorectal epithelium (29). PRL-1 and PRL-3 display activity to enhance cell motility and invasiveness and induce metastatic tumor formation in mice (13,86). All these observations suggest that PRLs play a critical role in cancer development and metastatic progression, and that PRLs are potential targets for anti-cancer therapeutic development. However, no clinically useful and specific inhibitors of PRLs have been reported, despite extensive efforts having been taken to identify them (103,104).

## 3.2 Hypothesis and Specific Aims

Since all PRLs are implicated in tumor progression and metastasis, there is considerable interest in identifying small molecule inhibitors targeting PRLs for novel anti-cancer agents. Although it is difficult to make isozyme-specific PRL inhibitors due to the high sequence similarity among the three PRLs and the unusual wide and shallow catalytic pockets of PRLs revealed by structure studies (21-23,137), there still are several small molecules reported to inhibit PRL activity (103-108). However, further

investigations are required to validate the specificity and efficacy of these compounds in inhibiting tumorigenesis and metastasis. On the other hand, since the structures of PRL-1 solved by us and others revealed an identical trimeric arrangement (22,23,137), interference with PRL trimerization would be an alternative to inhibition of the phosphatase activity. Trimerization provides a membrane-binding surface with polybasic residues and the adjacent prenylation group to anchor PRL-1 on the acidic inner membrane. Given the high homology among the three PRLs, trimerization revealed in PRL-1 may be a general property for all PRL enzymes (17). In addition, PRL-1 trimer formation appeared to be essential for the PRL-1-mediated cell growth and migration (17). Most importantly, PRLs are highly expressed in many human cancer types, but no evidence for point mutations in PRLs have been found, suggesting that overexpression-induced PRL trimerization may be important for malignancies. Thus, I hypothesized that **targeting the trimer interface of PRLs is a novel approach to develop small molecule inhibitors for cancer treatment.** To test this hypothesis, I developed two specific aims: 1) to identify small molecule inhibitors targeting PRL-1 trimer interface and blocking PRL-1 trimer formation; and 2) to test the anti-cancer activity of PRL-1 de-trimer inhibitors in cell based assays. These goals are designed to establish a novel strategy to develop PRLs inhibitors by targeting PRLs trimer interface and to demonstrate the potential value of PRLs trimer disruptor for anti-cancer therapy.

### 3.3 Materials and Methods

#### 3.3.1 Virtual screening

Asinex and ChemBridge subsets in ZINC (138) database were used as small molecule library for virtual screening, the coordinates were downloaded from ZINC website (http://zinc.docking.org) in mol2 file format. The monomer B of PRL-1 trimer

structure (23) (PDBID: 1ZCK) was used as receptor, and the coordinates were retrieved from the Protein Data Bank. DOCK6.2 program (139,140) was firstly used for rigid docking to result in a potential subset of PRL-1 trimer interface binding molecules, and then AutoDock4.01 software (141,142) was used for flexible docking to perform more accurate binding energy evaluation and get the most potent hit molecules.

In the first stage docking, the structure of monomer B was processed using the "Dock Prep" module in UCSF CHIMERA (143), then the docking region was defined through a standard pipeline of running *dms*, *sphgen*, *sphere_selector* and *showbox* program, and the energy scoring values were calculated by *grid* program. About 560000 small molecules (downloaded in 28 mol2 files, ~20000 molecules in each file) were submitted to *dock6.mpi* program to perform docking calculations simultaneously. During each docking, the small molecule was positioned by automated matching algorithm with 1000 orientations, the lowest interaction energy and related conformation was recorded. All ligands in each mol2 file were ranked according to their lowest interaction energy, and top 2000 were kept for the second stage docking, that is to say, 2000 × 28 = 56000 molecules were picked out for next screening.

In the secondary stage docking, the structure of monomer B was processed in AutoDockTools1.4 software, non-polar hydrogens were merged, Gasteiger charge and solvation parameter were added. The docking area was designated around the surface on the monomer B which constitute the BA or BC interface, and the energy grids of 51 × 51 × 63 points with 0.375 Å spacing on each axis were calculated for 17 atom types (H, HD, HS, C, A, N, NA, NS, OA, OS, F, P, SA, S, Cl, Br and I), as well as the electrostatic and desolvation potential using *autogrid4* program; On the other hand, each ligand structure was used to generate pdbqt and dpf files using *prepare_ligand4.py* and *prepare_dpf4.py*

scripts. Based on these prepared files, molecular docking was carried out in *autodock4* program as follows: 10 separate docking runs were performed for each ligand. In each docking run, the optimal binding conformation was achieved by Lamarckian Genetic Algorithm with Local Search (LGALS) method. After all ligands were docked, the lowest binding free energy of each ligand was extracted and ranked, and hit molecules were picked out through binding free energy comparisons, structure similarity analyses and binding mode inspections.

### 3.3.2 Cell culture and transfection

HEK293 cells, H1299 cells and MDA-MB-231 cells were grown in DMEM supplemented with 10% fetal bovine serum, penicillin (50 units/mL), and streptomycin (50 μg/mL) in a 37°C incubator containing 5% $CO_2$. HEK293 cells were seeded at 40% confluence in antibiotic-free medium and grown overnight. Transfection was performed using Lipofectamine 2000 from invitrogen according to the manufacturer's recommendations.

### 3.3.3 Immunoblotting and immunoprecipitation

HEK293 cells were grown to 70% confluency, washed with ice-cold phosphate-buffered saline, and lysed on ice for 30 min in lysis buffer supplemented with a complete protease inhibitor tablet (Roche). Cell lysates were cleared by centrifugation at 15000 rpm for 10 min. For immunoprecipitation, 3 μg of each antibody was added to 1 mg of cell lysate and incubated at 4 °C for 4 hrs with protein A/G-agarose beads. After being extensively washed, the protein complex was boiled with sample buffer, separated by SDS-PAGE, transferred electrophoretically to a nitrocellulose membrane, and immunoblotted with appropriate antibodies followed by incubation with horseradish

peroxidase-conjugated secondary antibodies. The blots were developed by the enhanced chemiluminescence technique (ECL kit, GE Biosciences).

### 3.3.4 *In vitro* and *in vivo* cross-linking assay

To assess the oligomeric state of PRL-1 *in vitro*, the $(His)_6$-tagged recombinant PRL-1 proteins were cross-linked with glutaraldehyde (Sigma, 25% glutaraldehyde solution, grade I). The reactions were performed in 20 μL solutions containing 5 μg of protein in phosphate-buffered saline (PBS, pH 7.5). Recombinant PRL-1 was treated with 10 μM compound for 30 min, and then cross-linked by incubating with 0.005% glutaraldehyde at room temperature for 10 min. The reaction was terminated by addition of pH 7.5 Tris-HCl (final concentration 50 mM) and 5 min incubation on ice. The samples were separated on SDS-PAGE and analyzed by Coomassie Blue staining. For *in vivo* cross-linking, HEK293 cells with 90% confluence were treated with 20 μM compound as indicated for 24 hours, and then fixed with 1% formaldehyde (Thermo, 16% formaldehyde solution) for 10 min at room temperature. Cells were washed twice in ice-cold PBS and lysed on ice for 30 min following by immunoprecipitation with HA antibody. The reaction mixtures were analyzed by SDS-PAGE and detected by immunoblotting with anti-HA antibody (Santa Cruz).

### 3.3.5 Wound healing assay

Cells were grown to 90% confluence in a 12-well plate at 37 °C in an atmosphere of 5% $CO_2$. A wound was created by scratching cells with a sterile 200 μL pipette tip. Cells were washed with PBS to remove the floating cells, and then treated with fresh medium containing 20 μM compound or DMSO. The wounds were photographed at 0 hour and 24 hours under ×10 magnitude microscope. Wound healing magnitude was

quantified by measuring the relative wound closure compared with control cells at 24 hours.

### 3.3.6 MTT assay

Cells were seeded in a 96-multiwell plate (1000 cells/well) containing DMEM, 10% fetal bovine serum at 37 °C in an atmosphere of 5% $CO_2$ overnight. Cells were then treated with various concentrations of compounds or DMSO for 24 and 48 hours. Cell proliferation was then determined by MTT assay as described previously (17) using a multiwall spectrophotometer (Victor 2, PerkinElmer Life Sciences). Data are presented as relative proliferation rate compared with control cells.

### 3.3.7 Cell migration assay

Cell migration was assessed as described previously (137) with some modifications. The assay was performed with Transwells (6.5 mM diameter; 8 μM pore size polycarbonate membrane) obtained from Corning (Costar, Acton, MA). Cells ($3.75 \times 10^5$) in 1.5 mL of serum-free medium were placed in the upper chamber, whereas the lower chamber was loaded with 2.5 mL of medium containing 10% FBS. Cells were then treated with 10 μM of different compounds as indicated. After 24 hour incubation (37 °C, 5% $CO_2$), the total number of cells that had migrated into the lower chamber was counted with a hemacytometer. Data are presented as relative migration rate compared with control cells.

### 3.3.8 Expression and purification of PRL-1

PRL-1 without tag (residues 4-160) was sub-cloned into pET21a. For protein expression, PRL-1 was transformed into *Escherichia coli* BL21-(DE3). Transformed cells were grown at 37°C in Luria broth (LB) containing 100 mg/mL ampicillin for 4 hrs until the OD600 reached 0.6, and then induced for overnight at room temperature with

0.4 mM IPTG. Cells were harvested by centrifugation (6000 rpm for 15 min at 4 °C), and the cell pellets from 1.5 L of LB medium were suspended in 30 mL of ice-cold buffer A consisting of 50 mM NaCl, 20 mM MES (pH 5.8), and 1 mM EDTA. In this stage, trypsin inhibitor and PMSF were also added to buffer A to final concentration of 0.05 mg/mL and 0.1 mM, respectively. The suspensions were passed twice through a French Press at 1000 psi, and the cell lysates were centrifuged at 4 °C for 30 min at 15000 rpm. The supernatants were mixed with 0.5 g beads of CM Sephadex C50 (Sigma-Aldrich) at 4 °C for 1 h, and then the mixture was transferred to an empty column. The column was washed by 200 mL of buffer A, and then eluted with 20 mL of buffer B (500 mM NaCl, 20 mM MES (pH 5.8), 5 mM DTT). The elution was dialyzed for 6 hrs at 4 °C against 1 L buffer A, and then loaded onto a Mono S column equilibrated at 4 °C with buffer A. The column was washed with 10 mL of buffer A and then eluted with a 40 mL of linear gradient of 0 to 1 M NaCl in buffer A. The column fractions were analyzed by measuring the absorbance at 280 nm and by carrying out SDS-PAGE analysis. The fractions were combined and concentrated at 4 °C to ≤ 1 mL using an Amicon concentrator and then loaded onto a gel filtration column Superdex 75. The column was eluted with buffer A, and fractions which contain protein were combined and concentrated to 6 mg/mL and stored at −80 °C. The sample PRL-1 was shown to be homogeneous by SDS-PAGE analysis.

### 3.3.9 Crystallization and data collection

For co-crystallization of PRL-1 with Analog-3, 100 μL 6 mg/mL PRL-1 was mixed with 6 μL stock of Analog-3 (10 mM in DMSO), then crystals were grown by vapor diffusion in hanging drops at 4°C, room temperature, 30°C and 37 °C respectively. Drops containing 1:1 volumes of protein in stock buffer and reservoir solutions were

equilibrated against the reservoir solution A (1.9 M amino sulfate, 100 mM sodium acetate, pH 4.6 ~ 4.9). The crystals were observed after 2 weeks (for 37° C), or 7 weeks (for 30 °C), or half year (for room temperature); No crystals were observed under 4 °C condition in 8 months. The crystals gotten in different temperature showed the same shape (long and thin rod cluster). The crystals (grown at 37 °C) was transferred into a reservoir solution B (90% saturated lithium sulfate, 0.5 mM Analog-3, 5% DMSO), soaked for 1 second, then flash-cooled in liquid nitrogen. X-ray data were collected at 100 K at SBC-CAT beamline 19-BM at the Advanced Photon Source (Argonne, IL) equipped with a mosaic CCD detector. The crystals belong to space group $C222_1$ with the following unit cell parameters: a = 46.07 Å, b = 76.47 Å and c = 86.87 Å. There is one protein molecule in the asymmetric unit. All data were processed with HKL3000 (144).

### 3.3.10 Structural refinement of PRL-1•Analog-3

The structure of PRL-1•Analog-3 was solved by molecular replacement using the program Molrep (145). The structure of PRL-1 (PDB entry code 1ZCK) (23), without the solvent molecules and other small molecules, was used as a search model. The map revealed the density for the bound Analog-3 (Figure 15). The structure was refined to 1.90 Å resolution with the program CNS1.1 (146), first using simulated annealing at 2,500 K, and then alternating positional and individual temperature factor refinement cycles. The progress of the refinement was evaluated by the improvement in the quality of the electron density maps, and the reduced values of the conventional *R* factor ($R = \Sigma_h||F_o| - |F_c||/\Sigma_h|F_o|$), and the free *R* factor (4.2% of the reflections omitted from the refinement) (123). Electron density maps were inspected and the model was modified on an interactive graphics workstation with the program WinCoot (147). Finally, water

molecules were added gradually as the refinement progressed. They were assigned in the $F_o$ - $F_c$ difference Fourier maps with a 3σ cutoff level for inclusion in the model. Molecular graphics were prepared by using Pymol (www.pymol.sourceforge.net).

### 3.4 Results

#### 3.4.1 Identification of small molecule compounds targeting PRL-1 trimer interface

Based on the observation that PRL-1 trimerization is critical for its role in promoting tumorigenesis and metastasis (17), we tested our hypothesis that targeting PRL-1 trimer interface may be a novel approach for developing anti-cancer drug. Utilizing *in silico* virtual screening, we searched the Asinex and ChemBridge subsets in ZINC small molecule database and tried to find compounds that could disrupt PRL-1 trimer formation. As shown in Figure 10A (Generated by Zhihong Yu), the monomer B in the PRL-1 trimer structure (PDBID: 1ZCK) was selected as receptor for docking calculations, the surface on the monomer B which constitutes the BA interface (mainly including residues 122 to 142), or BC interface (mainly including residues 11 to 18, 35 to 43, and 91 to 99) was defined as two docking regions, then the successive docking calculations using DOCK6.2 and AutoDock4.01 program were carried out respectively targeting BA and BC interface. By combining the top-ranked binding molecules of BA and BC interface and performing structure similarity analyses, we identified 56 hit molecules with diverse structure that may promisingly bind at either BA or BC interface (Figure 11). To select the most efficient compound(s), we used multiple protein and cell-based assays, which are summarized in Figure 10B and shown in more details in Figure 12.

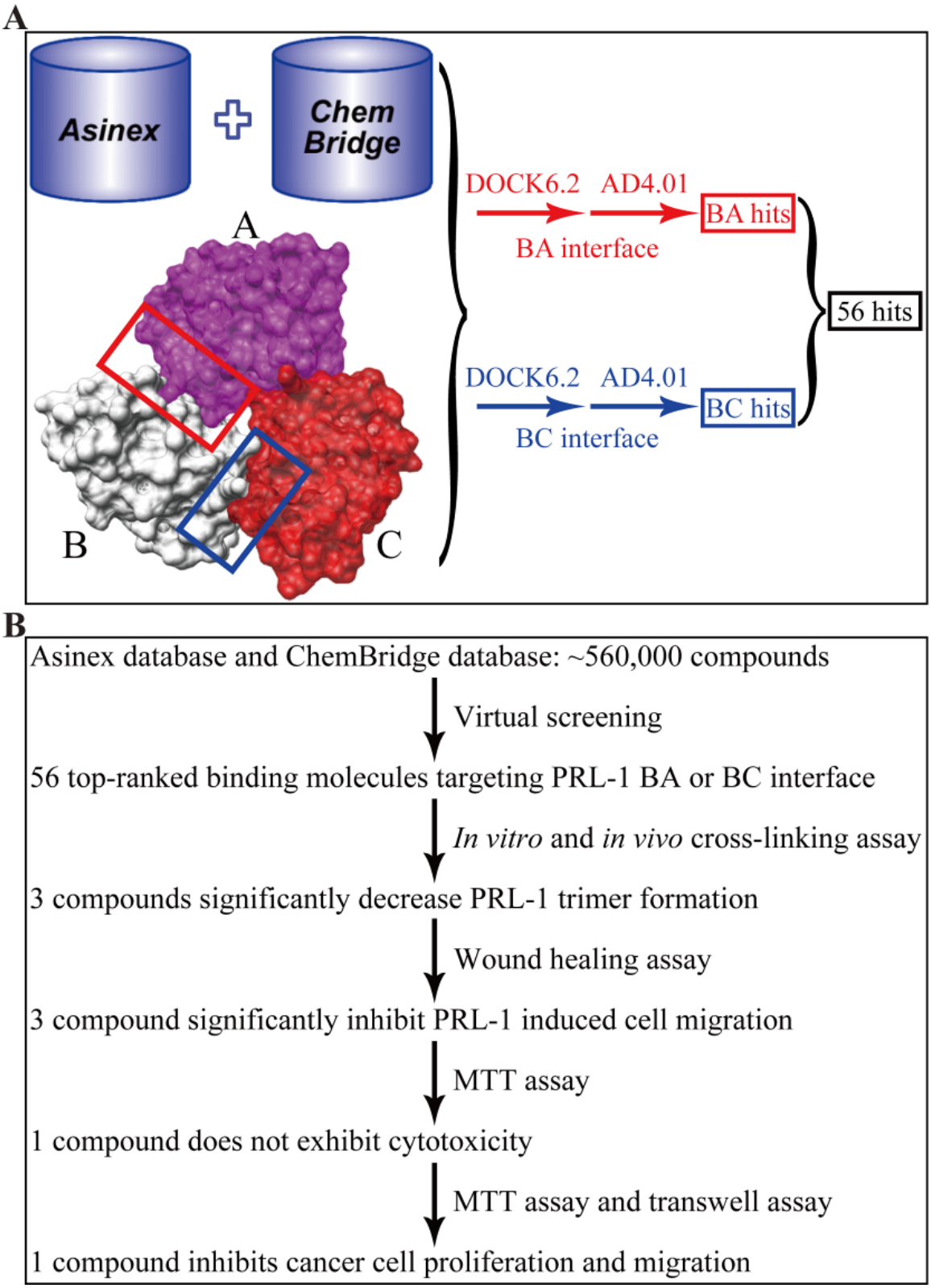


**Figure 10. Identification of small molecule compounds targeting PRL-1 trimer interface.**

**A.** The schematic diagram of the computer-based screening process. BA_interface is the interface between monomer B and monomer A of PRL-1. BC_interface is the interface between monomer B and monomer C of PRL-1. DOCK6.2 and AD4.01 are software used for virtual screening. Asinex and ChemBridge are chemical databases we used in the experiment. The figure is created using PyMol (DeLano Scientific; http:/www.pymol.org). **B.** Screening steps and tests we performed to select PRL-1 trimer disruptors. Panel A was generated by Zhihong Yu.

Specifically, to confirm the efficiency of those compounds to disrupt PRL-1 trimer formation, we employed the *in vitro* cross-linking assay. We screened all 56 hits by incubating recombinant PRL-1 protein with 10 μM each compound for 30 min following incubation with 0.005% cross-linker glutaraldehyde for another 10 min. A representative gel and its quantification by trimer/monomer relative ratio are shown in Figure 12A. Compound 3 (Cmpd-3), Compound 26 (Cmpd-26) and Compound 43 (Cmpd-43) could decrease PRL-1 trimer formation by 23%, 18% and 38% respectively. To further validate the efficiency of these three compounds to disrupt PRL-1 trimerization in cells, we performed *in vivo* cross-linking assay (Figure 12B). Consistent with *in vitro* assays, 20 μM Cmpd-3, -26 and -43 could disrupt PRL-1 trimer formation by 40%, 60% and 80% respectively in HEK293 cells. The structures of these three compounds were shown in Figure 12C. Collectively, these results indicate that Cmpd-3, -26 and especially -43 are effective PRL-1 trimer disruptors.

### 3.4.2 PRL-1 trimer disruptors inhibit PRL-1-induced cell proliferation and migration

It has been shown that PRL-1 overexpression induces cell proliferation and migration. We have provided evidence that PRL-1 trimer formation is essential for its function in promoting cell proliferation and migration (17). To test whether PRL-1

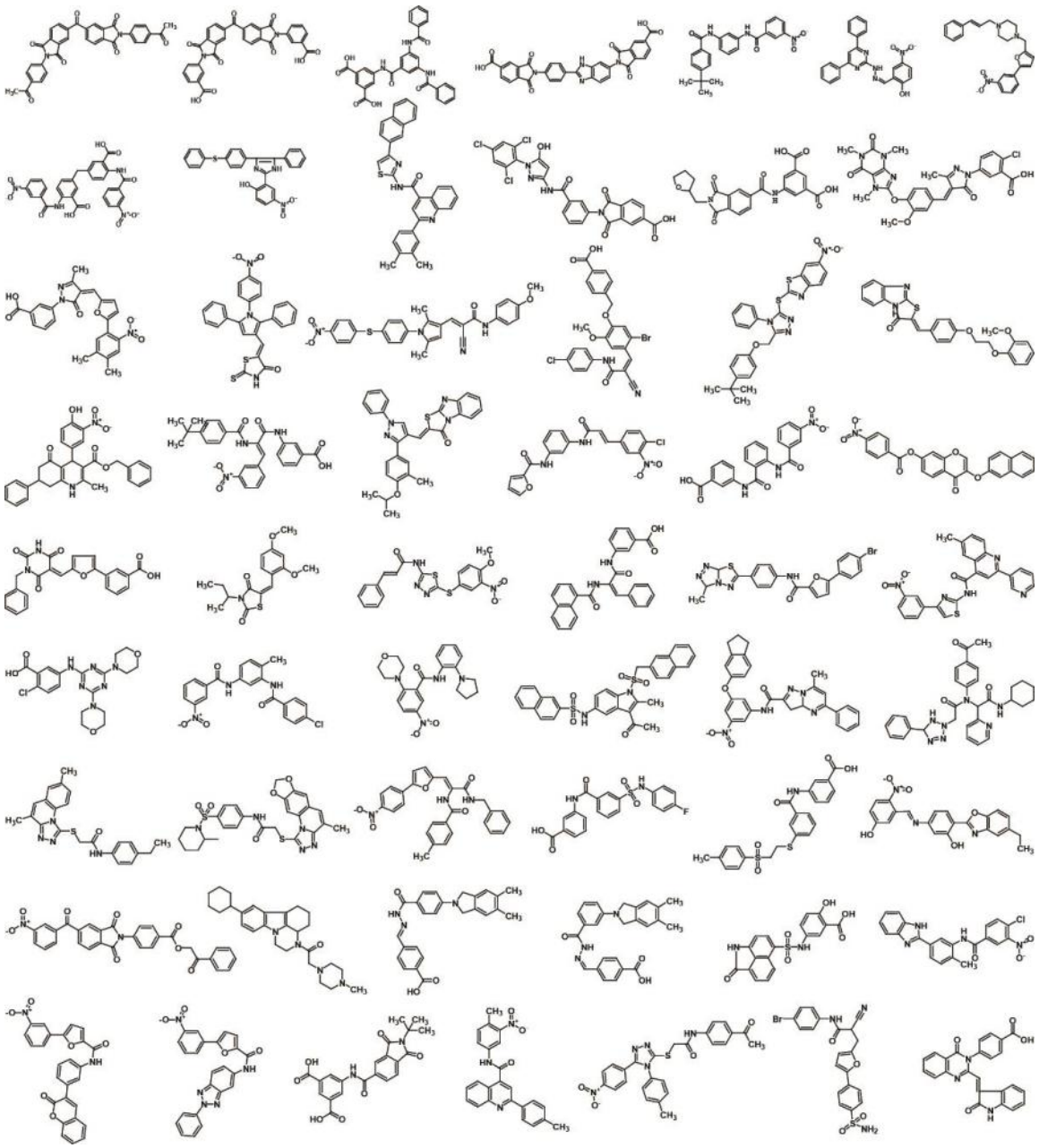

**Figure 11. 56 hits targeting PRL-1 trimer interface were identified by virtual screening.**

Asinex and ChemBridge subsets in ZINC (138) database were used as small molecule library for virtual screening as described in Materials and Methods. About 560,000 small molecules were analysed by docking calculations simultaneously. 56 hit molecules with diverse structure were identified as potential PRL-1 trimer disruptors. The chemical structures of these 56 hits were shown.

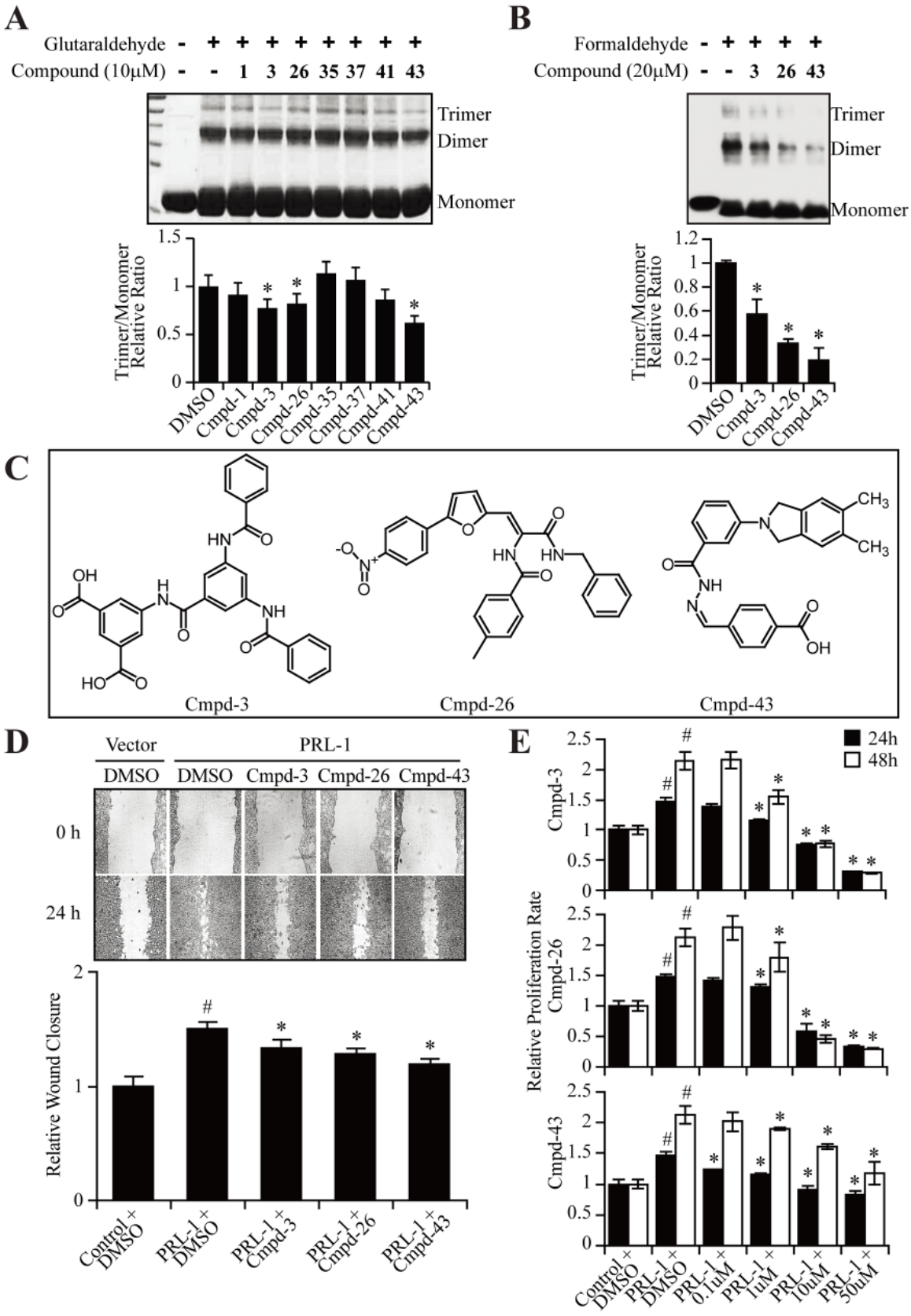
A
Glutaraldehyde - + + + + + + + +
Compound (10μM) - - 1 3 26 35 37 41 43
Trimer
Dimer
Monomer
Trimer/Monomer Relative Ratio
DMSO
Cmpd-1
Cmpd-3
Cmpd-26
Cmpd-35
Cmpd-37
Cmpd-41
Cmpd-43
B
Formaldehyde - + + + +
Compound (20μM) - - 3 26 43
Trimer
Dimer
Monomer
Trimer/Monomer Relative Ratio
DMSO
Cmpd-3
Cmpd-26
Cmpd-43
C
Cmpd-3
Cmpd-26
Cmpd-43
D
Vector
PRL-1
DMSO
DMSO
Cmpd-3
Cmpd-26
Cmpd-43
0 h
24 h
Relative Wound Closure
Control + DMSO
PRL-1 + DMSO
PRL-1 + Cmpd-3
PRL-1 + Cmpd-26
PRL-1 + Cmpd-43
E
24h
48h
Cmpd-3
Cmpd-26
Cmpd-43
Relative Proliferation Rate
Control + DMSO
PRL-1 + DMSO
PRL-1 + 0.1uM
PRL-1 + 1uM
PRL-1 + 10uM
PRL-1 + 50uM

**Figure 12. Effect of Cmpd-3, -26 and -43 on PRL-1 induced cell migration and proliferation.**

**A.** A representative SDS-PAGE profile of how we further confirm whether the PRL-1 trimer interface hits decrease PRL-1 trimer formation by in vitro cross-linking assay. **B.** Selected compounds from the in vitro cross-linking assay screening were tested for their ability of inhibiting PRL-1 trimer formation in cells by in vivo cross-linking assay. **C.** Structures of Cmpd-3, -26 and -43. **D.** Cmpd-3, -26 and -43 were tested for their ability of inhibiting PRL-1 induced migration by wound healing assay as described in Methods. **E.** Quantification of the MTT assay by measuring the relative proliferation rate as described in Methods. # $P<0.05$ compared with control group; * $P<0.05$ compared with PRL-1 without compound treatment group. Data represent mean (SD) value from at least 3 independent experiments.

trimer disruptors inhibit PRL-1's biological function of promoting cell proliferation and migration, we assayed the compound activity in PRL-1 induced cell proliferation and migration. In wound healing assay, consistent with previous reports, PRL-1 overexpression promoted cell migration by 1.5 fold compared to vector control (Figure 12D). 20 μM Cmpd-3, -26 and -43 significantly delayed wound closure induced by PRL-1 overexpression. In MTT assays, PRL-1 overexpression increased cell proliferation by 1.5 fold at 24 hours and 2.2 fold at 48 hours compared to vector control. Treatment with Cmpd-3, -26 and -43 could significantly decrease PRL-1 induced cell proliferation in a dose-dependent manner (Figure 12E). These results demonstrate that PRL-1 trimer disruptors, Cmpd-3, -26 and -43, could also inhibit PRL-1's function in promoting cell proliferation and migration. Among these three compounds we tested, Cmpd-3 and -26 have increased cell toxicity with high concentration, and Cmpd-43 has the best inhibition effect and no cell toxicity at high concentration (Figure 12E). Therefore, we chose Cmpd-43 as PRL-1 trimer disruptor to validate our hypothesis in the following experiments.

Proper analogs could help us to understand which part of the compound is critical for its activity. To further characterize the property of Cmpd-43, we searched the ChemBridge compound database, purchased four analogs of Cmpd-43 and compared the activity of the analogs with Cmpd-43. Compound structures are shown in Figure 13A. In particular, Analog-2 has the most different structure which does not contain the 4-Iminomethyl-benzoic acid group, suggesting that it may behave differently from Cmpd-43. Analog-1 does not have two methyl groups on the isoindoline group. Analog-3 has the furan ring replacing the benzoic acid group. Analog-4 has the pyrocatechol group replacing the benzoic acid group. These three analogs are highly similar to Cmpd-43 with only side chain differences, indicating that they may have the similar activity as Cmpd-43. To validate our hypothesis, we assayed the activity of these four analogs along with Cmpd-43 by MTT assay for cell proliferation and Transwell assay for cell migration. Not surprisingly, Analog-1, -3 and -4, but not Analog-2, could inhibit PRL-1 induced cell proliferation in a dose-dependent manner (Figure 13B). Analog-1, -3 and -4, but not Analog-2 at 10 μM also significantly reduced PRL-1-induced migration (Figure 13C). Specifically, Analog-1 and -4 could inhibit PRL-1 induced cell proliferation and migration but less efficient than Cmpd-43. Analog-3 has even better effect in inhibiting PRL-1 induced cell proliferation and migration than Cmpd-43. As we expected, Analog-2 has no effect in inhibiting either cell proliferation or migration, suggesting that the 4-Iminomethyl-benzoic acid group is critical for Cmpd-43's inhibitory activity. From these analog experiments, we found not only several compounds that either have similar (Analog-1 and 4) effect with or even better (Analog-3) effect than Cmpd-43 in inhibiting PRL-1 induced cell proliferation and migration, but also a control compound (Analog-2)

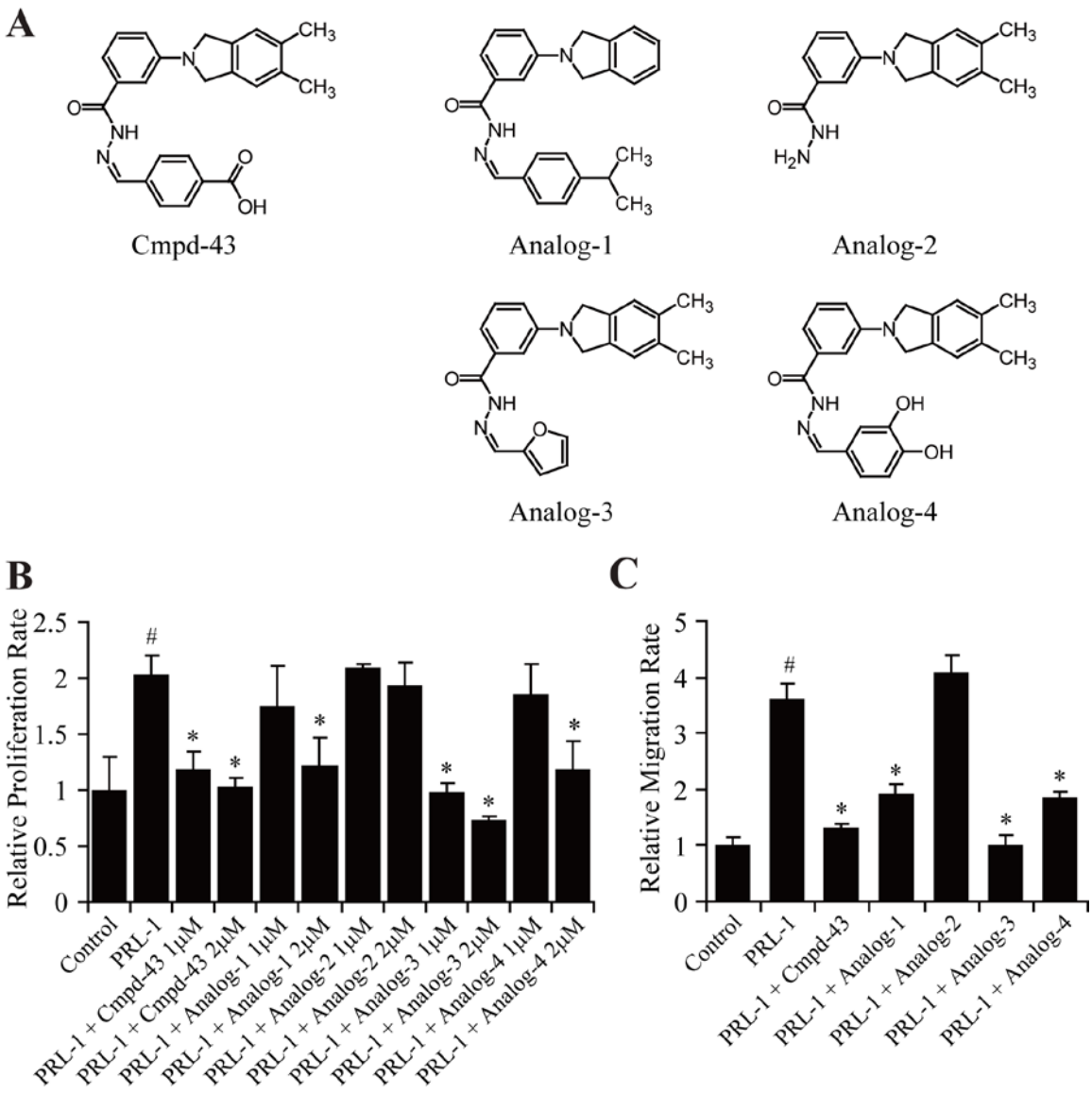


**Figure 13. Effect of Cmpd-43 and its analogs on PRL-1 induced cell migration and proliferation.**

**A.** Structures of Cmpd-43 and its analogs. **B.** The relative proliferation rate of PRL-1 overexpressing cells pretreated with Cmpd-43 and its analogs at two different concentrations. **C.** The relative migration rate of PRL-1 overexpressing cells pretreated with Cmpd-43 and its analogs. # $P<0.05$ compared with control group; * $P<0.05$ compared with PRL-1 without compound treatment group. Data represent mean (SD) value from at least 3 independent experiments

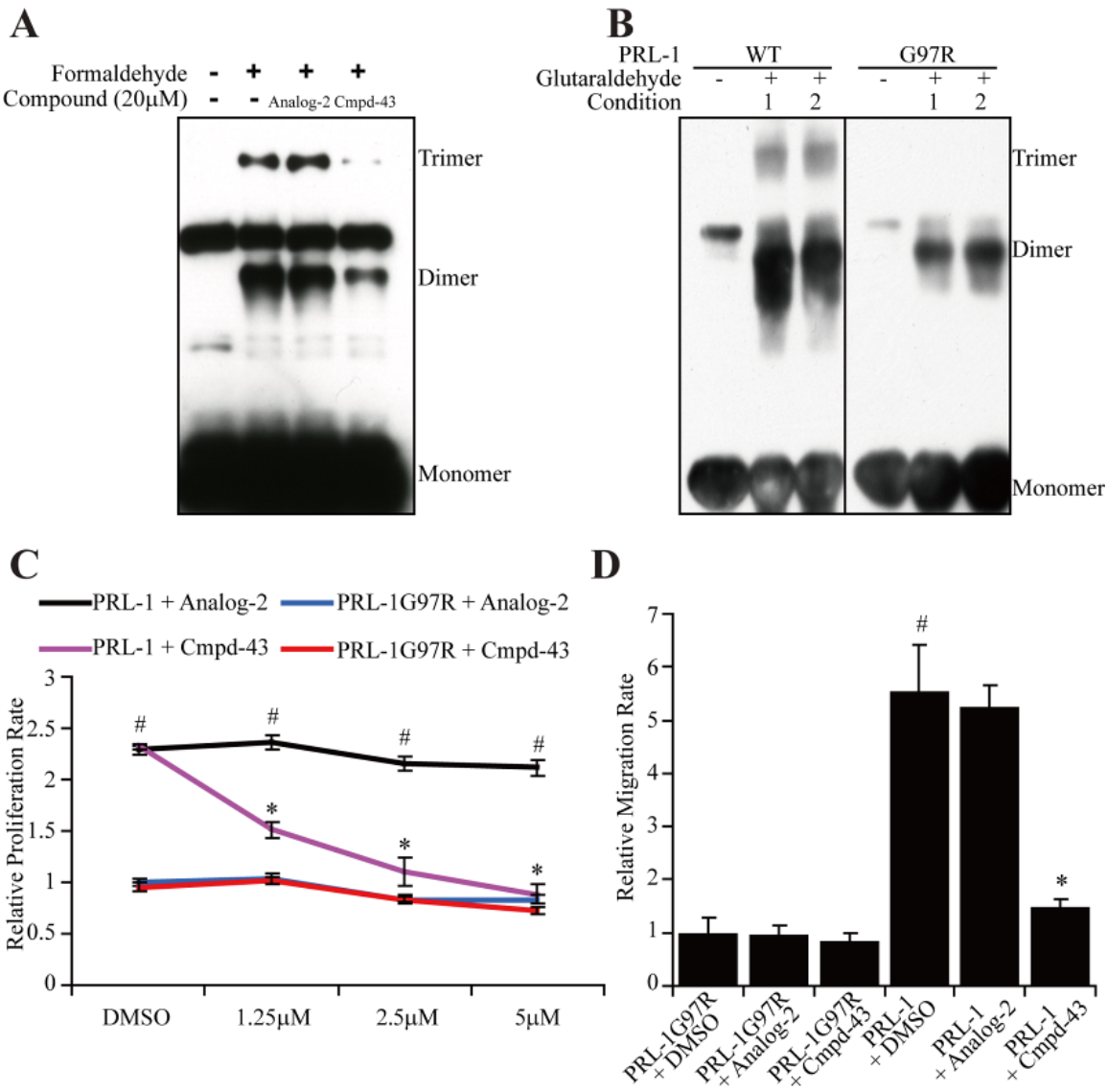


**Figure 14. The comparison between Cmpd-43 and Analog-2.**

**A.** The effect of Cmpd-43 and Analog-2 in inhibiting PRL-1 trimer formation by in vivo cross-linking assay. **B.** Trimer formation of PRL-1 WT or PRL-1 G97R tested by in vitro cross-linking assay at two conditions. Condition 1: Cross-linked 10 min at RT; condition 2: Cross-linked 30 min at 4°C. **C.** The relative proliferation rate of either PRL-1 WT or PRL-1 G97R in the presence of Cmpd-43 or Analog-2 at different does **D.** The relative migration rate of either PRL-1 WT or PRL-1 G97R in the presence of Cmpd-43 or Analog-2. # $P<0.05$ compared with PRL-1 G97R control group; * $P<0.05$ compared with PRL-1 with Analog-2 treatment group. Data represent mean (SD) value from at least 3 independent experiments.

that has no effect to inhibit PRL-1's cell function. With these useful chemical tools, we could further validate our hypothesis.

To confirm that it is indeed through disrupting PRL-1 trimerization that Cmpd-43 inhibits PRL-1-induced cell phenotype, we compared the efficiency of Cmpd-43 and Analog-2 in inhibiting PRL-1 trimer formation by *in vivo* cross-linking assay. As shown in Figure 14A, 20 μM of Cmpd-43 significantly decreased PRL-1 trimer formation in cells, while Analog-2 has no effect in disrupting PRL-1 trimerization. To further validate the specificity of Cmpd-43, we utilized PRL-1 G97R, which has defective trimer formation as shown previously (17). Here we also confirmed the impaired trimerization of PRL-1 G97R in two different conditions by *in vitro* cross-linking assay (Figure 14B). Then we performed MTT assay and Transwell assay to compare the activity of Cmpd-43 or Analog-2 in inhibiting wild-type PRL-1 or PRL-1 G97R induced cell proliferation and cell migration. As shown in Figure 14C, PRL-1 G97R has significantly decreased cell proliferation rate compared to wild-type PRL-1. Treatment with Analog-2 was unable to inhibit cell proliferation of wild-type PRL-1, while treatment with Cmpd-43 could significantly decrease PRL-1 induced cell proliferation in a dose-dependent manner. However, both Analog-2 and Cmpd-43 had no effect in decreasing cell proliferation of PRL-1 G97R. Consistently, PRL-1 G97R has significant reduced cell migration ability compared to wild-type PRL-1. 10 μM of Cmpd-43, but not Analog-2, was capable of decreasing wild-type PRL-1 induced cell migration. However, neither Analog-2 nor Cmpd-43 are able to inhibit cell migration of PRL-1 G97R (Figure 14D). All these data suggested that Cmpd-43 specifically impaired PRL-1 induced cell function via directly disrupting PRL-1 trimerization.

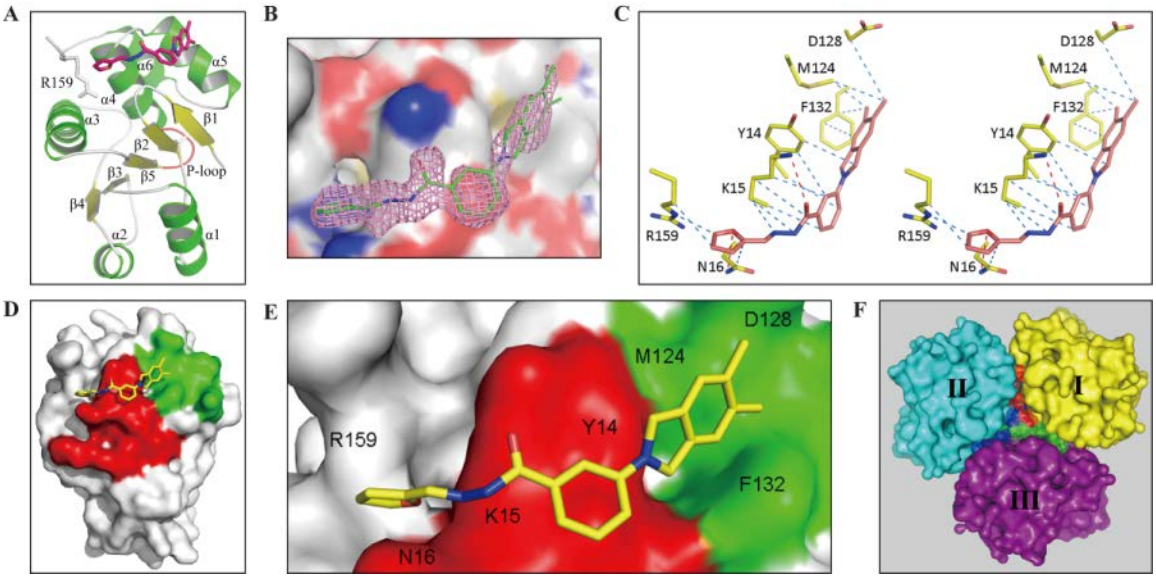


**Figure 15. The crystal structure of PRL-1 complex with Analog-3.**

**A.** Overall structure of PRL-1•Analog-3. P-loop is shown in red. Analog-3 binds to the back of active site and is shown by stick model. **B.** Unbiased *Fo*-*Fc* omit map of analog-3 contoured at 3.0σ. **C.** Stereo diagram of the binding interactions between PRL-1 and Analog-3. Color scheme for carbon atoms: residues of PRL-1, yellow; Analog-3, light red. Hydrophobic contacts are shown in cyan dash lines, polar contacts are shown in red. **D.** Overall structure of PRL-1•Analog-3. PRL-1 is shown in surface representation; Analog-3 is shown in stick model. The interfaces between molecule B and C is shown in red; green for molecule B and A. **E.** Enlarged view of PRL-1 binding with Analog-3. The residues involved in interactions with Analog-3 are marked in PRL-1 surface representative. **F.** Overlay of PRL-1•Analog-3 with PRL-1 trimer. The PRL-1 trimer is shown in surface representative; Analog-3 of PRL-1•Analog-3 complex is shown in transparent surface representative. All figures were created with PyMol (DeLano Scientific; http:/www.pymol.org) by Sijiu Liu.

### 3.4.3 Crystal structures of PRL-1•Analog-3

To determine the molecular basis of PRL-1 de-trimerization by Cmpd-43, we co-crystallized PRL-1 (residues 4-160) with Analog-3 of Cmpd-43. The 3D structure of PRL-1•Analog-3 was solved by molecular replacement using the coordinates of PRL-1 apo form (PDB entry code: 1ZCK) (23) as a search model and refined to 1.90 Å resolution. The details of the crystals and structure solution are summarized in Table 3.

The overall structure of PRL-1•Analog-3 (Figure 15A, generated by Sijiu Liu) is quite similar with the initial model we used for molecular replacement. Like other members of the PTP superfamily, the PRL-1 adopts a compact α+β structure comprising a central five-stranded β sheet surrounded by four α helixes on one side and two α helixes on the other side. The PTP signature motif ($H^{103}CVAGLGR^{110}$) forms a loop (P loop) at the base of the active site pocket.

**Table 3. Data collection and refinement statistics for PRL-1•Analog-3 complex.**

| | |
|---|---|
| Space group | $C222_1$ |
| Cell dimensions | a=47.07, b=76.47, c=86.87 Å |
| Data collection | |
| Resolution range (Å) | 50.0 – 1.84 |
| No. of unique reflections | 13,768 |
| Completeness (%) | 98.0 |
| Redundancy | 5.7 |
| $R_{merge}$[a] | 0.113 |
| Refinement | |
| Resolution range (Å) | 50.0 – 1.9 |
| No. of reflections used ($F \geq 2.0\delta(F)$) | 11,091 |
| Completeness (%) | 87.2 |
| No. of protein atoms | 1,230 |
| No. of inhibitors | 1 |
| No. of ions | 2 |
| No. of waters | 102 |
| $R_{work}$[b]/$R_{free}$[c] | 19.48/23.94 |
| r.m.s.d.[d] from ideal geometry | |
| Bond length (Å) | 0.007 |
| Bond angle | 1.23° |

[a] $R_{merge} = \Sigma_h\Sigma_i|I(h)_i - \langle I(h)\rangle|/\Sigma_h\Sigma_i I(h)_i$.

[b] $R_{work} = \Sigma_h|F(h)_{calcd} - F(h)_{obsd}|/\Sigma_h F(h)_{obsd}$, where $F(h)_{calcd}$ and $F(h)_{obsd}$ were the refined calculated and observed structure factors, respectively.

[c] $R_{free}$ was calculated for a randomly selected 3.6% of the reflections that was omitted from refinement.

[d] r.m.s.d., root mean square deviation.

The final atomic model encompasses residues 4-160 of PRL-1 in a complex with Analog-3, as revealed by the unbiased $F_o$-$F_c$ omit density map (Figure 15B, generated by Sijiu Liu). Analog-3 binds to the back of active site that lies 25Å away from the PRL-1 active site [defined by the P-loop ($H^{103}CVAGLGR^{110}$)]. This binding site is defined by α5 helix, α4-α5 loop, β1-β2 hairpin, and the side-chain Arg159. The furan ring of Analog-3 reaches to the C-terminus of PRL-1 and interacts with the side-chain of Arg159; the other side of Analog-3 contacts with residues Asp128 and Phe132 in α5 (Figure 15C, generated by Sijiu Liu). In previous studies, PRL-1 was always found in trimeric form in the crystalline state. This is true in either the apo form or in complex with a PRL-1 binding peptide (22,23,137). After we solved PRL-1•Analog-3 crystal structure, to determine whether PRL-1 is trimer or not in our new crystal structure, we checked the packing of PRL-1•Analog-3 in the crystal. Compared to PRL-1 trimer structure, there is no observable trimer pattern in the PRL-1•Analog-3 crystal structure, so our complex structure is not a trimer. There is a 2-fold axis that relates one monomer to another, but the interface between the two molecules is a small interface and consistent with only a crystallographic packing interface, not an interface that would be stable in dilute solution. So PRL-1 also is not a dimer in our crystal structure, instead, it is a monomer. The software PISA (148-150) was used to determine assemblies of PRL-1 in our crystal structure. The results from PISA further conformed that PRL-1 is a monomer in our structure (data not shown).

Detailed interactions between PRL-1 and Analog-3 are shown in Figure 15C (Generated by Sijiu Liu). A rich network of interactions ensures the precise positioning of the compound. For example, double ring in compound is engaged in hydrophobic interactions with Tyr14 in the β1-β2 hairpin, Met124 in the α4-α5 loop, and Phe132 in

α5. Two methyl groups on double ring contribute hydrophobic interactions with side-chain of Met124, Asp128 and Phe132. The phenyl ring in the middle of compound is within van der Waals contacts with Tyr14 and Lys15 in the β1-β2 hairpin. Hydrazide group in compound provides Van der Waals contacts with Lys15. The furan ring in the compound donates van der Waals contacts with Asn16 in the β1-β2 hairpin and Arg159 in the C-tail. Except that hydrophobic contacts between compound and protein, the binding mode also is stabilized by two polar interactions. One polar interaction is found between atom oxygen of furan ring and side-chain of Asn16, another is between oxygen of hydrazide and side-chain of Lys15 (Figure 15C).

### 3.4.4 Analog-3 binds to the PRL-1 trimer interface

In our previous papers (17,23,137), we reported that PRL-1 can form trimers in solution and in cells. In the trimer, each monomer interacts with two other monomers and forms two interfaces. For example, upon trimer formation, one interface was formed between molecule B (Figure 10A) and molecule C (Figure 10A) (BC interface, marked red in Figure 15D & 15E, generated by Sijiu Liu). This interface was defined by the α1 helix, the β1-β2 hairpin, and the α3-β5 loop in the molecule B, including residues Glu11, Thr13, Tyr14, Lys15, Asn16, Met17, Arg18, Pro96, and Gly97; The other interface was formed between molecule B (Figure 10A) and molecule A (Figure 10A) (BA interface, marked green in Figure 15D & 15E). This interface was defined by α4-α5 loop and α5 helix (residues 124-134) in molecule B, including residues Met124, Tyr126, Asp128, Val130, Gln131, Phe132. In the PRL-1•Analog-3 structure, Analog-3 binds to the back of active site that lies 25Å away from the PRL-1 active center. This binding site is defined by α5 helix, α4-α5 loop, β1-β2 hairpin, and the side-chain Arg159. In this binding mode, residue Arg159 in the C-tail; residues Tyr14, Lys15 and Asn16 in β1-β2

hairpin; residue Met124 in α4-α5 loop; residues Asp128 and Phe132 in α5 helix are involved in the interactions with PRL-1. The binding site overlaps with both BC interface and BA interface of trimer. Thus Analog-3 directly binds to the interface of trimer (Figure 15D & 15E) and blocks PRL-1 trimer formation. Additional, we superimposed three complex structures of PRL-1•Analog-3 into trimer strucrure of apo form of PRL-1, we found each Analog-3 in complex structure inserts into the trimer interface and causes strong steric hindrance against nearby Analog-3 in two other complex structures (Figure 15F, generated by Sijiu Liu). It further indicates that structure PRL-1•Analog-3 cannot form trimer, and it is a monomer.

### 3.4.5 Mutagenesis validated the critical residues for Cmpd-43 binding

In the crystal structure of PRL-1•Analog-3, residues Tyr14 and Phe132 provide hydrophobic interactions with Analog-3 of Cmpd-43. We hypothesized that once Tyr14 and Phe132 were mutated to Ala, PRL-1 will lose the ability to bind the compound. Thus, we next tested the trimer disrupting activity of Cmpd-43 in PRL-1 Y14A and PRL-1 F132A by *in vitro* cross-linking assay. We have shown that PRL-1 Y14A and F132A do not affect PRL-1 trimer formation (Figure 16A). Compared to wild-type PRL-1, which showed dramatically decreased trimerization in the presence of Cmpd-43, both PRL-1 Y14A and PRL-1 F132A had significant less response to Cmpd-43-induced trimer disruption (Figure 16A). Consistently, 10 μM of Cmpd-43 was less efficient to decrease cell migration mediated by PRL-1 Y14A and PRL-1 F132A than wild-type PRL-1 (Figure 16B). Taken together, Tyr14 and Phe132 of PRL-1 are critical for Cmpd-43 binding, further demonstrating the significance of these residues in PRL-1•Analog-3 interaction.

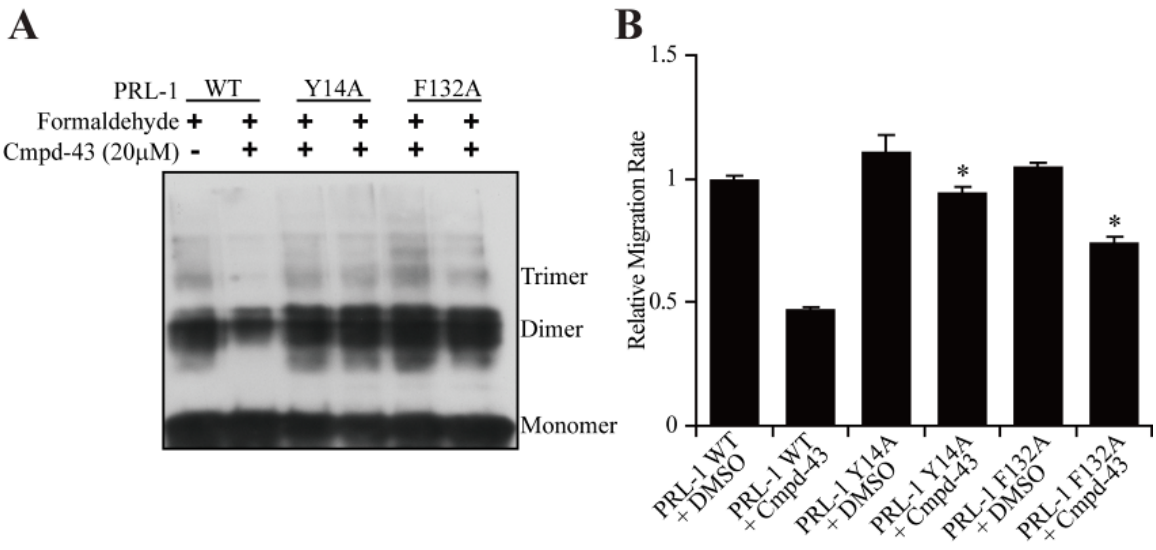


**Figure 16. Effect of Cmpd-43 on PRL-1 Y14A and F132A.**

**A.** The effect of Cmpd-43 in inhibiting PRL-1 Y14A and F132A trimer formation by *in vitro* cross-linking assay. **B.** The relative migration rate of PRL-1 Y14A and F132A in the presence of Cmpd-43. * $P<0.05$ compared with WT PRL-1 with Cmpd-43 treatment group. Data represent mean (SD) value from at least 3 independent experiments.

### 3.4.6 Cmpd-43 reduces the proliferation and migration in human breast cancer cell and lung cancer cell

Since the trimer interface is conserved among all PRLs, we proposed that PRLs could also form both homo- and hetero-trimers, and that Cmpd-43 could block both homo- and hetero-trimer formation. To test this hypothesis, we co-transfected each PRL with different tags into HEK293 cells and did immunoprecipitation assays. As we expected, although no interaction was detected in the absence of cross-linker (Figure 17A & 17B), HA-tagged PRL-3 could immunoprecipitate, and also form hetero-dimer or hetero-trimers with either Flag-tagged PRL-2 or GFP-tagged PRL-1 after cross-linking (Figure 17B, 17C & 17D). In addition, Flag-tagged PRL-2 could also interact with both HA-tagged PRL-3 and GFP-tagged PRL-1 and form hetero-dimers or hetero trimmers in

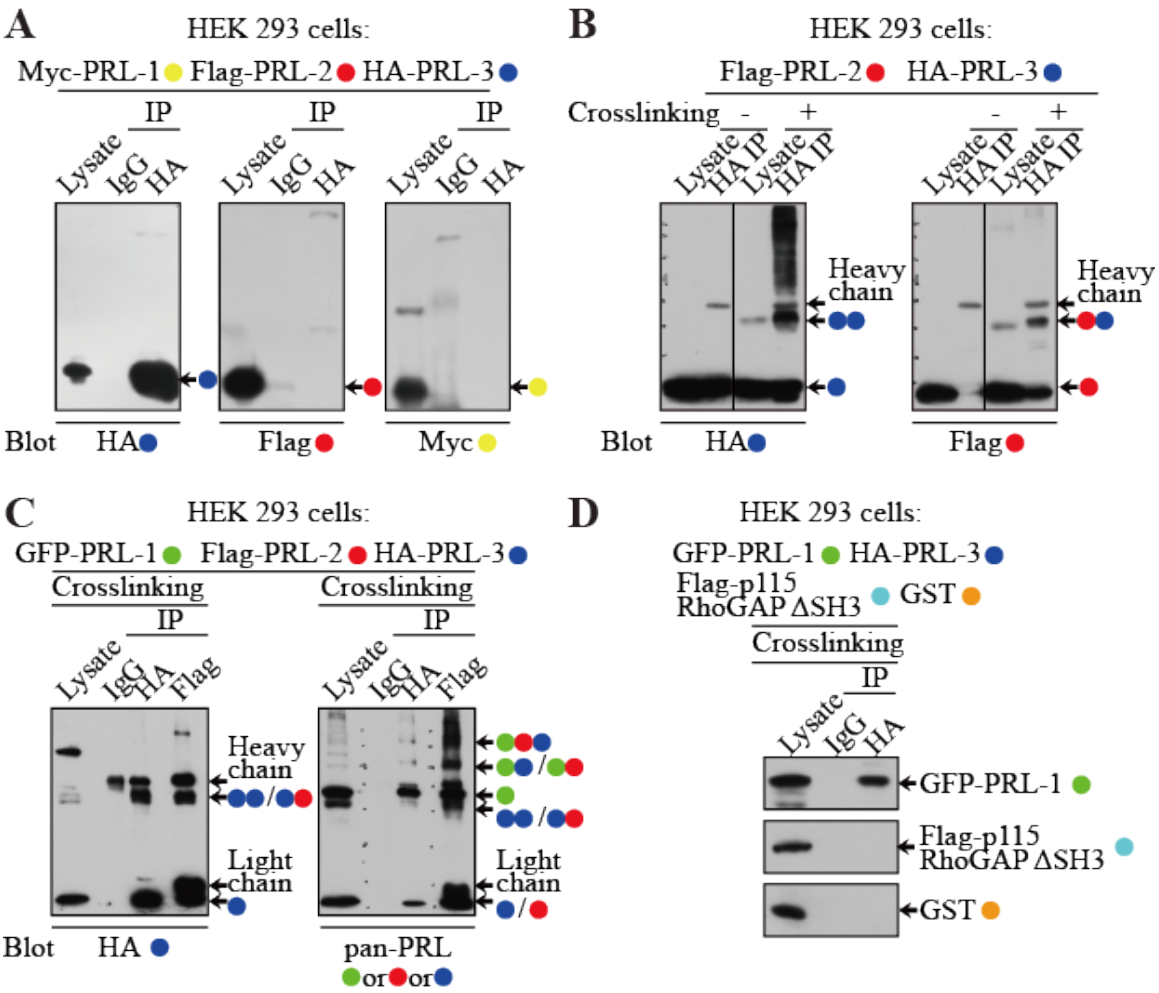


**Figure 17. PRLs form hetero-trimers.**

**A.** HA-PRL-3 cannot immunoprecipitate Myc-PRL-1 and Flag-PRL-2 in the absence of cross-linker. Cell lysates from HEK293 cells co-transfected with Myc-PRL-1, Flag-PRL-2 and HA-PRL-3 were subjected for immunoprecipitaion with HA antibody, then blotted with HA, Flag and Myc antibodies. **B.** HA-PRL-3 immunoprecipitated Flag-PRL-2 in the presence of cross-linker. Cell lysates from HEK293 cells co-transfected with Flag-PRL-2 and HA-PRL-3 were subjected for immunoprecipitation with HA antibody, then blotted with HA and Flag antibodies. **C.** HA-PRL-3 immunoprecipitated GFP-PRL-1, and Flag-PRL-2 immunoprecipitated HA-PRL-3 and GFP-PRL-1 in the presence of cross-linker. Cell lysates from HEK293 cells co-transfected with GFP-PRL-1, Flag-PRL-2 and HA-PRL-3 were subjected for immunoprecipitaion with HA and Flag antibody, then blotted with HA and pan-PRL antibodies. **D.** HA-PRL-3 immunoprecipitated Flag-PRL-2 but not Flag-p115 RhoGAP/ΔSH3 or GST in the presence of cross-linker. Cell lysates from HEK293 cells co-transfected with GFP-PRL-1, HA-PRL-3, Flag-p115 RhoGAP/ΔSH3 and GST were subjected for

immunoprecipitaion with HA antibody, and blotted with pan-PRL, Flag and GST antibodies.

the presence of cross-linker (Figure 17C). To rule out the possibility of non-specificity effect of cross-linking, we also co-transfected GFP-PRL-1 and HA-PRL-3 with two other proteins, Flag-tagged p115 RhoGAP/ΔSH3 and GST, that are presumably not associated with PRLs. We found that HA-PRL-3 only immunoprecipitated GFP-PRL-1 but not Flag-p115 RhoGAP/ΔSH3 or GST from the lysate (Figure 17D). These data suggested that all PRLs are biochemically equivalent in terms of trimerization, and that Cmpd-43 will disrupt trimer interface among all PRLs with no selectivity.

Given the similar function of all PRLs in promoting cancer progression, Cmpd-43 is a novel anti-cancer agent by targeting the interface of both homo-trimer and hetero-trimer of PRLs. To test the anti-cancer efficacy of Cmpd-43, we assayed the effect of Cmpd-43 in inhibiting cell proliferation and migration in human cancer cell lines. Breast adenocarcinoma cancer cell line MDA-MB-231 and lung cancer cell line H1299 were used in the experiment. It has been shown that knockdown of PRL-1 in H1299 cells significantly decrease cell proliferation and migration (88). PRL-2 knockdown in metastatic MDA-MB-231 breast cancer cells decreased anchorage-independent growth and cell migration (35). As shown in Figure 18A, Analog-2 has no effect in inhibiting cell proliferation of MDA-MB-231 and H1299 cells, while treatment with Cmpd-43 could significantly reduce cell proliferation in MDA-MB-231 cells and H1299 cells in a dose-dependent manner. H1299 cell is much more sensitive to Cmpd-43 treatment than MDA-MB-231 cells, suggesting Cmpd-43 has some specificity in different cell types. On the other hand, 10 μM of Cmpd-43 but not Analog-2 could significantly decrease cell migration in both MDA-MB-231 cells and H1299 cells (Figure 18B). All these data

suggest that Cmpd-43 could inhibit cancer cell proliferation and migration, and may represent a lead compound of anti-cancer agent.

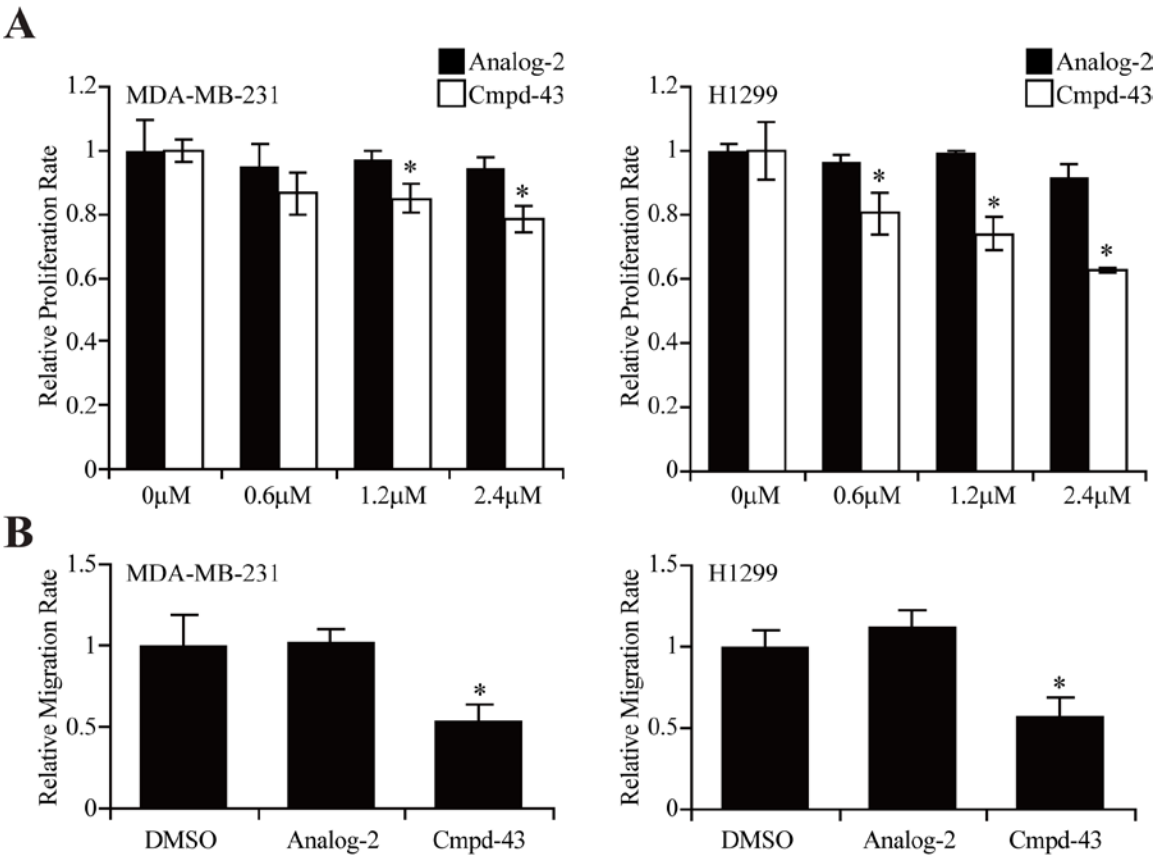


**Figure 18. Effect of Cmpd-43 on breast cancer cell MDA-MB-231 and lung cancer cell H1299.**

**A.** The relative proliferation rate of MDA-MB-231 cells (left panel) and H1299 cells (right panel) in the presence of Cmpd-43 or Analog-2 at different does. **B.** The relative migration rate of MDA-MB-231 cells (left panel) and H1299 cells (right panel) in the presence of Cmpd-43 or Analog-2. * $P<0.05$ compared cancer cells with Analog-2 treatment group. Data represent mean (SD) value from at least 3 independent experiments.

### 3.5 Discussion

PRL-1 is believed to be an oncogene and contributes to various human malignancies (34,36,151). Phosphatase activity of PRL-1 is required for its oncogenic property (17). However, PRL-1 crystal structure indicates that the catalytic cleft of PRL-

1 is extremely shallow and wide (22,23,137), suggesting that targeting PRL-1 active site for small molecule inhibitors is very difficult. Several groups have reported compounds that display inhibitory activity against the PRL phosphatases, including pentamidine (103) and rhodanine (104). However, the toxicity of these compounds is an issue due to low specificity. We also have tried very hard to find specific PRLs inhibitors by high throughput screening, but unfortunately, none of the small molecules are good PRLs inhibitors. Given that PRL-1 trimerization is critical for PRL-1's cellular function of promoting proliferation and migration, it presents an opportunity for us to find good PRL-1 inhibitors by targeting the trimer interface.

This is the first study to inhibit PRL-1's biological function via disrupting PRL-1 trimer formation using small molecule compound. Starting from a virtual screening for searching small molecule compounds targeting PRL-1 trimer interface, we identified three compounds as potential PRL-1 timer disruptors. Biochemical and cellular studies validated that Cmpd-3, -26 and -43 impair PRL-1 trimer formation both *in vivo* and *in vitro*, and accordingly inhibit PRL-1 induced cell proliferation and migration. Based on the chemical structure of Cmpd-43, we searched ChemBridge chemical database and purchased 4 structurally related analogs. As expected, Analog-2, which has the most different structure from Cmpd-43, was unable to disrupt PRL-1 trimer formation and could not reduce PRL-1 induced cell proliferation and migration. Analog-1, -3 and -4, which have similar structures with Cmpd-43, could still inhibit PRL-1's cell function. Moreover, the trimerization deficient mutant PRL-1 G97R, which has dramatically low cell proliferation and migration ability compared to wild-type PRL-1, has no response to both Cmpd-43 and Analog-2 for cell proliferation and migration. Structural analyses revealed that, PRL-1 alone exists as a trimer in crystalline state, but the complex of PRL-

1 with Analog-3 (Cmpd-43 analog) was a monomeric arrangement. Cmpd-43-binding deficient mutants PRL-1 Y14A and F132A lose the response to Cmpd-43 in decreasing trimer formation and inhibiting cell migration. Finally, Cmpd-43 could also inhibit cell proliferation and migration in breast cancer cell line MDA-MB-231 and lung cancer cell line H1299. Together, all the results demonstrated that targeting PRL-1 trimer interface could be a novel method for anti-cancer agent, and that Cmpd-43 represents a lead compound that inhibits PRL-1 biological function in human cancer cells.

As shown by us and work by others, PRLs could form homo-trimers (17,22,23,137). In addition, it is suggested that PRLs could also form hetero-trimers due to the conserved trimer interface among all PRLs. We confirmed the formation of hetero-trimer by immunoprecipitation assays (Figure 17), which also indicated that it is difficult to have selective trimer disruptors for each PRL isoform. Given that all PRLs have the same function of promoting tumorigenesis and metastasis (11,13,25,29,86,96), targeting all PRLs could be a reasonable therapeutic treatment for cancer. However, additional experiments are required to validate the significance of hetero-trimers. In summary, our study provides proof of concept for a design of the non-phosphatase activity based inhibitors that will target PRLs trimer interface and inhibit PRLs induced cell proliferation and migration in a clinically beneficial manner. In addition, targeting PRLs trimer interface seems to be a novel and promising approach to modulate the cell function of PRLs. Overall, our work provides conceptual support and rationale for design of PRLs trimer-disruptor based anti-cancer drugs.

# CHAPTER 4: GENERATION AND CHARACTERIZATION OF *PRL* KNOCKOUT MICE

## 4.1 Overview

PRLs play a positive role in cell signaling events and are suggested as oncogenes and therapeutic targets in several cancers (152,153). Overexpression of PRLs was frequently found in numerous tumor cell lines, and cells expressing high levels of PRLs exhibited enhanced proliferation, anchorage-independent growth, cell migration and invasion (11,12,69,86,95,96). Clinically, up-regulation of PRLs has been observed in many types of advanced stage tumors as well as metastatic lesions (153). It has been suggested that PRLs promote cell proliferation and migration through activation of several signaling pathways, including the Rho family of small GTPases, Src, ERK1/2, and PI3K (16,59,79,86,137). PRLs are strongly implicated as a driving force in malignancy, but limited knowledge is known about the exact physiological functions of these phosphatases. Our current understanding of PRLs came primarily from observations in clinical patient samples or cell culture models, either overexpressing or silencing PRLs. To define the biological function of endogenous PRLs in non-cancer cells, generation of genetic models with PRLs deletion is required.

## 4.2 Hypothesis and Specific Aims

Gene knockout in mouse model is a widely used genetic technique, in which a gene has been inactivated by replacing it or disrupting it with a piece of artificial DNA. The inactivation of a gene often results in mouse phenotypic alteration including appearance, behavior and other observable physical and biochemical characteristics. Information obtained from gene knockout in mice provides valuable clues about what this gene normally does in mice. Given that mice share many genes with humans,

characteristics observed from gene knockout mice may also give researchers a better understanding on how a related gene is involved in development and disease in humans. As we discussed previously, the amino acid sequences for all PRLs are conserved in human and mouse (Figure 2), suggesting that each PRL plays similar roles in human and mouse. This makes the mouse a good model organism to study the biological functions of PRLs *in vivo*. Thus, I hypothesized that **knockout mouse models lacking each of the individual *Prl* genes may provide substantial insight into the physiological function of PRLs *in vivo*.** To test this hypothesis, I proposed two specific aims: 1) to create *Prl-1*, *Prl-2* and *Prl-3* knockout mice, respectively; and 2) to characterize the phenotypes in *Prl-1*$^{-/-}$, *Prl-2*$^{-/-}$ and *Prl-3*$^{-/-}$ mice. The specific goal of this project is to generate and analyze *in vivo* mouse models with *Prl* deletion.

### 4.3 Materials and Methods

#### 4.3.1 Generation of *Prl-1* and *Prl-2* knockout mice by "gene-trapping" strategy

Heterozygous gene trap embryonic stem (ES) cell lines for *Prl-1* (Cell No.: CC0606; Mouse strain: 129P2/OlaHsd) and *Prl-2* (Cell No.: AQ0673; Mouse strain: 129P2/OlaHsd), containing an insertional mutation in mouse *Prl-1* and *Prl-2* locus respectively, were purchased from Mutant Mouse Regional Resource Centers (MMRRC). The ES cells were injected into blastocysts from C57BL/6J mice, and the resulting chimeric males with successful germ line transmission of the mutant allele were intercrossed with C57BL/6J females to generate F1 offspring. Knockout mice were generated by crossing heterozygous male with females. Genotyping of F1 offspring was performed by PCR. Primer sequences are listed in Table 4.

### 4.3.2 Construction of *Prl-3* gene-targeting vector

To generate a *Prl-3*-null allele, a targeting vector consisting of a 2.2-kb 5′ arm of homologous genomic sequence, LacZ (β-galactosidase) cassette, a neomycin resistance (PGK-Neo$^r$) cassette, a 5.2-kb 3′ arm of homologous genomic sequence followed by a DTA (Diphtheria Toxin A-chain gene) cassette was constructed. Briefly, the 5′ arm of the targeting vector was amplified from PRL-3 bacterial artificial chromosome (BAC) clone 116F7 and was inserted into the BamHI and XhoI sites of pKO vector. The 5.2-kb 3′ arm was amplified from PRL-3 BAC clone and was constructed into the SalII and NotI sites of pKO vector.

### 4.3.3 Generation of *Prl-3* knockout mice by homologous recombination

The targeting vector was linearized by PmeI and electroporated into ES cells in the Transgenic and Knock-Out Mouse Core at Indiana University Simon Cancer Center. The transfected ES cells were treated with neomycin for positive selection, and the DTA gene, which inhibits protein synthesis, was used as the negative selection marker. Genomic DNA was prepared from selected ES cells, and the various clones were screened by Southern blot analysis using DNA probes as described in Figure 19. Positive clones were identified and injected into blastocyst of C57BL/6J donors. Injected blastocysts were transplanted into pseudo-pregnant females. Chimeric animals with successful germ line transmission of the mutant allele were intercrossed with C57BL/6J females to generate F1 offspring. Knockout mice were generated by crossing heterozygous male with females. Genotyping of F1 offspring was performed by PCR. Primer sequences are listed in Table 4. Experiments on mice were carried out in accordance with the regulations of The Institutional Animal Care and Use Committees at Indiana University.

**Table 4. Primers used in genotyping, RT-PCR and Southern blot.**

| Genotyping | Forward primer | Reverse primer | Product |
|---|---|---|---|
| *Prl-1* wild-type allele | gcagacaagtgaactgtagaaattc | agtgtagcacacttctaccgttcca | 633 bp |
| *Prl-1* mutant allele | gcagacaagtgaactgtagaaattc | acgacgggatcctctagag | 852 bp |
| *Prl-2* wild-type allele | acagtatggatgagtagaatc | gttgctccttggttattctcac | 623 bp |
| *Prl-2* mutant allele | acagtatggatgagtagaatc | gttttcccagtcacgacgttg | 746 bp |
| *Prl-3* wild-type allele | atagaggacactgctctgcggccg | tccacagactgcaatggtcac | 834 bp |
| *Prl-3* mutant allele | atagaggacactgctctgcggccg | gattaagttgggtaacgcca | 520 bp |
| **RT-PCR** | **Forward primer** | **Reverse primer** | **Product** |
| *Prl-1* | gaagaggccgtctccactaa | atcccaggattgcgattaca | 195 bp |
| *Prl-2* | ggctgtaacagggtggaaga | gccaccaacatctgggtact | 302 bp |
| *Prl-3* | ggtgctctggactctcaagg | tgacccctactctgtcctg | 307 bp |
| *Rpl7* | gctgcggattgtggagccatac | cctccatgcagatgatgccaaac | 170 bp |
| **Southern Blot** | **Forward primer** | **Reverse primer** | **Product** |
| 5'arm probe | tagtaggctctgctgtgcaag | cagcttcatatgcgcacac | 600 bp |
| 3'arm probe | atccaaggaacagcaaagct | attgcctggacacttagacttg | 540 bp |

### 4.3.4 Southern blot

Genomic DNA extracted from ES cells was digested by XbaI, BamHI, NarI or ScaI respectively. After digestion, the DNA fragments were separated by electrophoresis in 0.7% agarose gels and transferred to Hybond-N+ membranes. $^{32}$P-labeled probes were made using the multiprime-labeling system (Amersham). The labeling DNA templates (5' probe size: 600 bp, 3' probe size: 540 bp) were generated by PCR using primers list in Table 4. Hybridizations were carried out at 60°C overnight in hybridization buffer.

### 4.3.5 RNA extraction and quantitative RT-PCR

Total RNA was extracted from tissues using Trizol reagent (Invitrogen) and treated with DNase I (Promega). Reverse transcription was performed using the SuperScript III one-step RT-PCR system (Invitrogen) at 55°C with gene-specific primers. Quantitative PCR was performed using SYBR Green I master mix on a

LightCycler 480 (Roche Applied Science), with RPL7 as the housekeeping gene control. All primers were listed in Table 4.

### 4.3.6 Western Blot analysis

Tissues were lysed in lysis buffer supplied with phosphatase and protease inhibitor mixture (Roche Applied Science). Equal amounts of protein were resolved by SDS-PAGE, transferred to nitrocellulose membrane and subjected to immunoblotting. Anti-PRL-1, anti-PRL-1/2, and anti-PRL-3 antibodies were kindly provided by Dr. Qi Zeng. All other antibodies were from Cell Signaling Technology.

### 4.3.7 X-gal staining

Samples were fixed in 4% PFA on ice for 1 hr, incubated in PBS/0.01%NP-40 for 4 hrs, and stained in β-gal substrate (1 mg/mL X-gal, 5 mM $K_3Fe(CN)_6$, 5 mM $K_4Fe(CN)_6$, 1 mM EGTA, 0.01% NP-40 in 1xPBS) for 48h at 37°C. ). Once staining was complete, tissues were re-fixed in 4% PFA overnight and cleared via use of increasing concentrations of glycerol (10–50%) for whole-mount imaging.

### 4.3.8 Histology

Tissues were fixed in 4% paraformaldehyde overnight at 4°C, embedded in paraffin, serially sectioned (10 μm), and stained with H&E according to standard methods. For immunohistochemistry, deparaffinized sections were boiled in 10 mM sodium citrate (pH 6.0) for 10 min to unmask antigen. Sections were then incubated with diluted antibodies (1:50-1:100) at 4 °C overnight. Signals were detected by VECTASTAIN Elite ABC kit and developed using diaminobenzidine substrate from Vector Laboratories (Burlingame, CA). Images were captured on a Leica DM2500 stereomicroscope. All images are representative of at least three samples.

### 4.3.9 Statistical analysis

Statistical significant differences were calculated using student's t-test or $\chi^2$ test and represented by asterisks: **P<0.05, **P<0.01, ***P<0.001*.

## 4.4 Results

### 4.4.1 Generation of *Prl-1*and *Prl-2* knockout mice by "gene-trapping"

Gene-trapping is a fast and easy way to introduce insertional mutations across the mammalian genome and to obtain gene-deficient alleles. In order to quickly obtain knockout mice for all *Prl*s, we collaborated with Dr. Shou Weinian's lab in the Department of Pediatrics, and searched the catalog in Mutant Mouse Regional Resource Center (MMRRC) for the availability of *Prl-1*, *Prl-2* and *Prl-3*-trapped ES clones. Even though *Prl-3*-trapped ES clones were not available, there were multiple clones for both *Prl-1* and *Prl-2*-trapped ES cells. The *Prl-1*, *Prl-2* and *Prl-3* genes are located on chromosome 1, 4 and 15 of the mouse genome, respectively. All three genes consist of 6 exons with start codon in exon 2 and stop codon in exon 6. Thus, exon 1 and the majority of the exons 2 and 6 are noncoding sequences once they are transcribed. To completely delete *Prl-1* or *Prl-2* gene, we chose ES clones with insertion site upstream of the ATG start codon in exon 2.

We generated *Prl-1* deficient mice using targeted ES cell clone (CC0606 obtained from MMRRC) with the gene trap vector pGT01 inserted into exon 2 (upstream of ATG start codon) of the mouse *Prl-1* locus (Figure 19A). Similarly, *Prl-2* knockout mice were generated using a gene trap ES cell clone (AQ0673 obtained from MMRRC), in which a gene trap cassette pGT01 was inserted into the first intron of the mouse *Prl-2* gene (Figure 19A). The gene trap vector contains a splice-acceptor sequence upstream of the reporter gene β-geo (fusion of beta-galactosidase and neomycin phosphotransferase

II) and a premature polyadenylation signal downstream of β-geo. The insertion of the gene trap cassette would eliminate endogenous gene expression, and express β-geo fusion protein derived by the endogenous gene promoter. The single insertion site was confirmed by sequencing analyses.

ES cells with *Prl-1* or *Prl-2* trapped allele were injected into C57BL/6 blastocysts respectively to generate chimeric embryos. Then pseudo-pregnant female mice were injected with chimeric embryos in each uterine horn and produced chimeric mice with mixed black and agouti coat color. Germline transmission was confirmed by examining the genotypes in the offsprings of chimeric males mated with C57BL/6J females. Cross-mating of F1 heterozygous mice gave offsprings with all three genotypes (Figure 19D).

### 4.4.2 Generation of *Prl-3* knockout mice by homologous recombination

Homologous recombination in embryonic stem cells was used to create *Prl-3* knockout mice. In cooperation with Dr. Weinian Shou's lab, we designed a targeting vector with a 5' arm consisting of 2.2kb sequence upstream of the ATG start in exon 2 and a 3' arm that is a 5.2kb sequence downstream of exon 6 in order to completely eliminate *Prl-3* gene expression. Once homologous recombination occurs, the whole coding sequence for *Prl-3* will be replaced with beta-galactosidase and neomycin cassette, and endogenous *Prl-3* promoter will instead drive the expression of beta-galactosidase. A bacterial artificial chromosome (BAC) containing mouse *Prl-3* gene was used as a template to amplify each arm for construction of the targeting vector. The sequence confirmed arms were then inserted into multiple cloning sites of pKO-DTA plasmid. The targeting vector was linearized by PmeI and then electroporated into mouse ES cells in the Transgenic and Knock-Out Mouse Core at Indiana University Simon

Cancer Center. Following transfection, PGK-driven neomycin expression was necessary for positive selection in the presence of G418 to eliminate non-transfected cells, while expression of Diphtheria Toxin A-chain (DTA) was used as negative selection to get rid of cells with random integration.

250 ES cell clones were selected and then genotyped by Southern blot analysis. Two external probes, 5' probe and 3' probe (comprising approximately 300 bp corresponding to exon 6 of the *Prl-3* locus), were radiolabeled and used to detect the targeted mutation. Genomic DNA of ES cell clones were digested by XbaI or BamHI for determination of 5' recombination, and NarI or ScaI for detection of 3' recombination. The 5' probe will detect a specific 4.8kb or 20kb band with XbaI or BamHI digestion respectively, while the 3' probe will recognize a 9.8kb or 20kb fragment with NarI or ScaI digestion respectively (Figure 19B). Five out of 250 ES cell clones were confirmed to have undergone homologous recombination. The Southern blot assays for a representative clone were shown in Figure 19C.

ES cells with heterozygous *Prl-3* allele were injected into C57BL/6 blastocysts. Chimeric embryos were implanted into pseudo-pregnant female mice. Chimeric mice with mixed black and agouti coat color were mated to C57BL/6J females, and offspring were confirmed for successful germline transmission as evidenced by genotyping with heterozygous alleles. Breeding F1 heterozygous mice gave offspring with all three genotypes (Figure 19D).

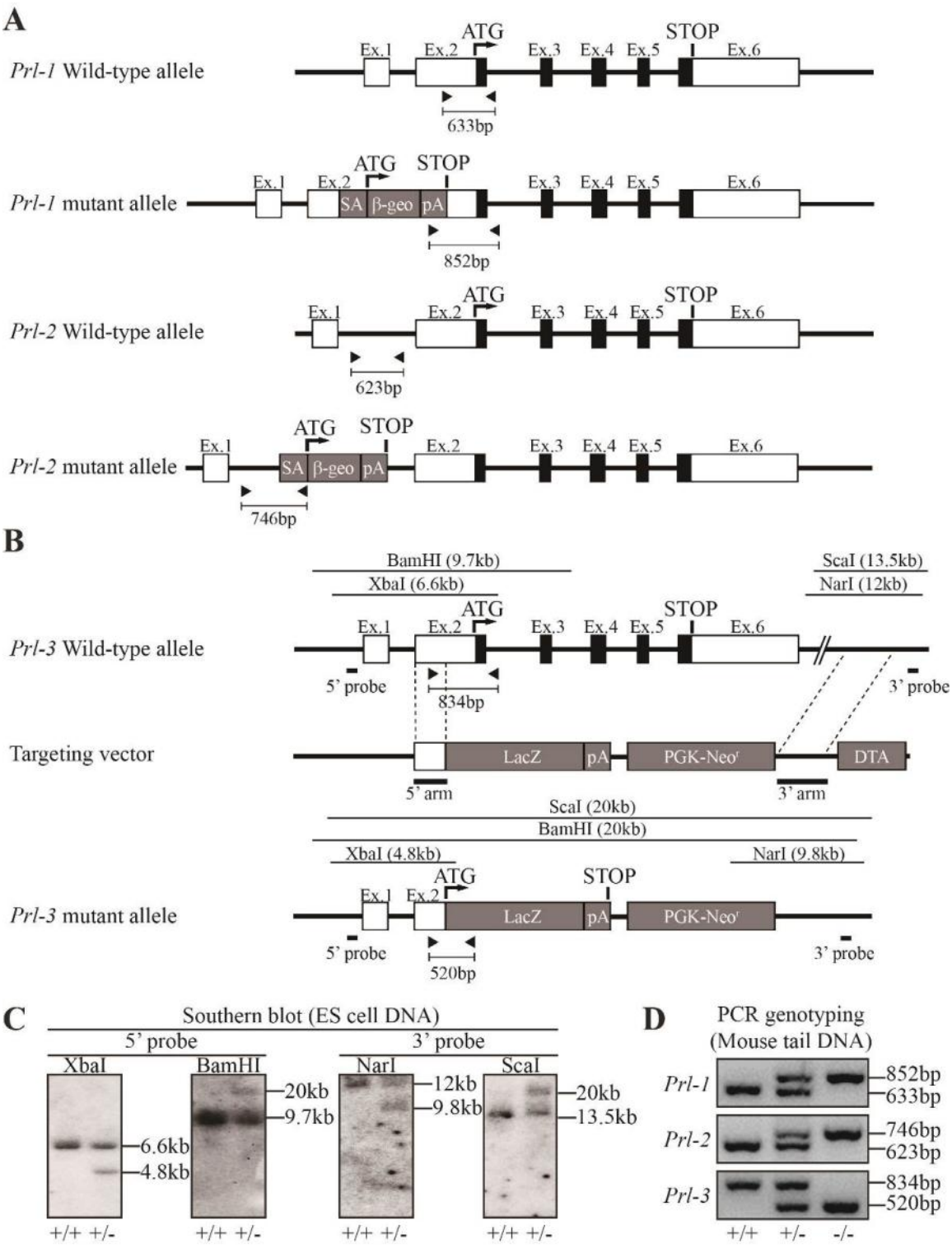


**Figure 19. Generation of *Prl-1*, *Prl-2* and *Prl-3* deficient mice.**

**A.** "Gene-trapping" strategy for generating *Prl-1* and *Prl-2* deficient mice. Genomic structure for wild-type *Prl-1* and *Prl-2*, as well as gene-trapped *Prl-1* and *Prl-2* were shown. Rectangles indicate exon segments, with coding sequence shaded. A splice-

acceptor sequence upstream of the reporter gene β-geo (fusion of beta-galactosidase and neomycin phosphotransferase II) and a downstream premature polyadenylation signal was inserted in the exon 2 of *Prl-1* gene and intron 1 of *Prl-2* gene. Genotyping primers and product size were labeled. **B.** Gene targeting strategy for generating *Prl-3* knockout mice. Genomic structure for wild-type and mutant *Prl-3*, as well as structure of targeting vector were shown. Rectangles indicate exon segments, with coding sequence shaded. Targeting arms (5' arm and 3' arm) were labeled. Probes (5' probe and 3' probe) used for Southern blot analysis were indicated. The fragment and expected size after digestion with each of the enzymes (XbaI, BamHI, NarI and ScaI) were indicated. Genotyping primers and product size were labeled. **C.** Southern blot for *Prl-3* homologous recombination. Genomic DNA from wild-type ES cells and *Prl-3*-targeted ES cells were either digested with XbaI or BamHI and probed with 5' probe, or digested with NarI or ScaI and probed with 3' probe. 5' probe gives a specific 4.8kb band and 20kb band in targeted ES cell DNA after XbaI and BamHI digestion, respectively; while 3' probe gives a specific 9.8kb band and 20kb band in targeted ES cell DNA after NarI and ScaI digestion, respectively. The size for each band was indicated. **D.** PCR strategy for genotyping using mouse tail DNA.

### 4.4.3 Validation and examination of *Prl-1*, *Prl-2* and *Prl-3* deficient mice

To determine the knockout of *Prl-1*, *Prl-2* and *Prl-3* gene product, we first examined gene deletion at mRNA level by quantitative RT-PCR. Total mRNAs were extracted from thymus of either wild-type, *Prl-1*-null or *Prl-2*-null mice to determine the deletion of *Prl-1* or *Prl-2*. Since previous report indicated that PRL-3 expression is restricted in heart and muscle (14), we chose to examine PRL-3 mRNA level from muscle. As shown in Figure 20A, I was unable to detect *Prl-1* mRNA in thymus of *Prl-1*-null mice. *Prl-2* mRNA was also not detectable in the same organ from *Prl-2*-null mice. *Prl-3* mRNA can only be amplified from muscle of wild-type but not from that of *Prl-3*-null mice. The results here demonstrated that both "gene-trapped" deletion of *Prl-1* and *Prl-2*, and "gene-targeted" deletion of *Prl-3* were successfully achieved.

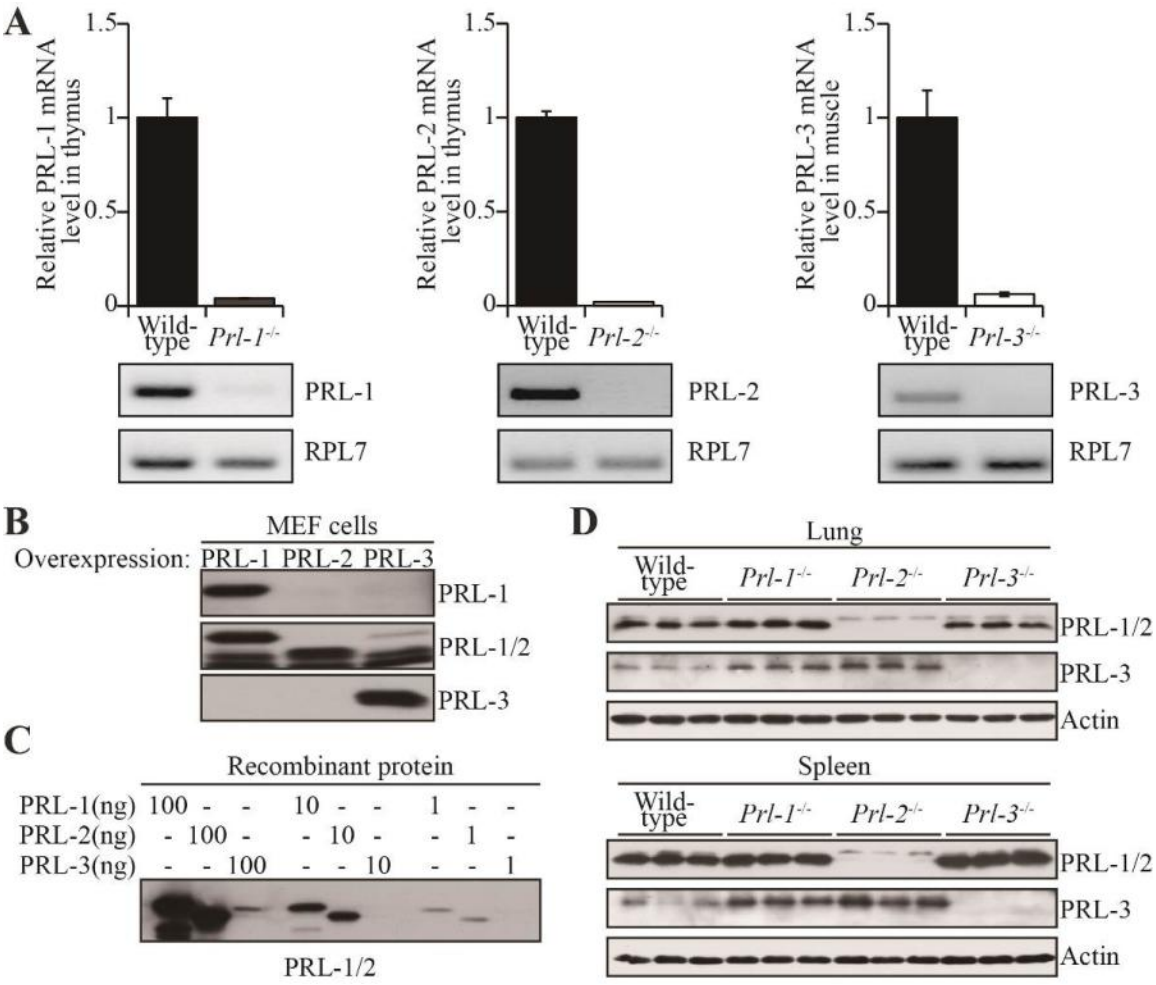


**Figure 20. Gene deletion resulted in knockout of PRLs at both mRNA and protein level.**

**A.** Quantitative RT-PCR analysis was used to detect the deletion of PRL-1 and PRL-2 mRNA from thymus, and to detect the deletion of PRL-3 mRNA from muscle. After RT-PCR, samples were subjected to agarose gel analysis. **B.** The specificity of PRL antibodies were measured by Western blot on cell lysates from MEF cells with overexpression of individual PRLs. PRL-1 antibody only recognizes overexpressed PRL-1; PRL-3 antibody only recognizes overexpressed PRL-3; while PRL-1/2 antibody recognizes overexpressed PRL-1, PRL-2 and PRL-3 (upper bands), as well as endogenous PRL-1 and PRL-2 (lower bands). **C.** Specificity and affinity of PRL-1/2 antibody were determined by detecting recombinant PRL proteins. **D.** Endogenous PRL-1, PRL-2 and PRL3 protein products were determined by Western blot on lung and spleen lysates from wild-type, *Prl-1*-null, *Prl-2*-null or *Prl-3*-null mice.

Then gene knockout at protein level needs to be further validated by Western blot. However, the specificities of commercially available antibodies are not adequate to differentiate individual PRLs due to the highly similar amino acid sequence among all PRLs. I would like to thank Dr. Qi Zeng and her colleagues for generating and kindly sending us PRL-1, PRL-1/2 and PRL-3 antibodies (32). We measured the specificity of these three antibodies by detecting protein lysates from MEF cells individually overexpressing PRL-1, PRL-2 or PRL-3 (Figure 20B). PRL-1 and PRL-3 antibodies specifically recognized PRL-1 and PRL-3, respectively, while PRL-1/2 antibody cross-reacted with all three PRLs with much higher affinity to PRL-1 and PRL-2. To further evaluate the affinity and specificity of PRL-1/2 antibody, different amount of recombinant PRL-1, PRL-2 and PRL-3 proteins were loaded on the gel and then immunoblotted with PRL-1/2 antibody. The results showed that this antibody recognized both PRL-1 and PRL-2 at same level but displayed about 100-fold higher selectivity again PRL-3 (Figure 20C). Since PRL-2 is 6 amino acids shorter than PRL-1, PRL-1/2 antibody is able to distinguish endogenous PRL-1 and PRL-2 with such small difference in molecular weight. Therefore, protein lysates from lung and spleen were assayed for the presence of endogenous PRL-1, PRL-2 and PRL-3 protein product by combining PRL-1/2 antibody and PRL-3 antibody. While detectable in samples from wild-type and *Prl-3* knockout, endogenous PRL-1 and PRL-2 proteins did not exist in *Prl-1*-null and *Prl-2*-null mice, respectively. PRL-3 was detectable in wild-type, *Prl-1*-null and *Prl-2*-null lung and spleen, but not in *Prl-3*-null samples (Figure 20D). Interestingly, deletion of either *Prl-1* or *Prl-2* result in an up-regulation of PRL-3 at the protein level, suggesting that mice evolved a compensatory mechanism among different PRL isoforms to ensure a proper cellular PRL level for its biological function (Figure 20D).

Previous studies have documented that both PRL-1 and PRL-2 were found expressed in almost all organs, and PRL-1 expression level is relatively lower than PRL-2 (14,24,25), whereas PRL-3 is primarily expressed in organs and tissues that contain muscle cells, such as heart and skeletal muscle (14). However, the information gained from these studies may not be accurate due to lack of any negative control. Thus, the knockout mice we generated were perfect negative controls for exploring PRLs gene expression pattern. In addition, the mutant alleles have a LacZ cassette under the endogenous *Prl* promoter, providing a novel opportunity to visualize each PRL transcription in different organs and cell types by detecting LacZ expression. To re-examine the mRNA expression pattern of all PRLs, we assayed many tissue types from wild-type, *Prl-1*$^{-/-}$, *Prl-2*$^{-/-}$ and *Prl-3*$^{-/-}$ mice by LacZ staining. Unfortunately, LacZ signal can only be detected in organs from *Prl-2*$^{-/-}$ and *Prl-3*$^{-/-}$ mice but not *Prl-1*$^{-/-}$ mice, indicating that the LacZ gene inserted in the *Prl-1* locus is inactivated (Figure 21A). Compared to the background staining in wild-type control, *Prl-2*$^{-/-}$ mice displayed dark blue staining in all the organs we surveyed, further demonstrating the broad expression of PRL-2 in different organs and cell types.

In stark contrast to the previous study (14), *Prl-3*$^{-/-}$ mice showed positive staining in many organs including heart (both fetal and adult heart), skeletal muscle, lung and brain (Figure 21A & 21B), indicating a more broader expression pattern of PRL-3, which is consistent with the most recent report by Zimmerman *et al.* (111). Moreover, in contrast to the more uniform staining of PRL-2 in different cell types, the expression pattern of PRL-3 is restricted to specific tissues or cell types, as evidenced by the uneven distribution between cerebral cortex and cerebellum and robust expression in blood vessels between ribs and in the heart (Figure 21B).

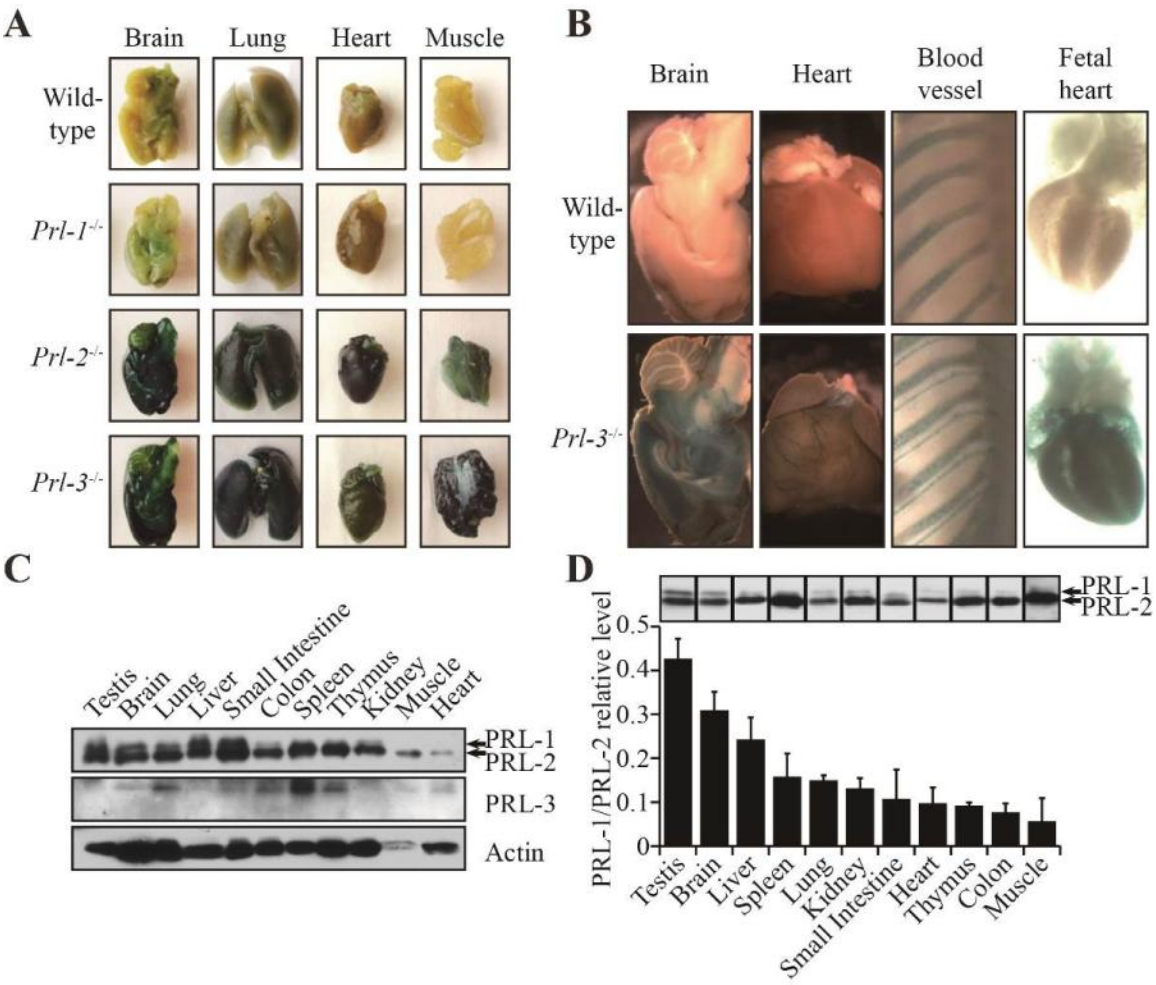


**Figure 21. Gene expression pattern for all PRLs.**

**A.** LacZ staining for different organs from wild-type, *Prl-1*, *Prl-2* or *Prl-3* knockout mice. **B.** Uneven distribution of LacZ staining in brain and blood vessels of *Prl-3*-null mice. **C.** PRL-1, PRL-2 and PRL-3 protein expression pattern in different organs from wild-type mice. **D.** Relative PRL-1/PRL-2 level in different organs of wild-type mice.

Another problem of previous studies is that they only measured the gene expression pattern at mRNA level by Northern blot or *in situ* hybridization. Owing to the low specificity and efficacy of antibodies, endogenous protein expression pattern of PRLs has not been well established. Thanks to our knockout mice for all PRLs, we have demonstrated the specificity of PRL antibodies in detecting endogenous PRL-1, PRL-2 and PRL-3 expression, which gives us strong confidence to measure the protein

expression pattern for all PRLs. Therefore, protein lysates from different organs were subjected to Western blot analysis using PRL antibodies. As shown in Figure 21C, PRL-1 and PRL-2 proteins are broadly expressed in all the organs we assayed. Given the same specificity of the antibody towards PRL-1 and PRL-2, the intensity of PRL-1 band (upper band) and PRL-2 band (lower band) reflects the relative level of endogenous PRL-1 and PRL-2. By comparing different organs, we found that overall PRL-1 protein level is relatively lower than PRL-2 in all organs we measured, from about 40% in testis to about 5% in muscle (Figure 21D). In contrast to the restricted expression pattern of PRL-3 as initial study suggested, we found endogenous PRL-3 protein is expressed in a more ubiquitous manner. As shown in Figure 21C, PRL-3 is detectable not only in heart and muscle as reported before, but also in several other organs such as brain, lung, colon, small intestine, spleen and thymus, which is in line with mRNA expression pattern determined by lacZ staining.

**Table 5. Distribution of offspring by heterozygous-heterozygous mating at weaning.**

| ***Prl-1*** | **+/+** | **+/-** | **-/-** | **n** | $\chi^2$ | ***p*** |
|---|---|---|---|---|---|---|
| Observed | 187 | 353 | 143 | 683 | 6.44 | <0.05 |
| Expected | 171 | 342 | 171 | | | |
| ***Prl-2*** | **+/+** | **+/-** | **-/-** | **n** | $\chi^2$ | ***p*** |
| Observed | 139 | 307 | 73 | 519 | 34.18 | <0.001 |
| Expected | 130 | 260 | 130 | | | |
| ***Prl-3*** | **+/+** | **+/-** | **-/-** | **n** | $\chi^2$ | ***p*** |
| Observed | 111 | 210 | 76 | 397 | 7.50 | <0.05 |
| Expected | 99 | 199 | 99 | | | |

### 4.4.4 Overall phenotypic characterization of *Prl-1*, *Prl-2* and *Prl-3* deficient mice

To characterize potential phenotypes, we first examined the birth rate of these *Prl* deficient mice by analyzing more than 400 pups produced by heterozygous mating for

each gene. Even though all possible genotypes were observed in the resulting offspring, the distribution did not exactly match the expected Mendelian ratios of 1:2:1 (Table 5). Among 683, 519 and 397 pups produced by *Prl-1*, *Prl-2* and *Prl-3* heterozygous mating, only 143, 73 and 76 animals are identified as knockouts. The numbers of knockout offspring are significantly less than the expected number of 170, 130 and 99, suggesting that deletion of individual *Prl* genes indeed causes survival disadvantage. However, further study is required to examine at which stage this partial lethality occurs.

Then, we measured the body weight of more than 20 males and females with different genotypes at weaning (4 weeks old). Even though *Prl-1*$^{-/-}$ and *Prl-3*$^{-/-}$ males did not exhibit a significant decrease in body mass compared to wild-type males, the body weight of *Prl-2*$^{-/-}$ male mice dropped 19 ± 12% (Figure 22A). This phenotype did not have gender differences as evidenced by a 22 ± 19% body weigh decrease in *Prl-2*$^{-/-}$ but not *Prl-1*$^{-/-}$ and *Prl-3*$^{-/-}$ females (Figure 22B). A detailed examination revealed that each organ from *Prl-2*$^{-/-}$ mice weighed below normal. Since the body weight of *Prl-2*$^{-/-}$ mice is also smaller, we normalized organ weights by expressing them relative to body weight in different genotypes, and found a similar organ/whole body weight ratio in lung, liver, thymus, kidney and heart within different genotypes (Figure 22C & 22D). However, testis from *Prl-2*$^{-/-}$ males and spleen from both *Prl-2*$^{-/-}$ males and females remained significantly smaller even when normalized to whole body weight (Figure 22C & 22D), indicating that the development of these organs are affected by deletion of *Prl-2*. Interestingly, the relative brain/body weight ratios of *Prl-2*$^{-/-}$ males and females were larger compared to those of the wild-type controls (Figure 22C & 22D). Histological analysis was performed on tissue sections from different genotypes by hematoxylin and

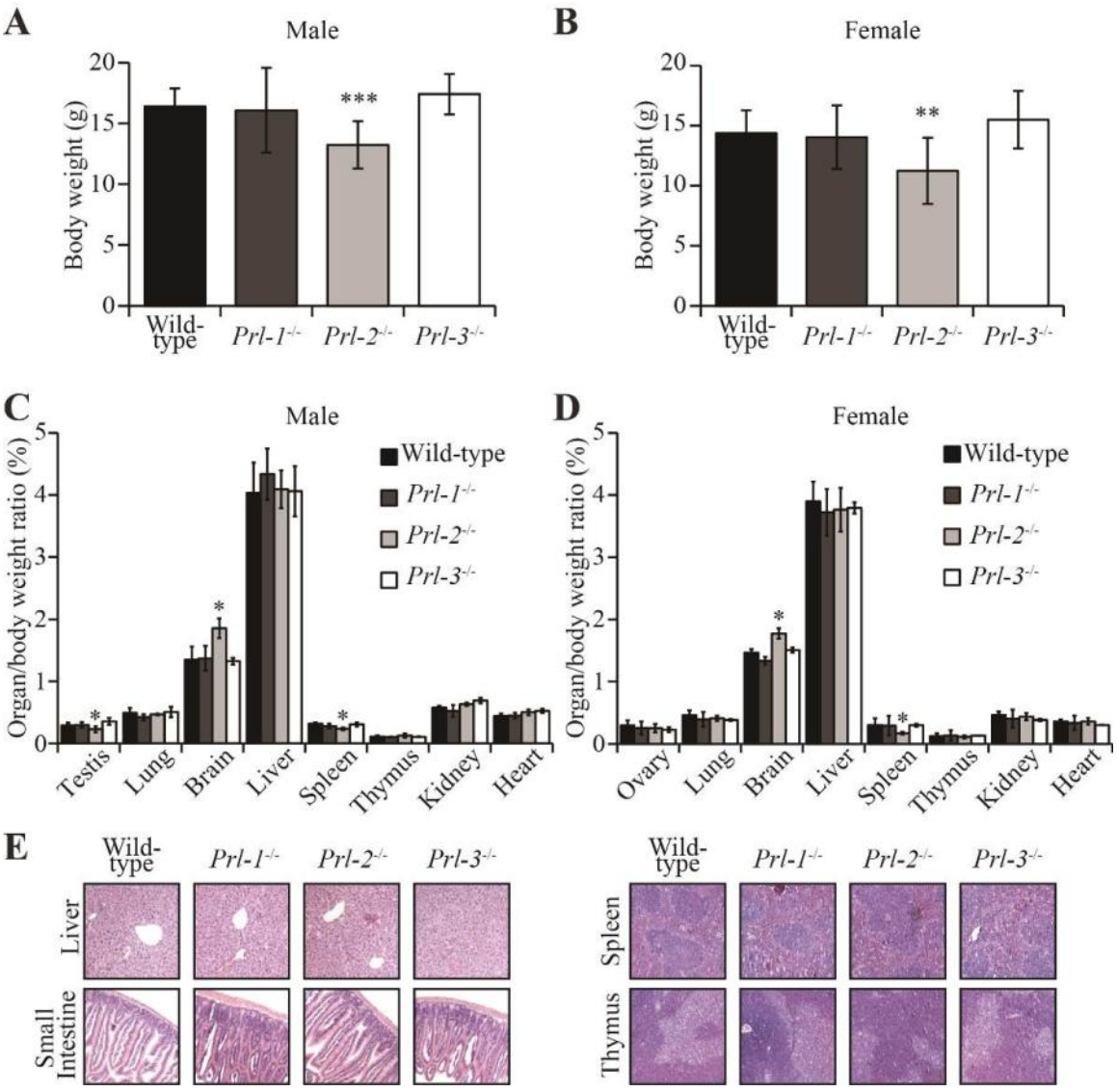


**Figure 22. Overall phenotypic characterization of *Prl-1*, *Prl-2* and *Prl-3* deficient mice.**

**A-B.** Body weights of 4-weeks-old male mice (**A**) or female mice (**B**) with different genotypes were determined. Body weights of *Prl-2*-null males and females were significantly less than those of wild-type, *Prl-1*-null and *Prl-3*-null males and females. **C-D.** Relative organ/body weight ratios of 3-months-old male mice (**C**) or female mice (**D**) were determined. Testis from *Prl-2*-nul males and spleen from both *Prl-2*-null males and females were significantly smaller than those from wild-type, even normalized by body weight. **E.** Histology of liver, small intestine, spleen and thymus from different genotypes were analyzed by H&E staining. No significant histological abnormalities were observed in *Prl-1*, *Prl-2* or *Prl-3* deficient mice.

eosin staining, and no significant abnormalities were observed (Figure 22E). It is noteworthy that despite the significantly smaller spleen/body weight ratio for *Prl-2*$^{-/-}$ mice, the overall histological structure of the *Prl-2* mutant spleen has no appreciable differences in comparison to that of the wild-type animal (Figure 22E).

### 4.4.5 *Prl-2* deletion causes placental insufficiency

Collaborating with Dr. Yuanshu Dong in our lab, we found the growth retardation displayed by *Prl-2*$^{-/-}$ mice starts from newborn mice and maintains throughout their adulthood. Lower weight of *Prl-2*$^{-/-}$ mice at birth suggests growth restriction during embryonic development. To examine whether this smaller body weight can also be observed in embryonic stage, timed mating with *Prl-2* heterozygous males and females was performed and the embryos were harvested at E16.5. As we expected, the weight of *Prl-2*$^{-/-}$ embryos was about 80% of that of the wild-type littermates (Figure 23A & 23B, generated by Yuanshu Dong). In addition, compared to wild-type littermates, the placental weight of the *Prl-2*$^{-/-}$ embryos was also reduced to about 80% (Figure 23A & 23C, generated by Yuanshu Dong), indicating impaired growth and development of both the placenta and embryo in *Prl-2*$^{-/-}$ mice.

Defects in placental development can negatively impact the placenta's ability to transport nutrients, thus leading to restricted fetal growth or even embryonic death (154). HE staining revealed that *Prl-2*$^{-/-}$ placenta had severely reduced decidua and spongiotrophoblast layers (Figure 23D, generated by Yuanshu Dong). Large islands of glycogen cells in spongiotrophoblast layer of wild-type placenta, readily recognizable by their vacuolated appearance, were almost absent in *Prl-2* mutant placenta. In addition, massive invasion of glycogen cells in the decidua layer in wild-type placenta was not

observed in mutant placenta, likely responsible for the lost volume of the decidua layer in *Prl-2* mutant mice (Figure 23D).

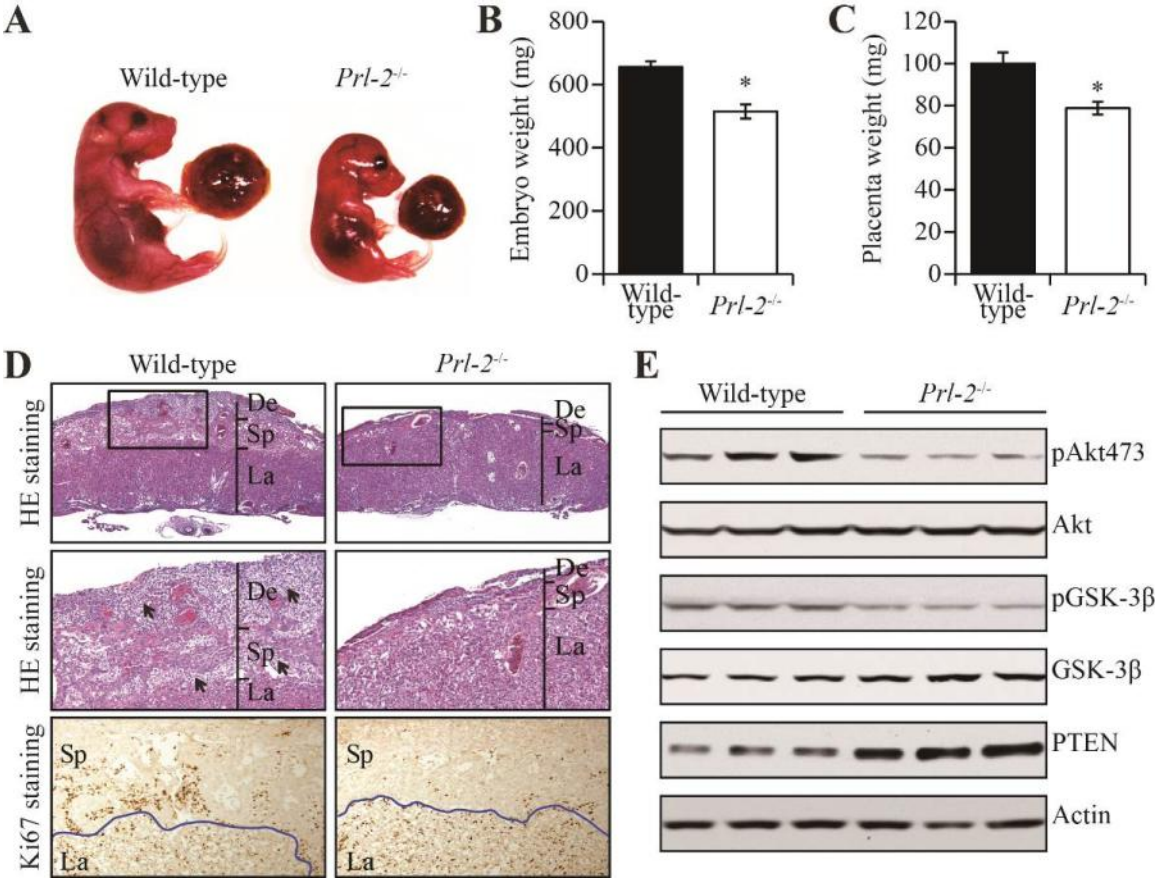


**Figure 23. *Prl-2* deletion causes placental insufficiency.**

**A.** Embryos and their connected placentas of a *Prl-2*$^{-/-}$ mouse and its wild-type littermate at E16.5. **B.** Weight of wild-type and *Prl-2*$^{-/-}$ embryos at E16.5 (n=9 for both genotypes). *P<0.005. **C.** Weight of wild-type and *Prl-2*$^{-/-}$ placentas at E16.5 (n=9 for both genotypes). *P<0.01. **D.** Histological examination of E16.5 placenta sections from *Prl-2*$^{-/-}$ mice and their wild-type littermates. (Upper panel) H&E stain at 25x. (Middle panel) H&E stain at 100x. Aarrowhead showed islands of glycogen cells. (Lower panel) IHC using antibody against Ki67 to monitor proliferating cells. The blue line showed the boundary between labyrinth and spongiotrophoblast layers. De, deciduas; Sp, spongiotrophoblast; La, labyrinth. **E.** Western blot analyses of signaling molecules using tissue lysates derived from *Prl-2*$^{-/-}$ or wild-type placenta. All panels were generated by Yuanshu Dong.

Examination of placenta at different stages further demonstrated that significant loss of spongiotrophoblast and glycogen cells in the spongiotrophoblast layer of *Prl-2*$^{-/-}$ mice occurred at or before E12.5, a time point when the three-layer placenta is just established and glycogen cells start to differentiate (155,156). To determine whether the cell loss in the spongiotrophoblast layer is due to increased apoptosis or decreased proliferation, TUNEL assay and Ki67 staining were performed on wild-type and *Prl-2*$^{-/-}$ placenta at E12.5. While there was no difference in the number of apoptotic cells, marked reduction in the number of proliferating cells was observed in the mutant spongiotrophoblast layer (Figure 23D). Thus decreased cell proliferation may be responsible for the reduced cell number and compromised development of the spongiotrophoblast layer in mutant *Prl-2* placenta.

To define the mechanism by which *Prl-2* deficiency decreases cell proliferation, we analyzed the activation status of several PRL-mediated pathways previously implicated in cell cultures. As shown in Figure 23E (Generated by Yuanshu Dong), Western blot of lysates prepared from wild-type and *Prl-2*$^{-/-}$ placenta showed that Akt phosphorylation is considerably lower in the *Prl-2*$^{-/-}$ samples. Furthermore, decreased phosphorylation of GSK-3β, a well-established Akt substrate, was also evident in mutant *Prl-2* placenta by Western blot (Figure 23E). A decrease in GSK-3β phosphorylation is expected to activate GSK-3β, which in turn will phosphorylate and inhibit glycogen synthase, leading to reduced glycogen production in *Prl-2* mutant placenta. As a key component of PI3K pathway, Akt is repressed by PTEN. To determine whether the decreased Akt phosphorylation in *Prl-2*$^{-/-}$ placenta is due to increased PTEN level, we examined lysates from wild-type and *Prl-2*$^{-/-}$ placenta for PTEN. Consistent with Akt inactivation, deletion of *Prl-2* gave rise to an increase in PTEN in placenta (Figure. 23E).

Taken together, the results suggest that *Prl-2* deficiency impaired placenta development by up-regulation of PTEN and thereby inactivation of Akt.

### 4.4.6 *Prl-2* plays an important role in spermatogenesis

We have mentioned earlier that, even though normalized by body weight, testis weight of *Prl-2*$^{-/-}$ males was still significantly smaller than that of wild-type controls (Figure 22C & 24A, generated by Yuanshu Dong), suggesting *Prl-2* plays a role in spermatogenesis. To determine whether the reduced testis size affects *Prl-2*$^{-/-}$ male reproduction, in collaboration with Dr. Yuanshu Dong, we set up mating cages of wild-type and *Prl-2*$^{-/-}$ males at 3 and 6 months old with wild-type virgin females for 6 consecutive days. While at both ages *Prl-2*$^{-/-}$ males produced similar number of vaginal plugs as the matching wild-type animals, the average litter size derived from *Prl-2*$^{-/-}$ males was smaller than that from females mated to wild-type males (Figure 24B, generated by Yuanshu Dong). Thus, while the sexual drive appeared to be normal, the reproductive ability of the *Prl-2*$^{-/-}$ male was compromised. Sperm counts were next measured to investigate the cause of reduced fertility in *Prl-2*$^{-/-}$ male. Indeed, *Prl-2*$^{-/-}$ epididymis contained significantly fewer spermatozoa than wild-type, especially at 6-month old (Figure 24C, sperm count $(3.1 \pm 1.3) \times 10^6$ for *Prl-2*$^{-/-}$ and $(13.3 \pm 0.6) \times 10^6$ for wild-type, generated by Yuanshu Dong). These results suggest that the impaired reproductive ability of *Prl-2*$^{-/-}$ male is due to lower sperm production.

The structure of *Prl-2*$^{-/-}$ testes was analyzed histologically to explore the cause for the reduced organ size and sperm count. In 6-month old mutant testes, abnormal clusters of cells could be frequently found in the lumen of seminiferous tubules (Figure 24D, generated by Yuanshu Dong). In addition, seminiferous tubules either totally or

partially devoid of germ cells were also observed in 6-month old *Prl-2*$^{-/-}$ testes, indicating a severe cell loss in these tubules (Figure 24D).

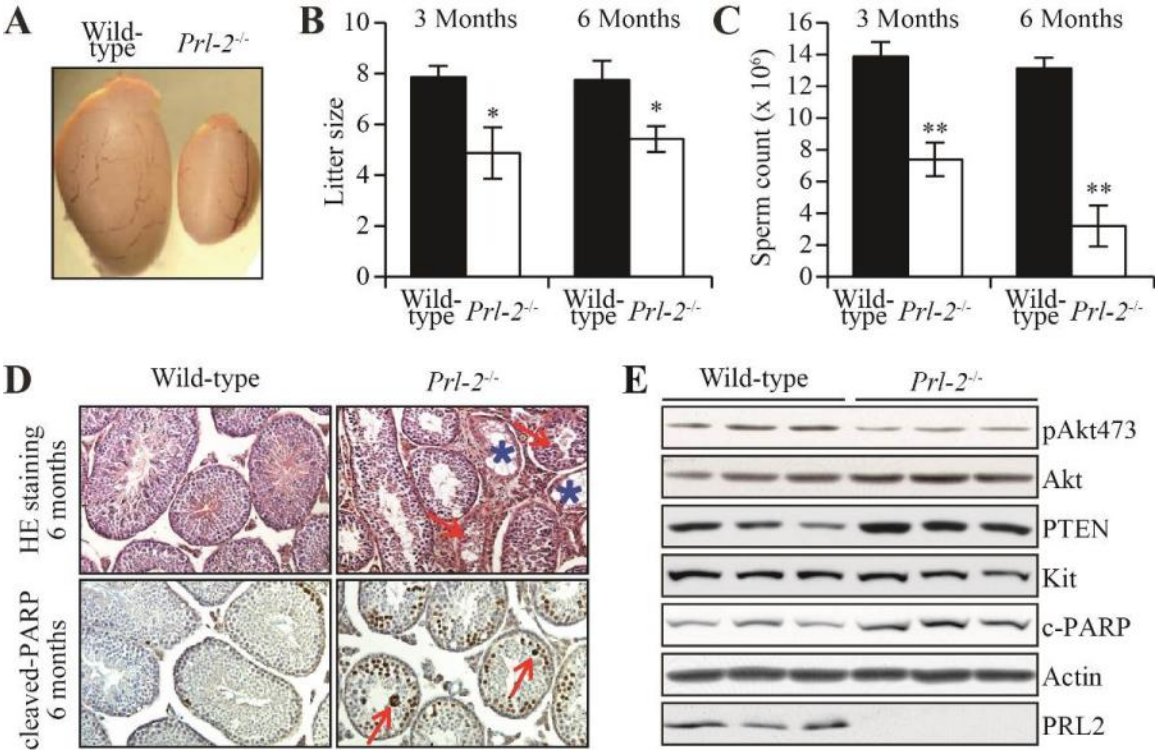


**Figure 24. *Prl-2* plays an important role in spermatogenesis.**

**A.** Picture of testis from wild-type and *Prl-2*$^{-/-}$ littermates at 3 months old. **B.** Mating experiment to assess the reproductive performance of wild-type and *Prl-2*$^{-/-}$ males by litter size. Each male was mated with 4 wild-type virgin females every day for 6 consecutive days. Plugged females were taken out and kept for pregnancy measurement. For 3 months old, WT: n=5, KO: n=8. For 6 months old, n=4 for each genotype. Data represent mean ± SEM. **C.** Sperm counts of wild-type and *Prl-2*$^{-/-}$ mice. Epididymis from one side of mice was removed, minced in BWW buffer, and incubated at 32 °C for 15 min. Sperm suspension was then added to hemocytometer to count total sperm number. n=5 for each genotype at each time point. Data represent mean ± SEM. **D.** Histological examination of testis sections from *Prl-2*$^{-/-}$ mice and their wild-type littermates at 6 months old. (Upper panel) H&E staining. Red arrows show aberrant cell clusters. Blue stars mark empty seminiferous tubules. (Lower panel) IHC with antibody against cleaved-PARP was used to monitor apoptotic cells. Red arrows mark the apoptotic cell cluster. n=3 for each genotype. **E.** Western blot analyses of signaling molecules using germ cells isolated from *Prl-2*$^{-/-}$ or wild-type testis. All panels were generated by Yuanshu Dong.

To determine whether the seminiferous hypocellularity was due to decreased proliferation or increased apoptosis, we performed immunohistological staining for PCNA (Proliferating Cell Nuclear Antigen, a proliferation marker) and cleaved PARP (Poly ADP-Ribose Polymerase, an apoptosis marker) on testis sections of *Prl-2*$^{-/-}$ and wild-type mice at 6 months of age. While the percentage of proliferating cells in the testis was similar between the two genotypes, the number of cleaved PARP positive cells was dramatically increased in the mutant germ cells, indicating that *Prl-2* deficiency primarily impair cell survival (Figure 24D). Thus aberrant germ cell apoptosis provides a potential mechanism to explain the hypotrophy of testis and decreased amount of sperms produced by testis in *Prl-2*$^{-/-}$ mice.

Since SCF-Kit pathway plays an important role in regulating the proliferation and survival of differentiating spermatogonia and spermatocytes, increased apoptosis observed in *Prl-2* deficient testis led us to examine signaling molecules involved in SCF-Kit pathway. Therefore, we isolated germ cells from *Prl-2*$^{-/-}$ and wild-type testis, and evaluated the activation status of Kit downstream molecules. As shown in Figure 24E (Generated by Yuanshu Dong), Akt phosphorylation in *Prl-2*$^{-/-}$ germ cells was only about 50% of that in wild-type, indicating that *Prl-2* deficiency impaired PI3K/Akt activation. To investigate the mechanism by which *Prl-2* attenuates PI3K/Akt activation, we first analyzed Kit expression in both wild-type and *Prl-2*$^{-/-}$ germ cells. No change in Kit expression was observed as a result of *Prl-2* deletion (Figure 24E). In placenta as mentioned previously, *Prl-2* deficiency led to up-regulation of PTEN, an antagonist of PI3K/Akt signaling pathway, and therefore decreased Akt activation. To examine whether this is also the case in testis, we measured PTEN protein level in germ cells isolated from wild-type and *Prl-2*$^{-/-}$ testes. Consistent with our observation in placenta,

PTEN protein level was 1.6 ± 0.3 fold higher in isolated germ cells of *Prl-2*$^{-/-}$ (Figure 24E). Therefore, impaired Akt activation in *Prl-2*$^{-/-}$ germ cells was due to increased PTEN expression, which suppressed Akt phosphorylation. Given the critical role of PI3K/Akt signaling in cell survival, it was not surprising that increased apoptosis, as evidenced by a 1.5 ± 0.2 fold increase in cleaved PARP protein level, was detected in *Prl-2* deficient germ cells (Figure 24E), which is consistent with immunohistochemistry data for cleaved PARP (Figure 24D) in *Prl-2*$^{-/-}$ testes. Together, the data indicate that impaired spermatogenesis in *Prl-2*$^{-/-}$ testis is primarily, if not solely, due to blockage of Kit-PI3K-Akt signaling, as a result of elevated PTEN expression.

### 4.4.7 *Prl-2* is important for hematopoietic stem cell self-renewal

The smaller spleen observed in *Prl-2*-null mice led us to investigate the role of *Prl-2* in hematopoiesis. In collaboration with Dr. Michihiro Kobayashi from Dr. Yan Liu's lab, we performed serial competitive bone marrow transplantation assays to examine whether *Prl-2* deficiency affects hematopoietic stem cell (HSCs) function. Equal numbers of donor and competitor bone marrow mononuclear cells (BMMCs) were transplanted into lethally irradiated recipient mice. Sixteen weeks after primary transplantation, the repopulating ability of *Prl-2*-null cells was significantly lower than wild-type cells (Figure 25A, generated by Michihiro Kobayashi).

To further establish that the self-renewal defect is HSC intrinsic, we purified wild-type and *Prl-2*-null LTHSCs ($CD48^{-}CD150^{+}$KSLs) and transplanted 200 of each into lethally irradiated recipient mice along with 300,000 wild-type competitor BMMCs. In this context, *Prl-2*-null HSCs exhibited a substantially lower contribution to peripheral blood production compared to control HSCs (Figure 25B, generated by

Michihiro Kobayashi), demonstrating that *Prl-2* plays an important role in HSC maintenance and loss of *Prl-2* impairs HSC self-renewal.

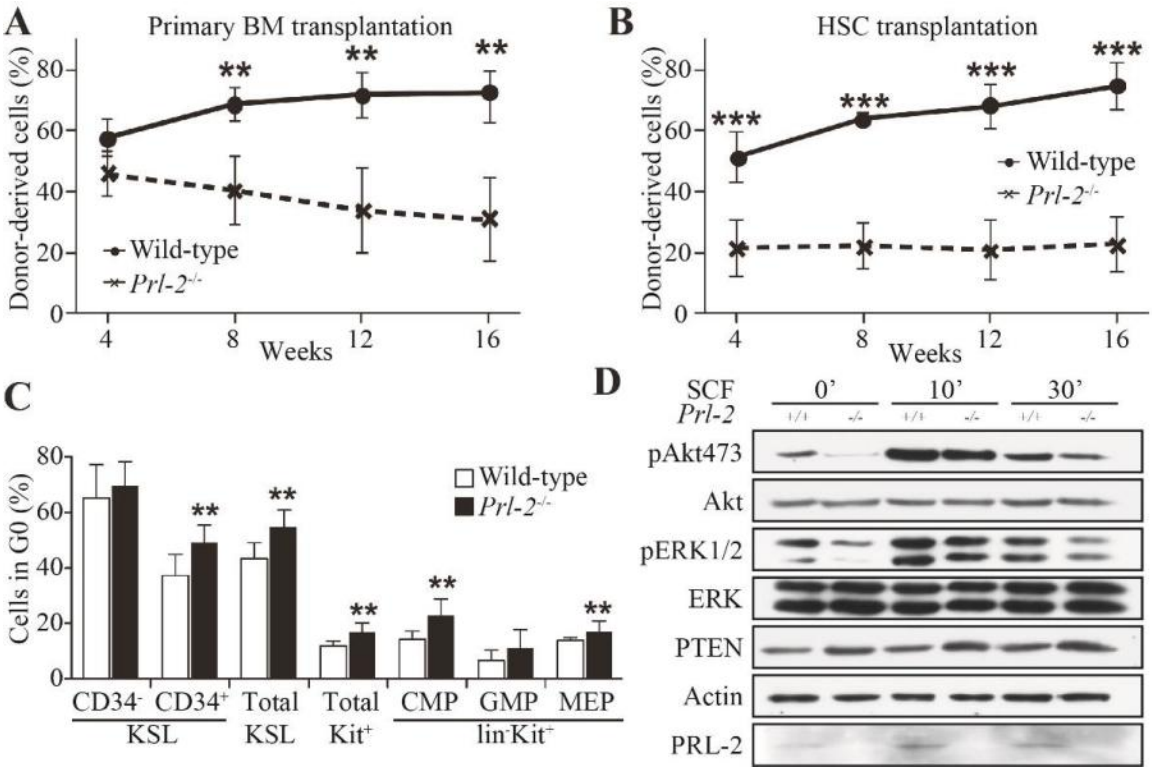


**Figure 25. *Prl-2* is important for hematopoietic stem cell self-renewal.**

**A.** Lethally irradiated recipient mice ($CD45.1^+$ and $CD45.2^+$) were transplanted with $5\times10^5$ bone marrow mononuclear cells (BMMCs) from wild-type and *Prl-2*-null mice ($CD45.2^+$) plus $5\times10^5$ competitor cells ($CD45.1^+$) in competitive repopulation assays. Graph shows the mean percentage (±SD) of donor-derived ($CD45.2^+$) cells in the peripheral blood post-transplantation, measured at monthly intervals. n=7 for each genotype. **B.** Lethally irradiated recipient mice ($CD45.1^+$ and $CD45.2^+$) were transplanted with 200 LT-HSCs ($CD48^-CD150^+$KSLs) from wild-type and *Prl-2*-null mice ($CD45.2^+$) plus $3\times10^5$ competitor cells ($CD45.1^+$) in competitive repopulation assays. Graph shows the mean percentage (±SD) of donor-derived ($CD45.2^+$) cells in the peripheral blood post-transplantation, measured at monthly intervals. n=7 for each genotype. **C.** Cell-cycle analysis of hematopoietic stem and progenitor cells was performed by staining with DAPI and Ki67 and analyzed by FACS. Data shown are the mean values ± SD. n=6 for each genotype. **D.** Western blot analysis of signaling molecules in wild-type and *Prl-2*-null $Kit^+$ cells following SCF stimulation. Panel A, B and C werer generated by Michihiro Kobayashi.

To assess the effect of *Prl-2* deficiency on proliferation, we stained *Prl-2*-null hematopoietic stem and progenitor cells with proliferation marker Ki67. While we detected normal number of Ki67 negative LT-HSCs, we found more Ki67 negative multipotent progenitor cells (MPPs) than normal (Figure 25C, generated by Michihiro Kobayashi), indicating that *Prl-2* null MPPs are more quiescent and less proliferative.

SCF/Kit signaling pathway is not only critical for germ cell survival, but also plays an important role in hematopoietic stem and progenitor cells maintenance. To decipher the molecular mechanisms underlying the HSPC proliferation defects seen in the *Prl-2*-null mice, we examined basal and SCF stimulated activation of Akt and ERK signaling in $Kit^+$ cells. We observed that the levels of pAkt473 and pERK1/2 are significantly lower in *Prl-2*-null $Kit^+$ cells compared with those in wild-type cells in the basal state (Figure 25D). *Prl-2*-null cells also displayed decreased activation of both pAkt and pERK1/2 at 30 minutes following SCF stimulation (Figure 25D), demonstrating that PRL-2 is important for sustaining SCF signaling in hematopoietic stem and progenitor cells.

To investigate the mechanism by which *Prl-2* deficiency attenuates Akt and ERK activation, we analyzed PTEN expression in both wild-type and *Prl-2*-null cells. PTEN is an antagonist of PI3K signaling pathway. In addition, PTEN has also been shown to negatively regulate the activation of the ERK pathway (157). We have shown that *Prl-2* deficiency led to elevated PTEN expression in both placenta and testis. We measured PTEN protein level in wild-type and *Prl-2*-null $Kit^+$ cells. As shown in Figure 25D, PTEN expression was $1.4 \pm 0.15$ fold higher in *Prl-2*-null samples. Therefore, the data indicated that impaired HSPC proliferation in the *Prl-2*-null mice is likely due to elevated PTEN expression, resulting in defect of SCF/Kit signaling transduction.

### 4.4.8 PRL-2 negatively regulates PTEN stability

Western blot of samples from placenta, testis and HSC suggested that loss of *Prl-2* elevated PTEN level. It was further evidenced by the down-regulation of PTEN as well as a higher basal Akt phosphorylation in HEK293 cells stably expressing FLAG-tagged PRL-2 (Figure 26A, generated by Yuanshu Dong). To determine whether PRL-2 affects PTEN protein stability, PRL-2 transfected or control HEK293 cells were treated with cycloheximide, which blocks protein synthesis. As shown in Figure 26B (Generated by Yuanshu Dong), PRL-2 overexpression promotes PTEN degradation, reducing its half-life from more than 36 hrs to around 10 hrs (Figure 26B). Treatment with 20 μM of the proteasome inhibitor MG132 did not significantly affect PTEN level in control cells, but did potently increase PTEN in PRL-2 expressing cells (Figure 26B), indicating that PRL-2 increases PTEN degradation through the proteasomal pathway. To further validate this, we generated GC-1 cell lines stably overexpressing Flag-tagged PRL-2. GC-1 cell was derived from mouse spermatogonia (158), which is physiologically relevant to the testis study. As shown in Figure 26C, increased PRL-2 expression (1-2-fold over endogenous PRL-2) in GC-1 cell lines results in 28 ± 5% reduction in PTEN level compared with the GC-1 vector control cells. Accordingly, PI3K/Akt signaling was activated, as evidenced by the 3.0 ± 0.3-fold increase in Akt phosphorylation in PRL-2 overexpressing GC-1 cells. To determine whether PRL-2 also controls PTEN at the level of protein stability as we had observed in HEK293 cells, GC-1 cells were treated with the protein synthesis inhibitor cycloheximide. As expected, PRL-2 overexpression promotes PTEN degradation, and reduces PTEN's half-life from much greater than 30 hrs to 24 hrs in GC-1 cells (Figure 26D). Thus, PRL-2 overexpression activates PI3K/Akt signaling by destabilizing PTEN in both HEK293 cells and GC-1 cells.

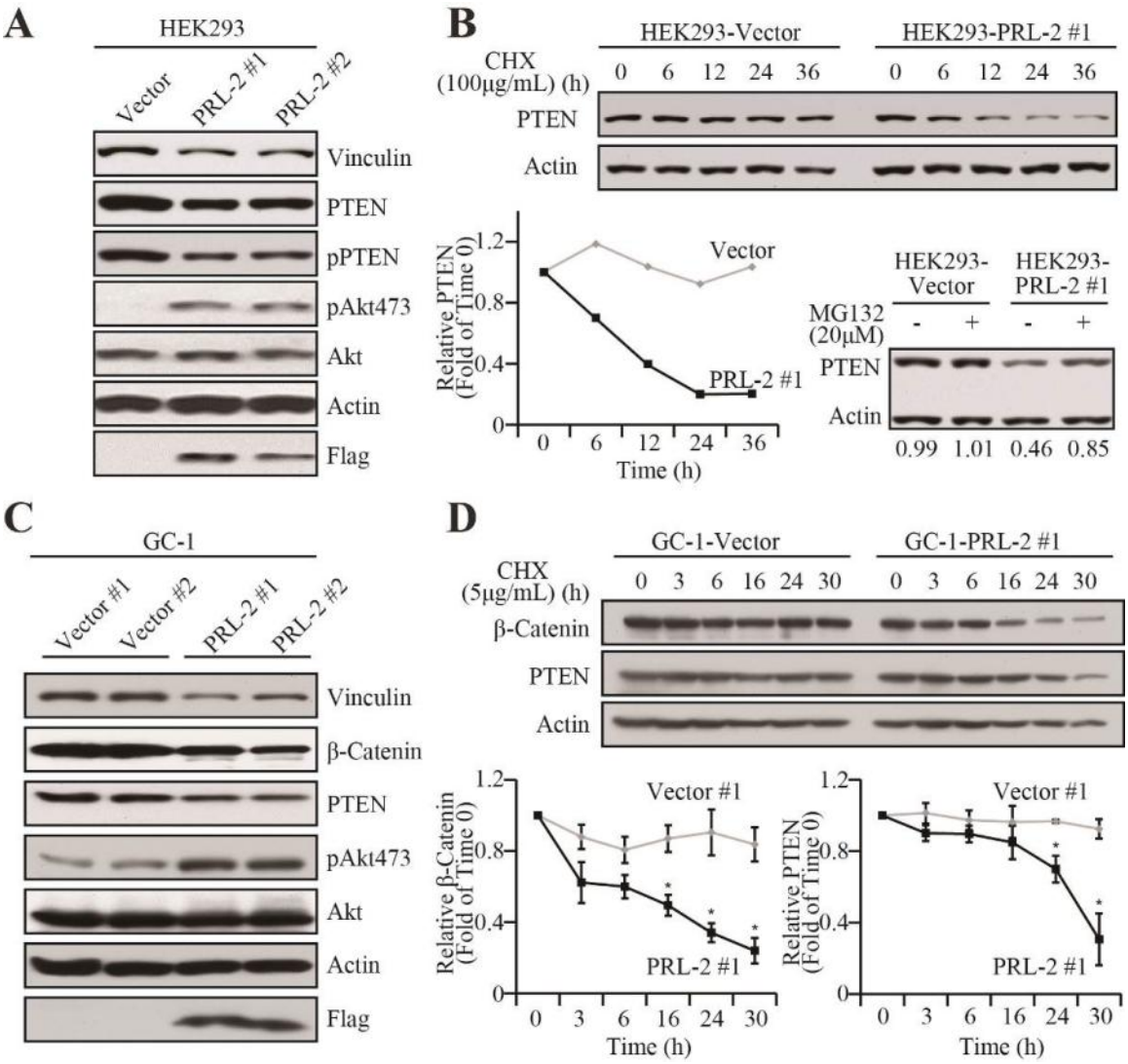


**Figure 26. PRL-2 negatively regulates PTEN stability.**

**A.** Western blot analysis of signaling molecules on cell lysates from PRL-2-HEK293 or vector control cells. **B.** PRL-2 negatively regulates PTEN stability in HEK293 cells. (Upper panel) Cycloheximide chase experiment. PRL-2-HEK293 stable cell line and its vector control were treated with cycloheximide (CHX) at 100 μg/mL, and cell lysates were then analyzed for PTEN and actin protein levels by Western blot. (Lower left panel) Quantitation of the cycloheximide chase experiment results. PTEN and actin signals were measured using ImageJ, and ratios of PTEN/actin were determined for each sample. The ratios were then calculated as folds of time 0 for each cell line as plotted. (Lower right panel) PRL-2-HEK293 cell line and its vector control were treated with 20 μM MG132 for 6 hrs. Cells were lysed and PTEN and actin protein levels analyzed by Western blot. **C.** Western blot analysis of signaling molecules on cell lysates from PRL-2-GC-1 or vector control cells. **D.** PRL-2 negatively regulates PTEN stability in

GC-1 cells. (Upper panel) Cycloheximide chase experiment. PRL-2-GC-1 stable cell line and its vector control were treated with cycloheximide (CHX) at 5 μg/mL, and cell lysates were then analyzed for PTEN, β-Catenin and actin protein levels by Western blot. (Lower panel) Quantitation of the cycloheximide chase experiment results. PTEN, β-Catenin and actin signals were measured using ImageJ, and ratios of PTEN/actin and β-Catenin/actin were determined for each sample. The ratios were then calculated as folds of time 0 for each cell line as plotted. Panel A and B were generated by Yuanshu Dong.

Phosphorylation of PTEN at Ser380, Thr382 and Thr383 enhances PTEN stability by protecting it from the proteasome-mediated degradation (159). Since PRL-2 is a protein phosphatase, we tested the hypothesis that PRL-2 destabilizes PTEN by removing phosphates from these sites. We analyzed PTEN phosphorylation at the S380/T382/T383 cluster and the total PTEN protein in vector control and PRL-2 expressing cells (Figure 26A). The ratios of phospho-PTEN/total PTEN were found to be constant as the levels of PRL-2 varied. Thus it appears that PRL-2 does not control PTEN phosphorylation at these sites.

One mechanism by which PTEN protein could be stabilized is through formation of a complex with MAGI2 and β-Catenin at the adherens junctions, which prevents PTEN from degradation (84). The adherens junctions component Vinculin plays an important role in maintaining the stability of the complex, because the complex is disrupted and PTEN level is reduced in cells lacking Vinculin. This led us to examine whether PRL-2 altered the expression of Vinculin. Lysates from vector and PRL-2 transfected cells were analyzed for Vinculin by Western blot. The results showed that Vinculin is down-regulated in PRL-2 over-expressing HEK293 cells (Figure 26A). Thus, one mechanism by which PRL-2 down-regulates PTEN may be through suppressing

Vinculin expression, which destabilizes PTEN by disrupting PTEN-MAGI-2-β-Catenin complex.

In line with this observation, we found that Vinculin expression decreased 41 ± 13% in PRL-2 overexpressing GC-1 cells (Figure 26C). Moreover, β-Catenin expression was also reduced by 29 ± 13% upon increased PRL-2 expression (Figure 26C). These observations support the notion that PRL-2 down-regulates PTEN via inhibition of Vinculin and β-Catenin expression, which likely leads to disruption of the PTEN-MAGI2-β-Catenin complex and exposes PTEN for degradation. Interestingly, the rate of β-Catenin degradation was also increased in PRL-2-overexpressing GC-1 cells (Figure 26D). More importantly, it appears that β-Catenin degradation ($t_{1/2}$ 16 h) precedes that of PTEN, indicating that the disassembly of the PTEN-MAGI2-β-Catenin complex may be responsible for PTEN degradation. Taken together, these results are in agreement with studies in HEK293 cells overexpressing PRL-2 and suggest that PRL-2 functions to destabilize the PTEN-MAGI2-β-Catenin complex to down-regulate PTEN, leading to enhanced PI3K/Akt signaling.

**4.5 Discussion**

Despite the apparent implication of PRLs in tumorigenesis and metastasis by plenty of information derived from cell culture, it is still unclear about the physiological function of these enzymes in mammals due to the absence of informative animal models. To establish the *in vivo* functions of all *Prls*, we sought to delete the three *Prls* individually in a mouse model. *Prl-1* and *Prl-2* knockout mouse lines were generated by the gene-trapping technology, while systemic deletion of *Prl-3* in mice was achieved by homologous recombination in ES cells. Deletion of PRL proteins was confirmed by quantitative RT-PCR using spleen mRNA, and Western blot analysis using lung and

spleen lysates from wild-type, *Prl-1*, *Prl-2* and *Prl-3*-null mice. A thorough examination on protein expression pattern of each PRL was performed by Western blot. As previous studies suggested, both PRL-1 and PRL-2 are broadly expressed in different organs in spite of relative lower expression level of PRL-1 than PRL-2. However, compared to the restricted expression pattern of PRL-3 in heart and skeletal muscle as suggested by previous report by Northern blot (14), we found a more ubiquitous protein expression pattern of PRL-3 in multiple organs including brain, lung, colon, small intestine, spleen, thymus, skeletal muscle and heart, which is consistent with recent studies by Zimmerman *et al.* (26,111).

Even though mice with deletion of each *Prl* genes are viable, the birth rate of these knockouts are significantly lower than the predicted Mendelian ratios, suggesting that all *Prl* genes are important for normal development, and deficiency of individual *Prl* genes causes partial perinatal lethality. While the body weights of *Prl-1* and *Prl-3*-null mice are comparable with their wild-type littermates, *Prl-2* knockouts are significantly smaller, suggesting a growth retardation phenotype in these animals with *Prl-2* deletion. Further investigation demonstrated that the smaller body weight of *Prl-2*-null embryo is due to impaired placental development as evidenced by thinner decidua and spongiotrophoblast layers and less glycogen cells observed in the placenta of *Prl-2*-null mice. Significantly decreased proliferation contributes to the loss of glycogen cells in the spongiotrophoblast layer. Normal placental development is essential for transporting nutrients, while impaired placenta function will lead to restricted fetal growth or even embryonic death (154). Furthermore, a careful anatomical examination revealed that testis and spleen from *Prl-2*-null mice were significantly smaller than those from wild-type mice, suggesting that PRL-2 may play important roles in spermatogenesis and

hematopoiesis. As expected, deletion of *Prl-2* causes impaired spermatogenesis and insufficient hematopoiesis due to increased germ cells apoptosis and decreased hematopoietic stem cell self-renewal, respectively. These developmental defects resulting from lack of *Prl-2* are in accordance with the oncogenic role of excess PRL-2 in tumorigenesis. However, these phenotypes were not observed in *Prl-1* or *Prl-3* mice, suggesting a possible compensation from more abundantly expressed PRL-2. Thus, it is interesting to generate and characterize *Prl-1*/*Prl-2*, *Prl-1*/*Prl-3* and *Prl-2*/*Prl-3* double knockout or even *Prl-1*/*Prl-2*/*Prl-3* triple knockout mice (see details in Chapter 5).

The mouse models with deficiency of each *Prl* genes are useful tools not only for studying the phenotypic alterations in the absence of each gene, but also for investigating the underlying mechanism of PRL actions. At the molecular level, these three defects observed in *Prl-2*-null mice converged to impaired PI3K/Akt signaling pathways, as evidenced by the lower basal Akt phosphorylation in placenta tissue, isolated germ cells and hematopoietic stem and progenitor cells from *Prl-2* deficient mice. The impaired PI3K/Akt activation in these samples is attributed to increased PTEN level in the absence of *Prl-2*, which is in agreement with cell based experiments that PRL-2 overexpression activates PI3K/Akt signaling by down-regulating PTEN. Mechanistically, PRL-2 negatively regulates PTEN protein level by destabilizing the PTEN-MAGI2-β-Catenin complex thereby exposing PTEN for degradation. It is in need of further investigation on how PRL-2 destabilizes the complex.

## CHAPTER 5: THE ROLE OF PRL-1 IN SPERMATOGENESIS

### 5.1 Overview

PRLs play a positive role in cell signaling events and are suggested as oncogenes and therapeutic targets in several cancers (152,153). Overexpression of PRLs was frequently found in tumor cell lines, and cells expressing high levels of PRLs exhibited enhanced proliferation, anchorage-independent growth, cell migration and invasion (11,12,69,86,95,96). Clinically, up-regulation of PRLs has been observed in many types of advanced stage tumors as well as metastatic lesions (153). It has been suggested that PRLs promote cell proliferation and migration through activation of several signaling pathways, including the Rho family of small GTPases, Src, ERK1/2, and PI3K (16,59,79,86,137). PRLs are strongly implicated as a driving force in malignancy, but limited knowledge is available regarding the exact physiological function(s) of these phosphatases. Our current understanding of PRLs came primarily from observations in clinical patient samples or cell culture models either overexpressing or silencing PRLs. To define the biological function of the PRLs, we generated PRL-1, PRL-2, and PRL-3 knockout mice (see details in Chapter 4) to study the effects of PRL deletion in the animal model.

### 5.2 Hypothesis and Specific Aims

We previously reported that *Prl-2* deficiency causes growth retardation in both embryos and adult mice due to placenta insufficiency (80), and that *Prl-2* deletion impairs male reproductive ability resulting from deficient spermatogenesis (81), and that deficiency of *Prl-2* led to insufficient hematopoiesis (83). Biochemically, all three phenotypes are caused by Akt inactivation as a result of up-regulation of the tumor suppressor PTEN in *Prl-2*$^{-/-}$. However, *Prl-1* deficient mice were viable, normally

developed and did not reveal any obvious phenotypic alteration compared to normal mice.

Since PRL-1 and PRL-2 share high amino acid sequence identity and similar tissue distribution in whole body and PRL-1 protein level is always lower than PRL-2, it is highly possible that PRL-2 can compensate for the loss of *Prl-1*. To further investigate the physiological role of PRL-1, I proceeded to generate *Prl-1*/*Prl-2* double knockout mice. Unfortunately, *Prl-1/Prl-2* double knockout is embryonic lethal. During this process, however, *Prl-1*$^{-/-}$/*Prl-2*$^{+/-}$ and *Prl-1*$^{+/-}$/*Prl-2*$^{-/-}$ mice were also generated and they were found to be viable and already show much severe testis phenotype compared to *Prl-1*$^{-/-}$ and *Prl-2*$^{-/-}$ mice, respectively. Similar to *Prl-2*$^{-/-}$, *Prl-1*$^{-/-}$/*Prl-2*$^{+/-}$ male mice also have impaired reproductive ability. More strikingly, *Prl-1*$^{+/-}$/*Prl-2*$^{-/-}$ male mice are completely sterile. Based on these observations, I hypothesized that **PRL-1 plays an important role in spermatogenesis**. I have two specific aims to test this hypothesis: 1) to characterize the testis phenotype, and to measure the reproductive function of *Prl-1*$^{-/-}$/*Prl-2*$^{+/-}$ and *Prl-1*$^{+/-}$/*Prl-2*$^{-/-}$ male mice; and 2) to elucidate the mechanism by which deletion of one additional *Prl-1* allele in the *Prl-2*$^{-/-}$ mice results in male sterility. These investigations are the first to definitively examine the role of PRL-1 in a knockout mouse model, and will provide the first *in vivo* evidence of an important role of PRL-1 in male reproductive system.

## 5.3 Materials and Methods

### 5.3.1 Generation of *Prl-1*$^{-/-}$/*Prl-2*$^{+/-}$ and *Prl-1*$^{+/-}$/*Prl-2*$^{-/-}$ mice

Generation and genotyping of *Prl-1*$^{-/-}$ and *Prl-2*$^{-/-}$ mice were previously described (Chapter 4, and Figure 19A). We obtained *Prl-1*$^{-/-}$/*Prl-2*$^{+/-}$ and *Prl-1*$^{+/-}$/*Prl-2*$^{-/-}$ mice by crossing the *Prl-1*$^{+/-}$/*Prl-2*$^{+/-}$ males with females. Mice used in this study were all on a

C57BL6/129P2 mixed genetic background. Experiments on mice were carried out in accordance with the regulations of The Institutional Animal Care and Use Committees at Indiana University.

### 5.3.2 Reproductive performance evaluation

Age matched wild-type, *Prl-1*$^{-/-}$, *Prl-2*$^{-/-}$, *Prl-1*$^{-/-}$/*Prl-2*$^{+/-}$ and *Prl-1*$^{+/-}$/*Prl-2*$^{-/-}$ males were each mated with 4 wild-type virgin females every day for 6 consecutive days. Vaginal plugs were monitored every morning, and plugged females were removed and replaced with virgin females. After 6 days, the total number of females plugged by each male was counted. Plugged females were kept for an additional month to determine the number of pregnant mice and their litter sizes. The percentage of pregnant mice among the plugged and the average litter size were calculated for each male.

### 5.3.3 Sperm Count

Caudal epididymis were isolated from age-matched male mice with different genotypes, minced in 10 mL BWW buffer (NaCl 5.54 g/L, KCl 0.356 g/L, $CaCl_2$•$2H_2O$ 0.250 g/L, $KH_2PO_4$ 0.162 g/L, $MgSO_4$•$7H_2O$ 0.294 g/L, $NaHCO_3$ 2.1 g/L, glucose 1.0 g/L, Sodium pyruvic acid 0.03 g/L, BSA 3.5 g/L), and incubated at 32 °C for 15 min. After mixed by pipetting, the motile and total sperm numbers were counted using hemocytometer.

### 5.3.4 Histology

Tissues were fixed in 4% paraformaldehyde (PFA) overnight at 4 °C, embedded in paraffin, serially sectioned (7 μm), and stained with H&E according to standard methods. For immunohistochemistry, de-paraffined and hydrated sections were subjected to antigen retrieval by boiling in 10 mM sodium citrate for 20 min. Sections were then incubated with diluted antibodies (1:50 – 1:400) at 4 °C overnight. Signals

were detected by VECTASTAIN Elite ABC kit and developed using DAB substrate from Vector laboratory (Burlingame, CA). Antibodies used were PLZF, Kit (Santa Cruz Biotechnology, CA), Vimentin, PCNA and cleaved PARP (Cell Signaling Technology, MA). Images were captured on a Leica DM2500 stereomicroscope. All images are representative of at least 3 samples.

### 5.3.5 Western blot analysis

Testes were lysed in lysis buffer supplied with phosphatase and protease inhibitor mixture (Roche Applied Science). Equal amounts of protein were resolved by SDS-PAGE, transferred to nitrocellulose membrane and subjected to immunoblotting. Anti-PRL-1/2 antibody was kindly provided by Dr. Qi Zeng. All other antibodies were from Cell Signaling Technology.

### 5.3.6 Statistical analysis

All statistical significant differences were calculated using student's t-test and represented by asterisks: $*P<0.05$, $**P<0.01$, $***P<0.001$.

## 5.4 Results

### 5.4.1 Generation and characterization of *Prl-1*$^{-/-}$/*Prl-2*$^{+/-}$ and *Prl-1*$^{+/-}$/*Prl-2*$^{-/-}$ mice

As I mentioned earlier, *Prl-1*$^{-/-}$ mice are viable and have no obvious phenotypic alterations compared to wild-type mice. In contrast, we have reported that *Prl-2* deficient mice showed growth retardation, impaired spermatogenesis and insufficient hematopoiesis (80,81,83). PRL-1 and PRL-2 share 86% amino acid sequence identity, and both PRL-1 and PRL-2 are broadly expressed in almost all organs, suggesting that PRL-1 and PRL-2 may have similar function. However, PRL-1 expression level is relatively lower than PRL-2, indicating that *Prl-2* could potentially compensate for *Prl-1* deficiency. Interestingly, relative PRL-1/PRL-2 protein level is significantly higher in

testis compared to all other organs, implicating that PRL-1 may also play a role in testis function (Figure 21D).

**Table 6. Distribution of offspring by double heterozygous-double heterozygous mating at weaning.**

| ***Prl-1*** | **+/+** | | | **+/-** | | | **-/-** | | | **n** | **$\chi^2$** | ***p*** |
|---|---|---|---|---|---|---|---|---|---|---|---|---|
| ***Prl-2*** | **+/+** | **+/-** | **-/-** | **+/+** | **+/-** | **-/-** | **+/+** | **+/-** | **-/-** | | | |
| Observed | 22 | 56 | 30 | 54 | 110 | 27 | 18 | 35 | 0 | 352 | 45.10 | <0.001 |
| Expected | 22 | 44 | 22 | 44 | 88 | 44 | 22 | 44 | 22 | | | |

To test whether *Prl-2* indeed compensates for loss of *Prl-1* and whether both PRL-1 and PRL-2 were required for spermatogenesis, we tried to generate *Prl-1*/*Prl-2* double knockout mice by crossing *Prl-1*/*Prl-2* double heterozygous males with females. We analyzed more than 300 pups, but none of them were double knockouts, suggesting that mice with both *Prl-1* and *Prl-2* deletion are embryonic lethal (Table 6). We made a lot of efforts to investigate at which stage the embryos are dead, and expected to isolate MEF cells from the double knockout embryos. However, we are still unable to get double knockout as early as embryo stage E9.5 days, indicating loss of both *Prl-1* and *Prl-2* results in early embryonic lethality. Fortunately, *Prl-1*$^{+/-}$/*Prl-2*$^{-/-}$ mice and *Prl-1*$^{-/-}$ /*Prl-2*$^{+/-}$ mice are viable, even though they displayed survival disadvantage as evidenced by the reduced birth rate (Table 6). PCR analysis was used to determine the deletion of *Prl-1* and *Prl-2* alleles (Figure 27A). Deletion of PRL protein products were determined by Western blot on lung lysates from mice with different genotypes using PRL-1/2 antibody (Figure 27B). To characterize the overall phenotypic changes, we first measured the body weight of more than 20 4-weeks-old males and females with different genotypes. As mentioned earlier, *Prl-2*$^{-/-}$ mice exhibited a roughly 20% decrease in body weight compared with wild-type and *Prl-1*$^{-/-}$ mice. More strikingly, the body weights of

*Prl-1*$^{-/-}$/*Prl-2*$^{+/-}$ and *Prl-1*$^{+/-}$/*Prl-2*$^{-/-}$ male mice decreased 38 ± 13% and 41 ± 10% compared with that of wild-type males, and 23 ± 16% and 27 ± 12% compared to the body weights of *Prl-2*$^{-/-}$ males. Similarly, body weights of *Prl-1*$^{-/-}$/*Prl-2*$^{+/-}$ and *Prl-1*$^{+/-}$ /*Prl-2*$^{-/-}$ female were also decreased 30 ± 13% and 26 ± 14% compared to wild-type females. However, even though *Prl-1*$^{-/-}$/*Prl-2*$^{+/-}$ and *Prl-1*$^{+/-}$/*Prl-2*$^{-/-}$ females are also smaller than *Prl-2*$^{-/-}$ females, no significant difference was observed (Figure 27C & 27D). More data points are needed to establish statistical significance.

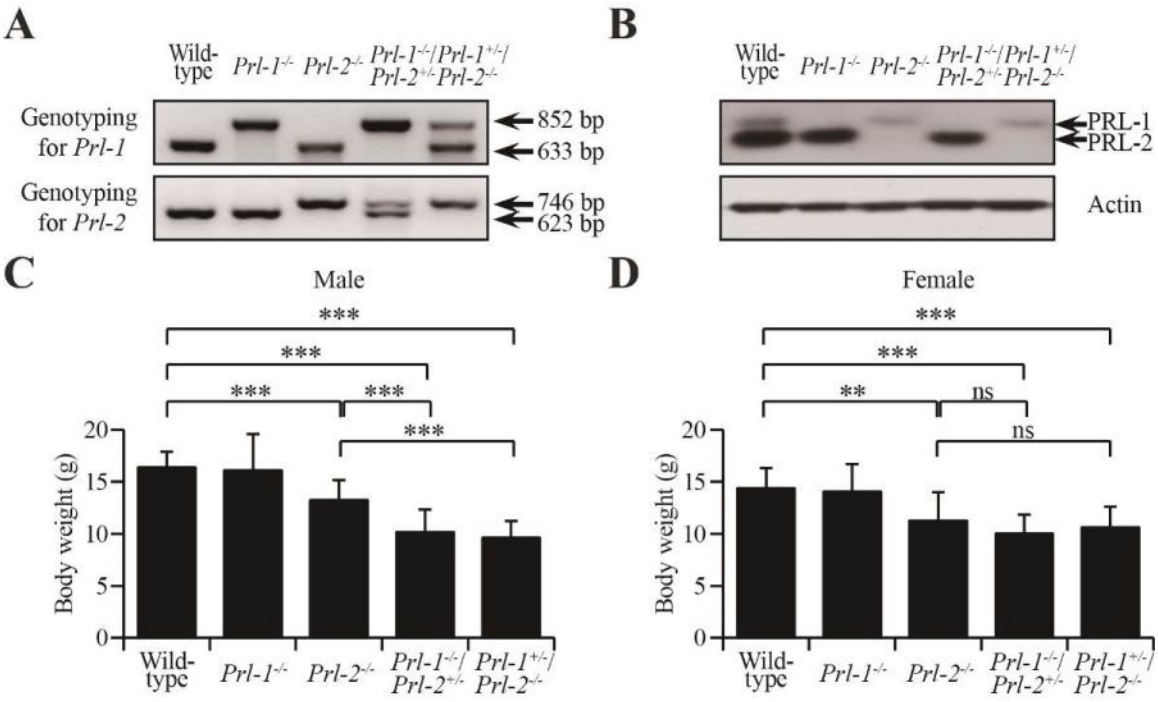


**Figure 27. Generation of *Prl-1*$^{-/-}$/*Prl-2*$^{+/-}$ and *Prl-1*$^{+/-}$/*Prl-2*$^{-/-}$ mice.**

**A.** PCR strategy for genotyping using mouse tail DNA. **B.** Endogenous PRL-1 and PRL-2 protein products were determined by Western blot on lung lysates from different genotypes. **C-D.** Body weights of 4-weeks-old male mice (**C**) or female mice (**D**) with different genotypes were determined. Body weights of *Prl-2*$^{-/-}$, *Prl-1*$^{-/-}$/*Prl-2*$^{+/-}$ and *Prl-1*$^{+/-}$/*Prl-2*$^{-/-}$ males and females were significantly less than those of wild-type and *Prl-1*$^{-/-}$ males and females. Body weights of *Prl-1*$^{-/-}$/*Prl-2*$^{+/-}$ and *Prl-1*$^{+/-}$/*Prl-2*$^{-/-}$ males were also significantly less than those of *Prl-2*$^{-/-}$ males.

### 5.4.2 *Prl-1* is essential for male reproductive ability

In order to evaluate the physiological function of PRL-1 in testis development, anatomical examination was performed on adult males with different genotypes. Our previous study (81) revealed that the testis of *Prl-2* null mice is about 50% smaller than that of wild-type mice (Figure 28A & 28B). Similarly, we found a 43 ± 8% reduction in testis weight of *Prl-2* null mice. Strikingly, deletion of a single allele of *Prl-1* gene from *Prl-2* null mice caused an additional 59 ± 16% reduction of testis size, indicating that *Prl-1* gene is indeed involved in testis development (Figure 28A & 28B). It is further strengthened by the discovery that the testes of *Prl-1*$^{-/-}$/*Prl-2*$^{+/-}$ male mice were also markedly smaller than those of wild-types (33 ± 14% reduction) (Figure 28A & 28B), despite the fact that testis development in either *Prl-1*$^{-/-}$ or *Prl-2*$^{+/-}$ mice is normal. Since the body weight of *Prl-1*$^{-/-}$/*Prl-2*$^{+/-}$ and especially *Prl-1*$^{+/-}$/*Prl-2*$^{-/-}$ mice was also reduced (Figure 27C), we normalized testis weight to body weight and still found a significant reduction of the testis/body weight ratio in *Prl-1*$^{-/-}$/*Prl-2*$^{+/-}$ and especially *Prl-1*$^{+/-}$/*Prl-2*$^{-/-}$ mice. As shown in Figure 28C, while testis/body weight ratio observed in *Prl-2*$^{-/-}$ males decreased 33 ± 16% compared to the wild-type animals, deletion of one more *Prl-1* allele resulted in a 69 ± 9% reduction in normalized testis size. Moreover, although no significant difference was observed in *Prl-1*$^{-/-}$ mice, the testis/body weight ratio of *Prl-1*$^{-/-}$/*Prl-2*$^{+/-}$ testis reduced 19 ± 12% compared to the wild-type mice (Figure 28C).

To determine whether the reduced testis size correlates with impaired reproductive ability, 3-months-old *Prl-1*$^{-/-}$/*Prl-2*$^{+/-}$ and *Prl-1*$^{+/-}$/*Prl-2*$^{-/-}$ male mice were mated with wild-type virgin females. These mice showed similar sexual desire measured by the percentage of female mice plugged by male mice (Figure 29A). However, the real

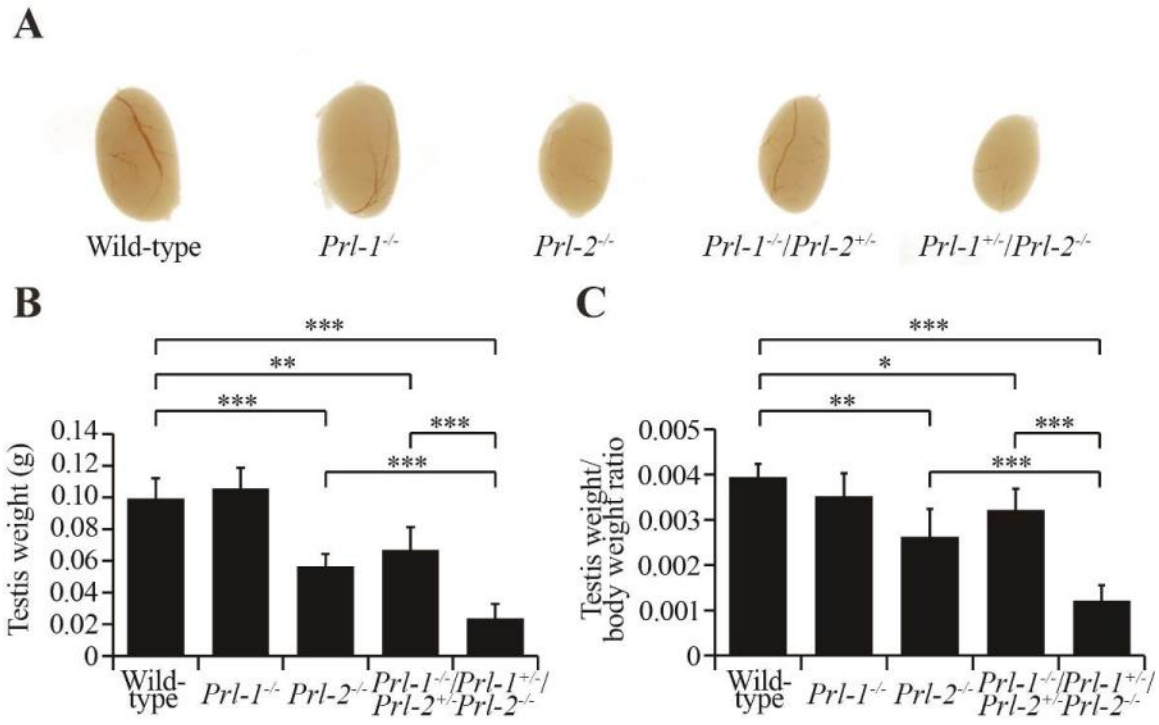


**Figure 28. *Prl-1* also contributes to the normal testis development.**

**A.** Representative testis picture from five different genotypes. **B-C.** Testis weights (B) or testis weight/body weight ratios (C) from five different genotypes were determined.

pregnant percentage after plugging, as well as the litter size from *Prl-1*$^{-/-}$/*Prl-2*$^{+/-}$ mice group were significantly lower compared to the wild-type group (Figure 29B & 29C). More strikingly, none of the females that were plugged by *Prl-1*$^{+/-}$/*Prl-2*$^{-/-}$ male mice were pregnant, indicating that a single *Prl-1* allele deletion in *Prl-2* deficient mice results in male infertility (Figure 29B & 29C). To further characterize the functionality of testis, the number of sperm from epididymis was directly counted using hemocytometer. In agreement with previous results (Figure 24C), the number of sperm from *Prl-2* KO mice was only 54 ± 18% of the wild-type controls (Figure 29D). Similarly, *Prl-1*$^{-/-}$/*Prl-2*$^{+/-}$ mice also showed significantly decreased sperm numbers (68 ± 9% of wild-type) (Figure 29D), suggesting that both *Prl-1* and *Prl-2* contribute to sperm production. Not

surprisingly, *Prl-1*$^{+/-}$/*Prl-2*$^{-/-}$ male mice lost 93 ± 5% of sperms in the epididymis (Figure 29D), which explained their sterility. Consistent with this observation, HE staining on caudal epididymis, where mature spermatozoa accumulate, also revealed that no morphologically normal spermatozoa were observed in the epididymis of *Prl-1*$^{+/-}$/*Prl-2*$^{-/-}$ mice (Figure 29E). Although more round-shaped non-spermatozoa cells were found in the epididymis of *Prl-2*$^{-/-}$ and *Prl-1*$^{-/-}$/*Prl-2*$^{+/-}$ mice, most of the cells are morphologically normal spermatozoa (Figure 29E). All these data imply that, in addition to PRL-2, PRL-1 also controls sperm production, which directly affects reproductive ability.

### 5.4.3 *Prl-1* is important for maintaining spermatogenesis

To investigate how PRL-1 is involved in controlling testis organ size and sperm production, the histological structure of male testis derived from different genotypes were analyzed by H&E staining. Even though the overall structures of seminiferous tubules of 3-month-old male mice were similar between different genotypes, the diameters of the seminiferous tubules were changed (Figure 30A & 30B). Consistent with our previous study (81), the diameter of the seminiferous tubules from the *Prl-2*$^{-/-}$ testis decreased 21 ± 6% in comparison to those from the wild-type and *Prl-1*$^{-/-}$ mice. There was also a 17 ± 3% and 27 ± 5% reduction in *Prl-1*$^{-/-}$/*Prl-2*$^{+/-}$ and *Prl-1*$^{+/-}$/*Prl-2*$^{-/-}$ testis size, respectively (Figure 30B). Moreover, loss of certain types of cells was evidenced by the “empty space” observed inside of the seminiferous tubules of *Prl-2*$^{-/-}$ testis, and this was even more severe in the *Prl-1*$^{+/-}$/*Prl-2*$^{-/-}$ testis (Black arrows in Figure 30A). In line with this observation, numerous round-shaped cells were released into the caudal epididymis of *Prl-2*$^{-/-}$ mice, and even more round-shaped cells were observed in the caudal epididymis of *Prl-1*$^{+/-}$/*Prl-2*$^{-/-}$ mice (Figure 29E). These data

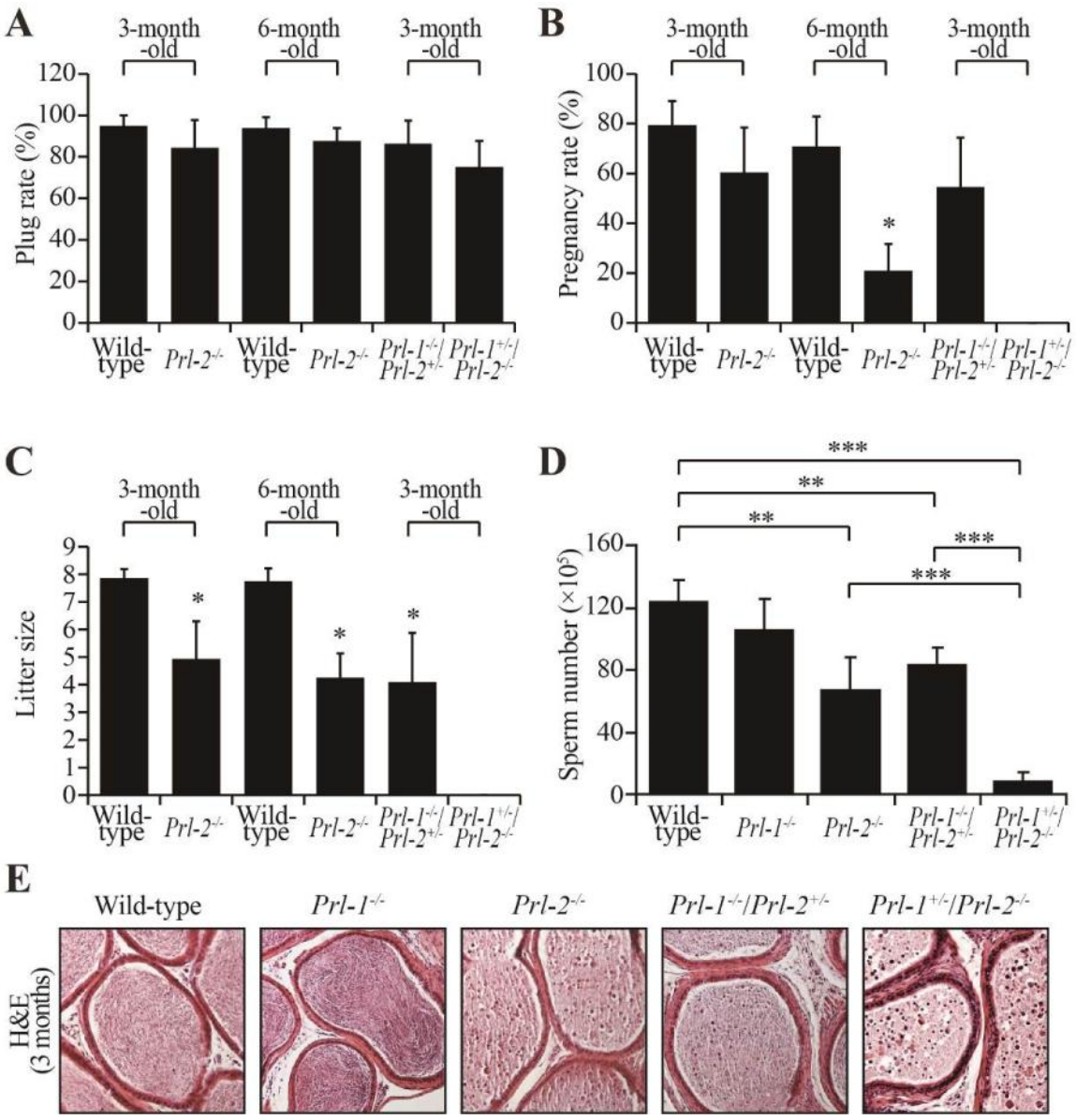


**Figure 29. Deletion one *Prl-1* allele in *Prl-2*$^{-/-}$ results in male infertility due to no sperm production.**

**A.** Sexual desire was measured by plug rate. **B-C.** Reproductive performance was measured by pregnancy rate **(B)** and little size **(C)**. **D.** The sperm number was determined by calculating the sperms from epididymis. **E.** Caudal epididymis sections from 3 months old male mice were histologically examined by H&E staining.

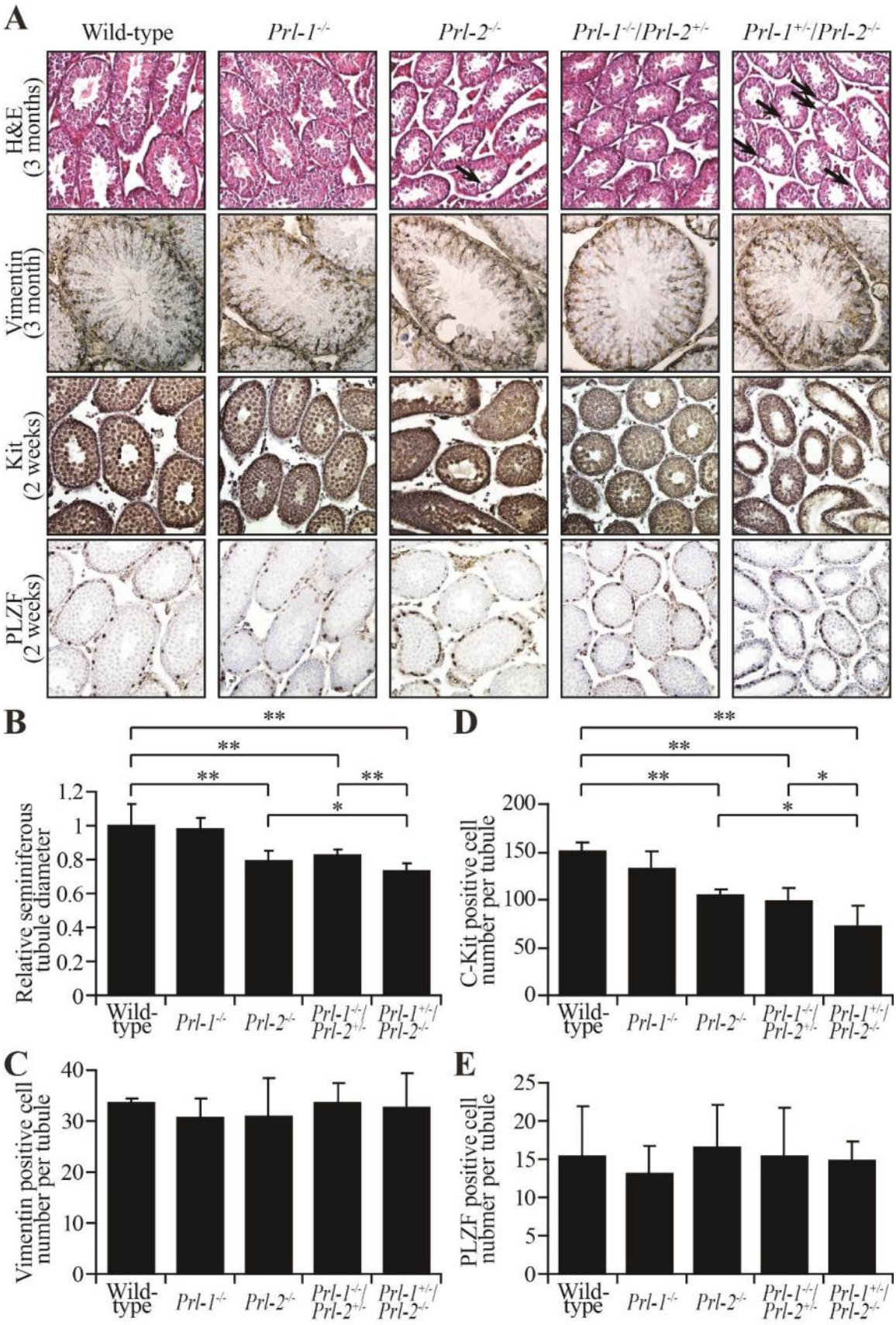
A
Wild-type
Prl-1-/-
Prl-2-/-
Prl-1-/-/Prl-2+/-
Prl-1+/-/Prl-2-/-
H&E (3 months)
Vimentin (3 month)
Kit (2 weeks)
PLZF (2 weeks)
B
Relative seminiferous tubule diameter
C
Vimentin positive cell number per tubule
D
C-Kit positive cell number per tubule
E
PLZF positive cell nubmer per tubule
Wild-type
Prl-1-/-
Prl-2-/-
Prl-1-/-/Prl-2+/-
Prl-1+/-/Prl-2-/-

**Figure 30. *Prl-1* also plays a role in maintaining spermatogenesis.**

**A.** Testis sections from 3 months or 2 weeks old male mice were histologically examined by H&E staining and immunohistochemical staining for Vimentin, PLZF and Kit. **B-E.** Relative seminiferous tubule diameters (**B**), number of Vimentin positive cell per seminiferous tubule (**C**), number of c-Kit positive cell per tubule (**D**) and number of PLZF positive cell per tubule (**E**) in testis sections from all five genotypes were quantificated. For each mouse, at least 20 tubules were counted. n=3 for each genotype. Data represent mean ± SD.

indicated that the reduced testis size is mainly attributed to decreased cellularity in the seminiferous tubules.

There are two major cell types within seminiferous tubules, Sertoli cells and germ cells. Sertoli cells are responsible for maintaining stem cell renewal, differentiation of spermatogonia into mature germ cells and the release of spermatozoa in the process of spermatogenesis. To determine whether the development and growth of Sertoli cells were normal and whether the number of Sertoli cells was affected, Vimentin (a Sertoli cell specific marker) staining was performed to visualize Sertoli cells from different genotypes by immunohistochemistry (Figure 30A). Even though the Sertoli cell structure was significantly affected in *Prl-2*$^{-/-}$ and *Prl-1*$^{+/-}$/*Prl-2*$^{-/-}$ testis, the number of Sertoli cells from all five genotypes was similar (Figure 30A & 30C), suggesting that reduced cellularity is possibly due to loss of germ cells but not Sertoli cells. Since Sertoli cells interact with germ cells in the seminiferous tubules (160,161), loss of germ cells would potentially affects the Sertoli cell organization in the seminiferous tubules.

Spermatogenesis is a process by which spermatozoa are formed from primordial germ cells by continuous mitosis and meiosis. Different types of germ cells are located in the seminiferous tubules from the base to lumen, including undifferentiated

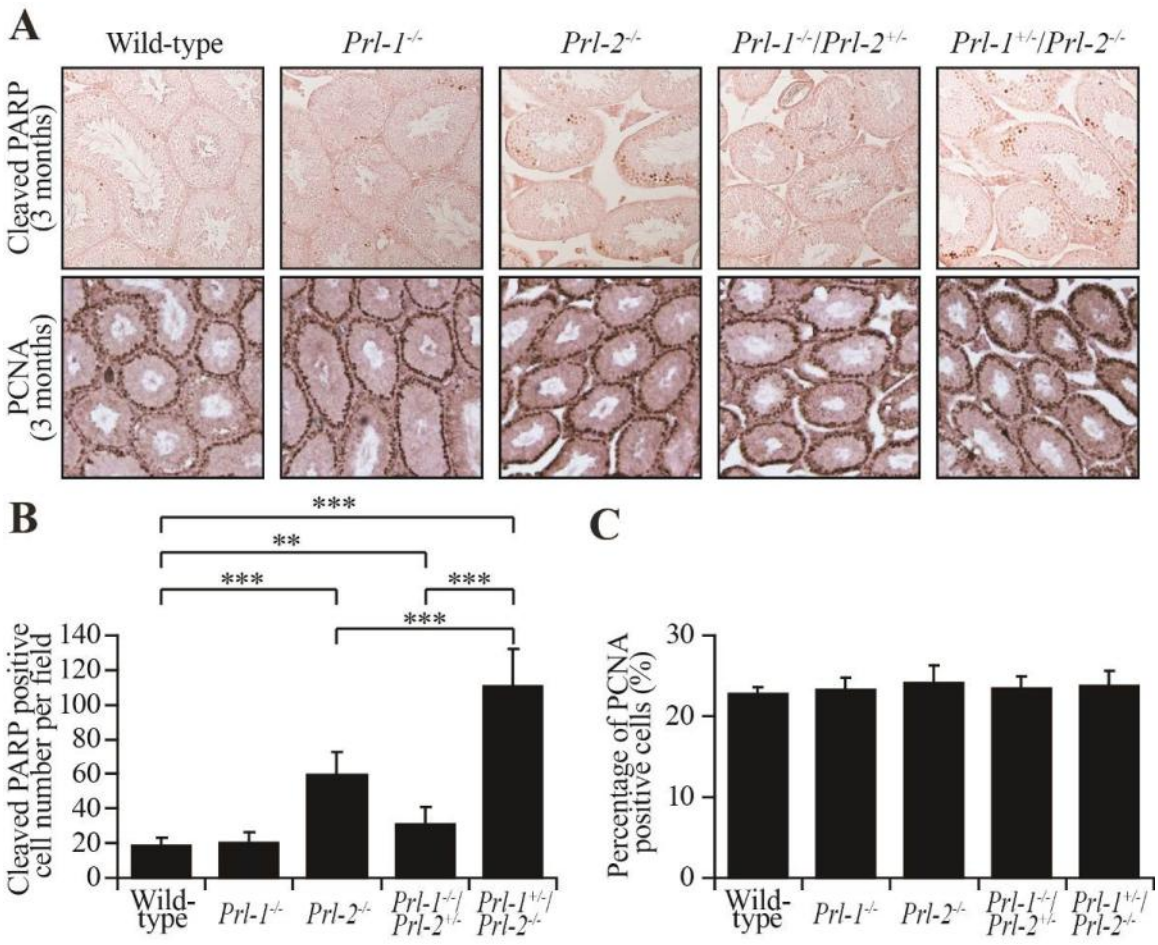


**Figure 31. *Prl-1* is also required to prevent germ cells from apoptosis.**

**A.** Testis sections from 3 month old male mice were histologically examined by immunohistochemical staining for Cleaved PARP and PCNA. **B-C.** Number of cleaved-PARP positive cell per field (**B**) and percentage of PCNA positive cells per tubule (**C**) in testis sections from five genotypes were determined. For each mouse, at least 10 fields or 20 tubules were counted. n=3 for each genotype. Data represent mean ± SD.

spermatogonia, differentiating spermatogonia, primary spermatocytes, secondary spermatocytes, round spermatid and elongated spermatid. To determine exactly which cell population is affected in the testis of different genotypes, PLZF staining (a specific marker for undifferentiated spermatogonia) and Kit staining (a specific marker for differentiating spermatogonia and primary spermatocytes) were performed (162,163). Our previous report suggested that testis structure alteration in *Prl-2* deficient mice

appears at 2-week-old (81). At this stage, Sertoli cells, undifferentiated spermatogonia, differentiating spermatogonia and primary spermatocytes are the major cell types residing in the seminiferous tubules (81). Thus, it is much easier for us to tell which cell population is altered. Since previous immunohistochemistry analysis indicated that differentiating spermatogonia and primary spermatocytes (Kit positive), but not undifferentiated spermatogonia (PLZF positive), are significantly reduced in *Prl-2*$^{-/-}$ testis, we hypothesized that deletion of one more *Prl-1* allele in *Prl-2*$^{-/-}$ testis will further aggravate the loss of Kit-positive cells. As shown in Figure 30A & 30E, the number of PLZF-positive cells is comparable in all five genotypes, suggesting that undifferentiated spermatogonia are not affected by deletion of *Prl-1* and *Prl-2*. However, Kit-positive cell number varied between genotypes (Figure 30A & 30E). Consistent with previous results, the number of Kit-positive cells in *Prl-2*$^{-/-}$ testis dropped 30 ± 4% compared to that of wild-type controls (Figure 30A & 30E). Comparable to *Prl-2*$^{-/-}$ testis, the Kit-positive cell number also decreased 35 ± 10% in *Prl-1*$^{-/-}$/*Prl-2*$^{+/-}$ testis (Figure 30A & 30D). As we expected, loss of Kit-positive cells are more pronounced in *Prl-1*$^{+/-}$/*Prl-2*$^{-/-}$ testis (58 ± 8% less than wild-type), in which many tubules are totally empty compared to *Prl-2*$^{-/-}$ and *Prl-1*$^{-/-}$/*Prl-2*$^{+/-}$ testis (Figure 30A & 30D). Taken together, the combination of *Prl-1*$^{+/-}$and *Prl-2*$^{-/-}$ intensified the Kit-positive germ cell loss observed in *Prl-2*$^{-/-}$ testis, leading to complete blockage of spermatogenesis and infertility.

### 5.4.4 *Prl-1* is also required to prevent germ cells from ectopic apoptosis

Spermatogenesis is a precisely controlled process including germ cell proliferation, differentiation, self-renewal and apoptosis. Germ cell loss occurs normally during spermatogenesis in all mammals, and control of germ cell apoptosis during spermatogenesis is especially important. To determine whether loss of Kit-positive germ

cells was due to decreased proliferation or increased apoptosis, we performed immunohistochemistry with PCNA (Proliferating Cell Nuclear Antigen, a proliferation marker) staining and cleaved PARP (Poly ADP-Ribose Polymerase, an apoptosis marker) staining to label proliferating cells and apoptotic cells respectively. As shown in Figure 31A & 31C, the percentage of proliferating cells in the testis was similar in all five genotypes. In contrast, the number of cleaved PARP positive cells was 3-fold higher in *Prl-2*$^{-/-}$ compared to wild-type or *Prl-1*$^{-/-}$ testis (Figure 31A & 31B). *Prl-1*$^{-/-}$/*Prl-2*$^{+/-}$ mice also showed a 1.6 fold higher apoptosis in seminiferous tubules compared to control groups (Figure 31A & 31B). More importantly, knocking out one additional *Prl-1* allele in *Prl-2*$^{-/-}$ increased another 3-fold of apoptosis compared to *Prl-2*$^{-/-}$ itself (Figure 31A & 31B). The aggravated phenotype of *Prl-1*$^{+/-}$/*Prl-2*$^{-/-}$ mice compared to *Prl-2*-null mice would then suggest an important role of PRL-1, in addition to PRL-2, in spermatogenesis by promoting Kit-positive germ cell survival.

**5.4.5 Loss of total PRL-1 and PRL-2 dose-dependently up-regulates PTEN level**

SCF-Kit is a major pathway that regulates the proliferation and survival of differentiating spermatogonia and spermatocytes. We have shown that in *Prl-2* deficient testis, SCF-Kit signaling is compromised as a result of elevated PTEN expression. Since deletion of one allele of *Prl-1* from *Prl-2* null mice showed aggravated phenotype, it is understandable to propose that PRL-1 share a same regulatory mechanism on PTEN stability with PRL-2. To further substantiate that PRL-1 also negatively regulates PTEN expression level in testis, we compared the PTEN protein level by Western blot in five genotypes (Figure 32). As we expected, PTEN expression was 33 ± 5% higher in *Prl-2*$^{-/-}$ testis compared to wild-type (Figure 32A & 32B). *Prl-1*$^{-/-}$ and *Prl-1*$^{-/-}$/*Prl-2*$^{+/-}$ testes also showed a 9 ± 11% and 21 ± 18% PTEN elevation, respectively (Figure 32A & 32B),

even though no statistical significance was observed. More obviously, PTEN protein level is further increased in *Prl-1*$^{+/-}$/*Prl-2*$^{-/-}$ testis and displayed a 67 ± 11% up-regulation than wild-type (Figure 32A & 32B).

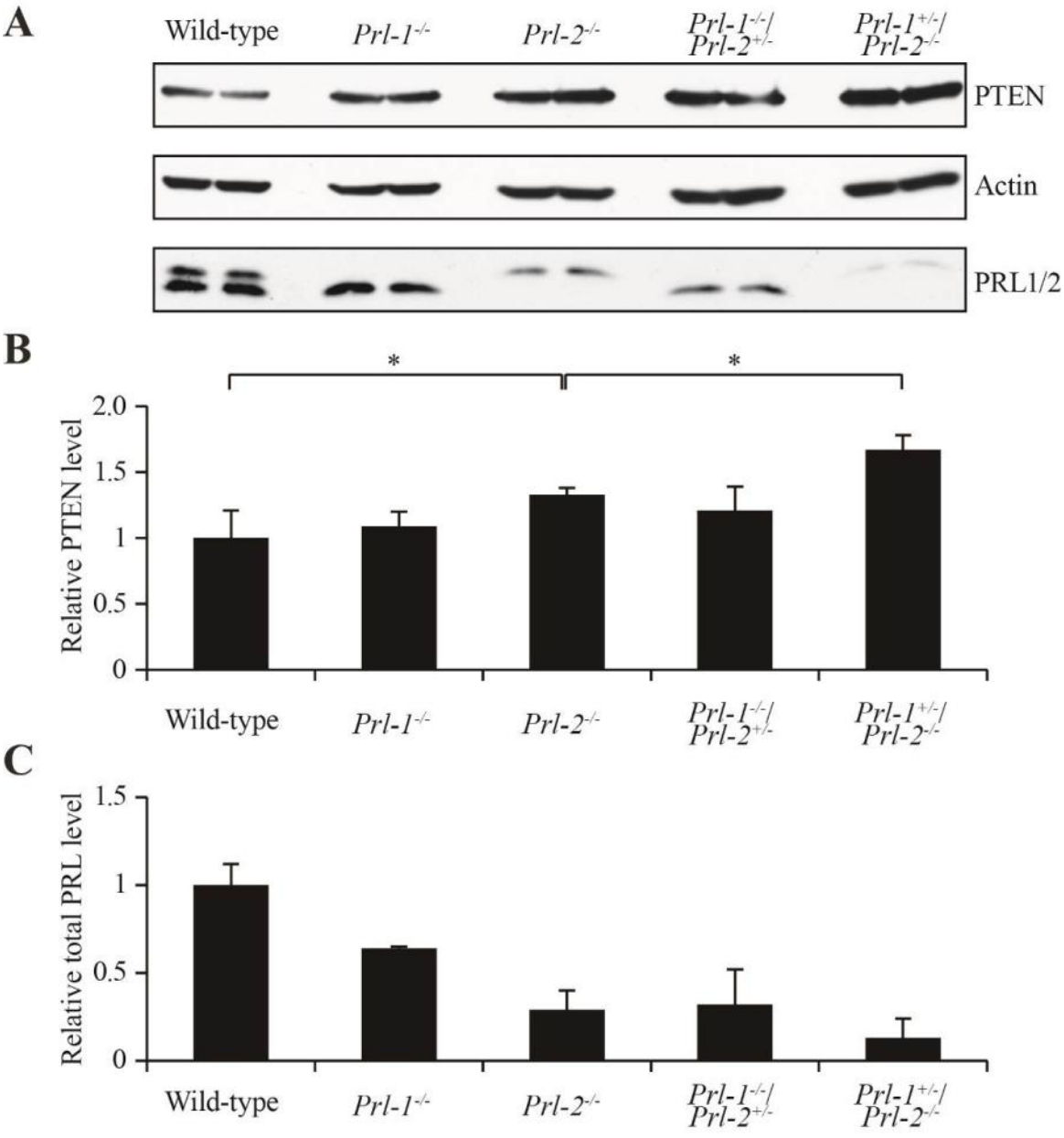


**Figure 32. Both PRL-1 and PRL-2 negatively regulate PTEN stability.**

**A.** Germ cells isolated from testis of male mice with different genotypes were analyzed for PTEN, PRL-1 and PRL-2by Western blot. **B.** Relative PTEN level normalized to Actin. **C.** Relative total PRL-1 and PRL-2 level normalized to Actin.

We also measured PRL-1 and PRL-2 protein level. If we assume PRL-1 and PRL-2 have similar function in regulating PTEN, and combined PRL-1 and PRL-2 protein level as total PRL level, we observed a 36 ± 1%, 71 ± 11%, 58 ± 20% and 83 ± 18% reduction of total PRL level in *Prl-1*$^{-/-}$, *Prl-2*$^{-/-}$, *Prl-1*$^{-/-}$/*Prl-2*$^{+/-}$ and *Prl-1*$^{+/-}$/*Prl-2*$^{-/-}$ testes, respectively (Figure 32A & 32C). More interestingly, we found a negative correlation between the total PRL level and the PTEN level, namely the less total PRL left, the more PTEN will be observed in the testis, suggesting that PTEN level is dose-dependently regulated by the total PRL-1 and PRL-2 level and that PRL-1 and PRL-2 are biochemically identical in terms of PTEN regulation.

Moreover, if we link the previous functional and histological study with total PRL level in testes from different genotypes, we still can find this negative correlation. For example, testis weight (Figure 28), reproductive ability (Figure 29), loss of Kit$^{+}$ germ cells (Figure 30) and increased apoptosis (Figure 31) are all dose-dependently associated with the total PRL levels, suggesting that both PRL-1 and PRL-2 are required for maintaining normal spermatogenesis and male reproductive ability. Even though further investigation is still required to fully establish the detailed mechanism, here we provide the first evidence that, in addition to PRL-2, PRL-1 also plays a significant role in maintaining spermatogenesis by down-regulation PTEN.

**5.5 Discussion**

The family of PRL phosphatases has three members, PRL-1, PRL-2 and PRL-3. The amino acid sequences of these three phosphatases are extremely similar, suggesting that they are biochemically equivalent. Numerous experiments supported this notion, because overexpression of any one member of this family induces similar cancer-associated phenotypes in cells. However, the *in vivo* function of these three phosphatases

may differ due to the different expression pattern and level. Among the three PRL isoforms, both PRL-1 and PRL-2 are broadly expressed in adult human tissues, while PRL-3 is primarily expressed in heart and skeletal muscle (14,25). PRL-2 has the most abundant expression compared to PRL-1's overall lower level in the same tissues or cell types (14,24,164). To investigate the physiological roles of PRLs, gene knockout mice lacking each *Prl* isoform are required. Recently, several studies on *Prl-2* and *Prl-3* deficient mice have been reported from our group and others (26,80,81,83,111). *Prl-2*-null mice displayed placenta dysfunction (80), impaired reproductive ability in male mice (81) and insufficiency in hematopoietic system (83), while *Prl-3*-null mice showed no obvious development problems but reduced colon cancer formation in the presence of carcinogen azoxymethane and dextran sodium sulfate (26), and *Prl-3* promotes VEGF signaling and endothelial cell motility (111). However, to date, there are no reports on gene targeted mouse models for disruption of the *Prl-1* genomic locus. Furthermore, given the similar but relatively lower expression pattern of PRL-1 compared to PRL-2, we were also interested in generating *Prl-1* and *Prl-2* double knockout mice.

This study is the first to reveal that PRL-1 also plays an important role in the spermatogenesis in addition to PRL-2. Previous report suggested that *Prl-2*$^{-/-}$ male mice display impaired reproductive ability, testis hypotrophy, and decreased sperm production as a result of compromised spermatogenesis, and ablation of PRL-2 expression causes ectopic germ cell apoptosis, which primarily affects the Kit-positive cell population. In contrast to *Prl-2*, *Prl-1*-null male mice show normal reproductive function comparable to wild-type controls. Considering the high similarity of sequence, and always higher expression level of PRL-2 than PRL-1 in all the organs, it is highly possible that, in *Prl-1*-null male testis, the original role of PRL-1 is maintained by PRL-2. In line with this

notion, *Prl-1*$^{-/-}$/*Prl-2*$^{+/-}$ male mice also have impaired reproductive ability, testis hypotrophy, and decreased sperm production similar to the phenotype observed in *Prl-2*$^{-/-}$ alone. Most strikingly, deletion of one additional allele of *Prl-1* in *Prl-2*-null male mice results in infertility. Compared to the subfertility of *Prl-2*-null mice, the infertile *Prl-1*$^{-/-}$ /*Prl-2*$^{+/-}$ male mice has an additional 50% reduction in testis weight, almost 2 fold higher apoptosis in Kit-positive germ cells and no sperm production, suggesting that PRL-1 plays an important role in maintaining the survival of Kit-positive germ cells in the testis. Mechanistically, *Prl-2* deletion results in Akt activation through up-regulating the expression of PTEN, which antagonizes PI3K by dephosphorylating phosphatidylinositol (3,4,5) triphosphate ($PIP_3$). In agreement with this mechanism, I have shown that the PTEN level is further increased in *Prl-1*$^{+/-}$/*Prl-2*$^{-/-}$ male testis, leading to enhanced ectopic apoptosis of Kit-positive germ cells. These data suggested that PRL-1 shares the same regulatory mechanism with PRL-2 on PTEN stability, and PRL-1 also exerts an essential role in promoting germ cell survival and maintaining the normal spermatogenesis.

It has been well established that the Kit-PI3K-Akt signaling pathway is critical for regulating the proliferation and survival of germ cells in testis. Animal models with Kit pathway component mutation or functional impairment also showed similar testicular phenotypes observed in the *Prl-1*$^{+/-}$/*Prl-2*$^{-/-}$ mice. Germline homozygous-null mutations of either *Scf* or *Kit* cause infertility in male mice owing to failure of germ cell development (165,166). Spermatogonia differentiation was blocked by application of Kit antibody (167). *Kit*$^{W\text{-}lacZ/+}$ mice with only one functional *Kit* allele has reduced spermatogenesis, less differentiating spermatogonia and higher apoptosis in testes of the heterozygous mice due to Kit haplodeficiency (168). Mice bearing a point mutation in *Kit* to specifically disrupt p85 binding exhibit male sterility due to decreased proliferation

and increased apoptosis of spermatogonia and the failure of producing sperms (169,170). Knock-in male mice with inactive p110β, an isoform of PI3K, are sub-fertile due to severe loss of Kit-positive cells (171). Since Akt is responsible for transducing the survival signal from Kit to downstream effectors (172), it is not surprising that *Akt1* knockout male mice are also sub-fertile with decreased testis size, attenuated spermatogenesis and increased germ cell apoptosis (172,173). Akt1 has also been reported to protect germ cells from radiation-induced apoptosis in testis (174), demonstrating an important survival function of Akt1 in spermatogenesis. Taken together the data support an essential role for the Kit-PI3K-Akt pathway in regulating the growth and survival of germ cells in testis. Our results suggest that, similar to PRL-2, PRL-1 may also promote SCF-Kit pathway in the testis by down-regulating PTEN. However, additional experiments should be done to validate that deletion one *Prl-1* allele in *Prl-2* deficient mice further attenuates the Kit-PI3K-Akt pathway leading to germ cell apoptosis and infertility.

Give the significant role of PTEN in down-regulating Kit-PI3K-Akt signaling, it is understandable that loss of heterozygosity in $Pten^{+/-}$ mice causes testicular germ cell cancer (175). PTEN is one of the most well-known tumor suppressors that frequently mutated, and commonly down-regulated in cancer (176). Loss of function mutations of PTEN or even a 20% reduction in PTEN expression can amplify PI3K signaling and promote tumorigenesis in a variety of experimental models of cancer (177). Previous study indicated that PRL-2 down-regulates PTEN through the disruption of adherens junctions components Vinculin and β-Catenin (81). Even if additional investigations are required to further demonstrate whether PRL-1 regulates PTEN through the same mechanism, our finding that both PRL-1 and PRL-2 down-regulate PTEN offers a

plausible explanation for the oncogenic potential of both PRL-1 and PRL-2 in promoting cell proliferation and migration. Together with the previous finding that PRL-3 also down-regulates PTEN through increasing its degradation (79), our animal studies suggested that PRLs could be potential therapeutic targets for cancer treatment by manipulating PTEN expression.

# CHAPTER 6: FINAL CONCLUSION AND FUTURE DIRECTION

## 6.1 Final conclusion

The overall goal of this dissertation is to gain insight into the biological function and therapeutic value of PRLs by biochemical and genetic approaches. The results presented in this dissertation explained the molecular mechanism by which PRL-1 activates ERK1/2 and RhoA; established a novel anti-cancer approach by disrupting PRL-1 trimerization; and examined the physiological role of PRLs in animal models. While PRLs have been studied extensively for their implication in tumorigenesis and metastasis, limited information is available on their natural substrates or binding proteins, which hindered the process of understanding on mechanisms at molecular level of PRL functions. In addition, although PRLs have been considered as potential therapeutic targets for cancer treatment, only a few PRLs inhibitors have been developed and the therapeutic potential of these active site inhibitors has not been well-studied. Moreover, while standard tissue culture systems contributed a lot to the current understanding of the oncogenic role of PRLs in human malignancies, little is known about their physiological function in *in vivo* processes. Therefore, in the PRL field, significant gaps exist between oncogenic implication and molecular mechanism, possibility as potential drug target and real therapeutic value, as well as well-established *in vitro* function and poorly understood *in vivo* function. This dissertation definitively filled these gaps and improved our understanding on PRLs biology.

Recent biochemical studies suggested that PRL-1 activates both ERK1/2 and RhoA of the Rho family small GTPases to facilitate cell proliferation and invasion. However, the mechanism by which PRL-1 up-regulates ERK1/2 and RhoA is still not established. In an effort to identify novel effectors of PRL-1, an unbiased phage display

screening against recombinant $(His)_6$-tagged PRL-1 was performed, and Peptide **1** (GWWSLIPPKYIT) was identified as a putative PRL-1 binding peptide. In a BLAST search, we found this peptide corresponds to a sequence motif in the SH3 domain of p115 RhoGAP, suggesting that this protein is a *bona fide* PRL-1 binding protein. Biochemical and cellular data suggested that the PRL-1 association with p115 RhoGAP relies on its SH3 domain. The co-crystal structure of PRL-1•Peptide **1** revealed that PRL-1 recognizes a conserved sequence motif in the canonical PxxP ligand binding site of the SH3 domain in p115 RhoGAP. p115 RhoGAP, a member of srGAP family, mainly expresses in nervous system and is implicated in cell migration and axon outgrowth. It has been shown that p115 RhoGAP associates with MEKK1, through which p115 RhoGAP inhibits ERK/MAP kinase signaling pathway. We found that the interaction between PRL-1 and p115 RhoGAP displaces MEKK1 from the inhibition of p115 RhoGAP and prevents the interaction between RhoA and p115 RhoGAP, leading to the ERK1/2 and RhoA activation, respectively. This study provides a potential mechanistic explanation for PRL-1 induced ERK1/2 and RhoA activation. Furthermore, two PRL-1-activated signaling pathways, MAP kinase and Rho GTPases, converge to the same protein, p115 RhoGAP.

Structural analysis of PRL-1 and PRL-3 revealed an identical trimeric arrangement (22,23,137). We have shown that trimerization is essential for the PRL-1-mediated cell growth and migration by providing a membrane-binding surface with C-terminal prenylation motif and the adjacent polybasic residues to anchor PRL-1 on the acidic inner membrane (17). To test the hypothesis that targeting PRL-1 trimer interface by small molecule inhibitors could block PRL-1 induced cell proliferation and migration, virtual screening was used to develop novel small molecule inhibitors targeting PRL-1

trimer interface. 56 hits were selected for further validation, and one of those compounds, Cmpd-43, was identified as potential PRL-1 trimer disruptors by biochemical assays. Cellular studies further demonstrated that Cmpd-43 reduced PRL-1-induced cell proliferation and migration. Analog-3, one of Cmpd-43 analogs, had similar cellular activity as Cmpd-43 in inhibiting PRL-1 mediated cell proliferation and migration. Most importantly, while the structure of PRL-1 alone is a trimer, co-crystal structure of PRL-1 with Analog-3 revealed a monomer structure of PRL-1, demonstrating that Analog-3 indeed blocked the trimer formation of PRL-1. Finally, Cmpd-43 effectively decreased the cell proliferation and migration in breast cancer cell line MDA-MB-231 and lung cancer cell line H1299, further implicating the potential therapeutic value of this compound in cancer treatment. All these data support our hypothesis that targeting PRL trimer interface is a novel strategy for anti-cancer treatment.

Even though extensive studies have been done to elucidate the role of PRL family of proteins in cancer development, we still know little about their physiological roles *in vivo*. To answer this question, we generated knockout mice deficient for individual *Prls*. While *Prl-1* and *Prl-3* knockout mice have no obvious developmental problems, *Prl-2*-null mice showed growth retardation, impaired male reproductive ability and ineffective hematopoiesis. Given the similar sequence identity and expression pattern, and the relative lower expression of PRL-1 compared to PRL-2, it is highly likely that PRL-1 plays a similar role with PRL-2 and PRL-2, to some extent, can compensate for loss of PRL-1. To reveal the physiological function of *Prl-1,* we tried to generate *Prl-1* and *Prl-2* double knockout mice. Even though we were unable to obtain any double knockout animal, deletion of one *Prl-1* allele in *Prl-2*-null mice already displayed significant smaller testis compared to *Prl-2*-null mice. Functionally, *Prl-1*$^{+/-}$

/*Prl-2*$^{-/-}$ mice are infertile due to no sperm production. Histological study revealed that *Prl-1*$^{+/-}$/*Prl-2*$^{-/-}$ males had dramatic reduction of Kit-positive germ cells in the seminiferous tubules due to enhanced ectopic apoptosis. At the molecular level, PTEN expression is further up-regulated in the testis of *Prl-1*$^{+/-}$/*Prl-2*$^{-/-}$ male mice compared to *Prl-2*-null mice, suggesting similar function of PRL-1 and PRL-2 in regulating PTEN stability. This study is the first to reveal the physiological role of PRL-1 in maintaining spermatogenesis by modulating Kic-PI3K-Akt signaling pathways.

Overall, this dissertation is an important milestone in understanding the biological function of PRLs. The results presented here explained the mechanism by which PRL-1 activates ERK1/2 and RhoA; explored the therapeutic value of targeting PRL-1 trimer interface for cancer treatment; established and characterized *Prl-1*, *Prl-2* and *Prl-3* knockout mice; and revealed a significant role of PRL-1 in spermatogenesis.

**6.2 Future Direction**

Although the results presented in this thesis provided mechanistic insight regarding the actions of PRLs, no definitive substrate(s) has been identified for the PRLs, which represents a significant obstacle to our understanding of the true biological role of PRLs. Given the multifunctional roles of PRLs in different signaling pathway, it is possible that PRLs can dephosphorylate many proteins. Indeed, substrate-trapping mutant PRL-2-C101S/D69A is able to pull-down several proteins including PTEN, p53 and β-Catenin, suggesting that these proteins are potential PRL-2 substrates. These candidates, as well as the phosphorylation sites, should be further validated for their potential as direct PRLs substrates.

The novel interaction between PRL-1 and p115 RhoGAP not only offers a mechanistic explanation for PRL-1 induced ERK1/2 and RhoA activation, but also

identifies a novel p115 RhoGAP binding site in PRL-1 for the development of anticancer therapeutics by blocking the interaction between PRL-1 and p115 RhoGAP. It is worthy of further investigation to screen small molecule inhibitors targeting the binding sites between PRL-1 and p115 RhoGAP. One may expect that treatment with such inhibitors could block the interaction between PRL-1 and p115 RhoGAP and the activation of ERK1/2 and RhoA signaling, leading to the inhibition of cell proliferation and migration. Additionally, the significance of the novel interaction between PRL-1 and p115 RhoGAP in the physiological condition is still unclear. Given the co-expression of PRL-1 and p115 RhoGAP in nervous system, it is highly possible that PRL-1 is involved in determining axon growth and cell migration in nervous system.

Cellular studies indicated that small molecule inhibitors targeting PRL-1 trimer interface effectively reduced PRL-1-mediated cell proliferation and migration in human cancer cells, but further evaluation using animal tumor models is required to measure the compound activity towards tumorigenesis and metastasis. Furthermore, the mechanism by which PRL-1 trimerization affects PRL-1-mediated signaling pathways also needs further investigation. Both of these future directions will benefit our understanding of the therapeutic significance of targeting PRL-1 trimerization.

Gene knockout mouse model offers an extremely valuable tool for studying the function of PRLs in development. Given the similar expression pattern and highly homologous sequence between PRL-1 and PRL-2, it is interesting to evaluate the phenotypes in double knockout mice. However, PRL-1 and PRL-2 double knockout mice are embryonic lethal in early stage, suggesting they play an essential role in embryonic development. Conditional gene knockout is required to overcome the early embryonic lethality of PRL-1 and PRL-2 double knockout mice. One great advantage of

the conditional knockout animal model is the ability to perform time-specific and/or tissue-specific knockout of interested gene. Time-specific gene deletion enables us to bypass the critical stage in embryonic development. Tissue-specific knockout facilitates our studies in distinguishing which specific cell type is responsible for the observed phenotypes. Finally, generating triple knockout that deletes all three PRLs could add considerable insight about the *in vivo* function of this PTP subfamily.

Given the implication of PRLs overexpression in cancer development, it is reasonable to expect that PRLs deficiency mice would develop fewer tumors. This is supported by recent reports that deletion of PRL-3 reduced colon tumors induced by carcinogen azoxymethane and dextran sodium sulfate (26). To date, different types of mouse tumor models have been established such as liver, breast, or leukemia (178,179). It would be very interesting to examine the effect of PRLs deletion in these cancer models. In addition, mice with heterozygous loss of PTEN and mice with homozygous loss of p53 develop spontaneous tumors in a variety of organs and tissues (180,181). Considering the direct regulation of PRLs on PTEN and p53, it is interesting to examine the effect of PRL deletion on spontaneous tumor development by crossing PRLs knockout mice with PTEN or p53 deficient mice. This could not only provide insight for the oncogenic role of PRLs, but also benefit our understanding of signaling pathways regulated by the PRLs.

Finally, it has been reported that adenoviral-mediated PTEN expression significantly inhibits tumor growth in multiple animal models (182-185), demonstrating that restoration of PTEN level may be an effective strategy for tumor therapy. Given the negative regulatory role of PRLs in PTEN stability, small molecule inhibitors of PRLs may increase PTEN expression. Unlike inhibitors of the PI3K-Akt pathway, PRLs

inhibitors may restore not only the canonical PTEN function but also tumor-suppressive nuclear activities of PTEN that are unrelated to its lipid phosphatase activity. Further investigation is necessary to explore the efficiency of PRLs inhibitors as new therapeutic approaches to a number of malignancies associated with gain-of-function mutations in the Kit gene. Furthermore, a combination of PRLs inhibitors with PI3K-Akt inhibitors may have synergistic effect in cancer treatment.

## REFERENCES


1. Tonks, N. K., and Neel, B. G. (2001) Combinatorial control of the specificity of protein tyrosine phosphatases. *Current opinion in cell biology* **13**, 182-195
2. Alonso, A., Sasin, J., Bottini, N., Friedberg, I., Friedberg, I., Osterman, A., Godzik, A., Hunter, T., Dixon, J., and Mustelin, T. (2004) Protein tyrosine phosphatases in the human genome. *Cell* **117**, 699-711
3. Julien, S. G., Dube, N., Hardy, S., and Tremblay, M. L. (2011) Inside the human cancer tyrosine phosphatome. *Nature reviews. Cancer* **11**, 35-49
4. Tartaglia, M., Niemeyer, C. M., Fragale, A., Song, X., Buechner, J., Jung, A., Hahlen, K., Hasle, H., Licht, J. D., and Gelb, B. D. (2003) Somatic mutations in PTPN11 in juvenile myelomonocytic leukemia, myelodysplastic syndromes and acute myeloid leukemia. *Nature genetics* **34**, 148-150
5. Bentires-Alj, M., Paez, J. G., David, F. S., Keilhack, H., Halmos, B., Naoki, K., Maris, J. M., Richardson, A., Bardelli, A., Sugarbaker, D. J., Richards, W. G., Du, J., Girard, L., Minna, J. D., Loh, M. L., Fisher, D. E., Velculescu, V. E., Vogelstein, B., Meyerson, M., Sellers, W. R., and Neel, B. G. (2004) Activating mutations of the noonan syndrome-associated SHP2/PTPN11 gene in human solid tumors and adult acute myelogenous leukemia. *Cancer research* **64**, 8816-8820
6. Wiener, J. R., Hurteau, J. A., Kerns, B. J., Whitaker, R. S., Conaway, M. R., Berchuck, A., and Bast, R. C., Jr. (1994) Overexpression of the tyrosine phosphatase PTP1B is associated with human ovarian carcinomas. *American journal of obstetrics and gynecology* **170**, 1177-1183
7. Wiener, J. R., Kerns, B. J., Harvey, E. L., Conaway, M. R., Iglehart, J. D., Berchuck, A., and Bast, R. C., Jr. (1994) Overexpression of the protein tyrosine phosphatase PTP1B in human breast cancer: association with p185c-erbB-2 protein expression. *Journal of the National Cancer Institute* **86**, 372-378
8. Mahlamaki, E. H., Barlund, M., Tanner, M., Gorunova, L., Hoglund, M., Karhu, R., and Kallioniemi, A. (2002) Frequent amplification of 8q24, 11q, 17q, and 20q-specific genes in pancreatic cancer. *Genes, chromosomes & cancer* **35**, 353-358

9. Yang, S. H., Seo, M. Y., Jeong, H. J., Jeung, H. C., Shin, J., Kim, S. C., Noh, S. H., Chung, H. C., and Rha, S. Y. (2005) Gene copy number change events at chromosome 20 and their association with recurrence in gastric cancer patients. *Clinical cancer research : an official journal of the American Association for Cancer Research* **11**, 612-620
10. Wu, C., Zhang, L., Bourne, P. A., Reeder, J. E., di Sant'Agnese, P. A., Yao, J. L., Na, Y., and Huang, J. (2006) Protein tyrosine phosphatase PTP1B is involved in neuroendocrine differentiation of prostate cancer. *The Prostate* **66**, 1125-1135
11. Diamond, R. H., Cressman, D. E., Laz, T. M., Abrams, C. S., and Taub, R. (1994) PRL-1, a unique nuclear protein tyrosine phosphatase, affects cell growth. *Molecular and cellular biology* **14**, 3752-3762
12. Cates, C. A., Michael, R. L., Stayrook, K. R., Harvey, K. A., Burke, Y. D., Randall, S. K., Crowell, P. L., and Crowell, D. N. (1996) Prenylation of oncogenic human PTP(CAAX) protein tyrosine phosphatases. *Cancer letters* **110**, 49-55
13. Zeng, Q., Dong, J. M., Guo, K., Li, J., Tan, H. X., Koh, V., Pallen, C. J., Manser, E., and Hong, W. (2003) PRL-3 and PRL-1 promote cell migration, invasion, and metastasis. *Cancer research* **63**, 2716-2722
14. Zeng, Q., Hong, W., and Tan, Y. H. (1998) Mouse PRL-2 and PRL-3, two potentially prenylated protein tyrosine phosphatases homologous to PRL-1. *Biochemical and biophysical research communications* **244**, 421-427
15. Zeng, Q., Si, X., Horstmann, H., Xu, Y., Hong, W., and Pallen, C. J. (2000) Prenylation-dependent association of protein-tyrosine phosphatases PRL-1, -2, and -3 with the plasma membrane and the early endosome. *The Journal of biological chemistry* **275**, 21444-21452
16. Fiordalisi, J. J., Keller, P. J., and Cox, A. D. (2006) PRL tyrosine phosphatases regulate rho family GTPases to promote invasion and motility. *Cancer research* **66**, 3153-3161
17. Sun, J. P., Luo, Y., Yu, X., Wang, W. Q., Zhou, B., Liang, F., and Zhang, Z. Y. (2007) Phosphatase activity, trimerization, and the C-terminal polybasic region are all required for PRL1-mediated cell growth and migration. *The Journal of biological chemistry* **282**, 29043-29051
18. Yu, L., Kelly, U., Ebright, J. N., Malek, G., Saloupis, P., Rickman, D. W., McKay, B. S., Arshavsky, V. Y., and Bowes Rickman, C. (2007) Oxidative stress-induced expression and modulation of Phosphatase of Regenerating Liver-1 (PRL-1) in mammalian retina. *Biochimica et biophysica acta* **1773**, 1473-1482

19. Skinner, A. L., Vartia, A. A., Williams, T. D., and Laurence, J. S. (2009) Enzyme Activity of Phosphatase of Regenerating Liver Is Controlled by the Redox Environment and Its C-Terminal Residues. *Biochemistry* **48**, 4262-4272
20. Ishii, T., Funato, Y., and Miki, H. (2013) Thioredoxin-related protein 32 (TRP32) specifically reduces oxidized phosphatase of regenerating liver (PRL). *The Journal of biological chemistry* **288**, 7263-7270
21. Kozlov, G., Cheng, J., Ziomek, E., Banville, D., Gehring, K., and Ekiel, I. (2004) Structural insights into molecular function of the metastasis-associated phosphatase PRL-3. *The Journal of biological chemistry* **279**, 11882-11889
22. Jeong, D. G., Kim, S. J., Kim, J. H., Son, J. H., Park, M. R., Lim, S. M., Yoon, T. S., and Ryu, S. E. (2005) Trimeric structure of PRL-1 phosphatase reveals an active enzyme conformation and regulation mechanisms. *Journal of molecular biology* **345**, 401-413
23. Sun, J. P., Wang, W. Q., Yang, H., Liu, S., Liang, F., Fedorov, A. A., Almo, S. C., and Zhang, Z. Y. (2005) Structure and biochemical properties of PRL-1, a phosphatase implicated in cell growth, differentiation, and tumor invasion. *Biochemistry* **44**, 12009-12021
24. Dumaual, C. M., Sandusky, G. E., Crowell, P. L., and Randall, S. K. (2006) Cellular localization of PRL-1 and PRL-2 gene expression in normal adult human tissues. *The journal of histochemistry and cytochemistry : official journal of the Histochemistry Society* **54**, 1401-1412
25. Matter, W. F., Estridge, T., Zhang, C., Belagaje, R., Stancato, L., Dixon, J., Johnson, B., Bloem, L., Pickard, T., Donaghue, M., Acton, S., Jeyaseelan, R., Kadambi, V., and Vlahos, C. J. (2001) Role of PRL-3, a human muscle-specific tyrosine phosphatase, in angiotensin-II signaling. *Biochemical and biophysical research communications* **283**, 1061-1068
26. Zimmerman, M. W., Homanics, G. E., and Lazo, J. S. (2013) Targeted deletion of the metastasis-associated phosphatase Ptp4a3 (PRL-3) suppresses murine colon cancer. *PloS one* **8**, e58300
27. Zhang, Z. Y. (2001) Protein tyrosine phosphatases: prospects for therapeutics. *Current opinion in chemical biology* **5**, 416-423
28. Arena, S., Benvenuti, S., and Bardelli, A. (2005) Genetic analysis of the kinome and phosphatome in cancer. *Cellular and molecular life sciences : CMLS* **62**, 2092-2099

29. Saha, S., Bardelli, A., Buckhaults, P., Velculescu, V. E., Rago, C., St Croix, B., Romans, K. E., Choti, M. A., Lengauer, C., Kinzler, K. W., and Vogelstein, B. (2001) A phosphatase associated with metastasis of colorectal cancer. *Science* **294**, 1343-1346
30. Kato, H., Semba, S., Miskad, U. A., Seo, Y., Kasuga, M., and Yokozaki, H. (2004) High expression of PRL-3 promotes cancer cell motility and liver metastasis in human colorectal cancer: a predictive molecular marker of metachronous liver and lung metastases. *Clinical cancer research : an official journal of the American Association for Cancer Research* **10**, 7318-7328
31. Bardelli, A., Saha, S., Sager, J. A., Romans, K. E., Xin, B., Markowitz, S. D., Lengauer, C., Velculescu, V. E., Kinzler, K. W., and Vogelstein, B. (2003) PRL-3 expression in metastatic cancers. *Clinical cancer research : an official journal of the American Association for Cancer Research* **9**, 5607-5615
32. Li, J., Guo, K., Koh, V. W., Tang, J. P., Gan, B. Q., Shi, H., Li, H. X., and Zeng, Q. (2005) Generation of PRL-3- and PRL-1-specific monoclonal antibodies as potential diagnostic markers for cancer metastases. *Clinical cancer research : an official journal of the American Association for Cancer Research* **11**, 2195-2204
33. Peng, L., Ning, J., Meng, L., and Shou, C. (2004) The association of the expression level of protein tyrosine phosphatase PRL-3 protein with liver metastasis and prognosis of patients with colorectal cancer. *Journal of cancer research and clinical oncology* **130**, 521-526
34. Wang, Y., Li, Z. F., He, J., Li, Y. L., Zhu, G. B., Zhang, L. H., and Li, Y. L. (2007) Expression of the human phosphatases of regenerating liver (PRLs) in colonic adenocarcinoma and its correlation with lymph node metastasis. *Int J Colorectal Dis* **22**, 1179-1184
35. Hardy, S., Wong, N. N., Muller, W. J., Park, M., and Tremblay, M. L. (2010) Overexpression of the protein tyrosine phosphatase PRL-2 correlates with breast tumor formation and progression. *Cancer research* **70**, 8959-8967
36. Radke, I., Gotte, M., Kersting, C., Mattsson, B., Kiesel, L., and Wulfing, P. (2006) Expression and prognostic impact of the protein tyrosine phosphatases PRL-1, PRL-2, and PRL-3 in breast cancer. *Brit J Cancer* **95**, 347-354
37. Wang, L., Peng, L., Dong, B., Kong, L., Meng, L., Yan, L., Xie, Y., and Shou, C. (2006) Overexpression of phosphatase of regenerating liver-3 in breast cancer: association with a poor clinical outcome. *Annals of oncology : official journal of the European Society for Medical Oncology / ESMO* **17**, 1517-1522

38. Hao, R. T., Zhang, X. H., Pan, Y. F., Liu, H. G., Xiang, Y. Q., Wan, L., and Wu, X. L. (2010) Prognostic and metastatic value of phosphatase of regenerating liver-3 in invasive breast cancer. *Journal of cancer research and clinical oncology* **136**, 1349-1357
39. Ustaalioglu, B. B., Bilici, A., Barisik, N. O., Aliustaoglu, M., Vardar, F. A., Yilmaz, B. E., Seker, M., and Gumus, M. (2012) Clinical importance of phosphatase of regenerating liver-3 expression in breast cancer. *Clinical & translational oncology : official publication of the Federation of Spanish Oncology Societies and of the National Cancer Institute of Mexico* **14**, 911-922
40. Dumaual, C. M., Sandusky, G. E., Soo, H. W., Werner, S. R., Crowell, P. L., and Randall, S. K. (2012) Tissue-specific alterations of PRL-1 and PRL-2 expression in cancer. *American journal of translational research* **4**, 83-101
41. Miskad, U. A., Semba, S., Kato, H., and Yokozaki, H. (2004) Expression of PRL-3 phosphatase in human gastric carcinomas: close correlation with invasion and metastasis. *Pathobiology : journal of immunopathology, molecular and cellular biology* **71**, 176-184
42. Li, Z. R., Wang, Z., Zhu, B. H., He, Y. L., Peng, J. S., Cai, S. R., Ma, J. P., and Zhan, W. H. (2007) Association of tyrosine PRL-3 phosphatase protein expression with peritoneal metastasis of gastric carcinoma and prognosis. *Surgery today* **37**, 646-651
43. Miskad, U. A., Semba, S., Kato, H., Matsukawa, Y., Kodama, Y., Mizuuchi, E., Maeda, N., Yanagihara, K., and Yokozaki, H. (2007) High PRL-3 expression in human gastric cancer is a marker of metastasis and grades of malignancies: an in situ hybridization study. *Virchows Archiv : an international journal of pathology* **450**, 303-310
44. Ooki, A., Yamashita, K., Kikuchi, S., Sakuramoto, S., Katada, N., Waraya, M., Kawamata, H., Nishimiya, H., Nakamura, K., and Watanabe, M. (2011) Therapeutic potential of PRL-3 targeting and clinical significance of PRL-3 genomic amplification in gastric cancer. *BMC cancer* **11**, 122
45. Da, N., Lu, A. P., Shou, C. C., and Li, J. Y. (2009) Expression of phosphatase regenerating liver 3 is an independent prognostic indicator for gastric cancer. *World J Gastroentero* **15**, 1499-1505
46. Ooki, A., Yamashita, K., Kikuchi, S., Sakuramoto, S., Katada, N., and Watanabe, M. (2009) Phosphatase of regenerating liver-3 as a prognostic biomarker in histologically node-negative gastric cancer. *Oncol Rep* **21**, 1467-1475

47. Matsukawa, Y., Semba, S., Kato, H., Koma, Y., Yanagihara, K., and Yokozaki, H. (2010) Constitutive Suppression of PRL-3 Inhibits Invasion and Proliferation of Gastric Cancer Cell in vitro and in vivo. *Pathobiology : journal of immunopathology, molecular and cellular biology* **77**, 155-162
48. Bilici, A., Ustaalioglu, B. B., Yavuzer, D., Seker, M., Mayadagli, A., and Gumus, M. (2012) Prognostic significance of high phosphatase of regenerating liver-3 expression in patients with gastric cancer who underwent curative gastrectomy. *Digestive diseases and sciences* **57**, 1568-1575
49. Polato, F., Codegoni, A., Fruscio, R., Perego, P., Mangioni, C., Saha, S., Bardelli, A., and Broggini, M. (2005) PRL-3 phosphatase is implicated in ovarian cancer growth. *Clinical cancer research : an official journal of the American Association for Cancer Research* **11**, 6835-6839
50. Ren, T., Jiang, B., Xing, X., Dong, B., Peng, L., Meng, L., Xu, H., and Shou, C. (2009) Prognostic significance of phosphatase of regenerating liver-3 expression in ovarian cancer. *Pathology oncology research : POR* **15**, 555-560
51. Lu, J. W., Chang, J. G., Yeh, K. T., Chen, R. M., Tsai, J. J., Su, W. W., and Hu, R. M. (2012) Increased expression of PRL-1 protein correlates with shortened patient survival in human hepatocellular carcinoma. *Clinical & translational oncology : official publication of the Federation of Spanish Oncology Societies and of the National Cancer Institute of Mexico* **14**, 287-293
52. Zhao, W. B., Li, Y., Liu, X., Zhang, L. Y., and Wang, X. (2008) Evaluation of PRL-3 expression, and its correlation with angiogenesis and invasion in hepatocellular carcinoma. *International journal of molecular medicine* **22**, 187-192
53. Mayinuer, A., Yasen, M., Mogushi, K., Obulhasim, G., Xieraili, M., Aihara, A., Tanaka, S., Mizushima, H., Tanaka, H., and Arii, S. (2013) Upregulation of protein tyrosine phosphatase type IVA member 3 (PTP4A3/PRL-3) is associated with tumor differentiation and a poor prognosis in human hepatocellular carcinoma. *Annals of surgical oncology* **20**, 305-317
54. Hassan, N. M., Hamada, J., Kameyama, T., Tada, M., Nakagawa, K., Yoshida, S., Kashiwazaki, H., Yamazaki, Y., Suzuki, Y., Sasaki, A., Nagatsuka, H., Inoue, N., and Moriuchi, T. (2011) Increased expression of the PRL-3 gene in human oral squamous cell carcinoma and dysplasia tissues. *Asian Pacific journal of cancer prevention : APJCP* **12**, 947-951

55. Zhou, J., Wang, S., Lu, J., Li, J., and Ding, Y. (2009) Over-expression of phosphatase of regenerating liver-3 correlates with tumor progression and poor prognosis in nasopharyngeal carcinoma. *International journal of cancer. Journal international du cancer* **124**, 1879-1886
56. Laurent, C., Valet, F., Planque, N., Silveri, L., Maacha, S., Anezo, O., Hupe, P., Plancher, C., Reyes, C., Albaud, B., Rapinat, A., Gentien, D., Couturier, J., Sastre-Garau, X., Desjardins, L., Thiery, J. P., Roman-Roman, S., Asselain, B., Barillot, E., Piperno-Neumann, S., and Saule, S. (2011) High PTP4A3 phosphatase expression correlates with metastatic risk in uveal melanoma patients. *Cancer research* **71**, 666-674
57. Ma, Y., and Li, B. (2011) Expression of phosphatase of regenerating liver-3 in squamous cell carcinoma of the cervix. *Medical oncology* **28**, 775-780
58. Liu, Y. Q., Li, H. X., Lou, X., and Lei, J. Y. (2008) Expression of phosphatase of regenerating liver 1 and 3 mRNA in esophageal squamous cell carcinoma. *Archives of pathology & laboratory medicine* **132**, 1307-1312
59. Achiwa, H., and Lazo, J. S. (2007) PRL-1 tyrosine phosphatase regulates c-Src levels, adherence, and invasion in human lung cancer cells. *Cancer research* **67**, 643-650
60. Hwang, J. J., Min, S. H., Sin, K. H., Heo, Y. S., Kim, K. D., Yoo, O. J., and Lee, S. H. (2012) Altered expression of phosphatase of regenerating liver gene family in non-small cell lung cancer. *Oncol Rep* **27**, 535-540
61. Yamashita, S.-i., Masuda, Y., Matsumoto, K., Okumura, Y., Matsuzaki, H., Kurizaki, T., Haga, Y., Katafuchi, S., Murayama, T., and Ikei, S. (2007) Down-regulation of the human PRL-3 gene is associated with the metastasis of primary non-small cell lung cancer. *Annals of thoracic and cardiovascular surgery: official journal of the Association of Thoracic and Cardiovascular Surgeons of Asia* **13**, 236-239
62. Kong, L., Li, Q., Wang, L., Liu, Z., and Sun, T. (2007) The value and correlation between PRL-3 expression and matrix metalloproteinase activity and expression in human gliomas. *Neuropathology* **27**, 516-521
63. Fagerli, U. M., Holt, R. U., Holien, T., Vaatsveen, T. K., Zhan, F., Egeberg, K. W., Barlogie, B., Waage, A., Aarset, H., Dai, H. Y., Shaughnessy, J. D., Jr., Sundan, A., and Borset, M. (2008) Overexpression and involvement in migration by the metastasis-associated phosphatase PRL-3 in human myeloma cells. *Blood* **111**, 806-815

64. Broyl, A., Hose, D., Lokhorst, H., de Knegt, Y., Peeters, J., Jauch, A., Bertsch, U., Buijs, A., Stevens-Kroef, M., Beverloo, H. B., Vellenga, E., Zweegman, S., Kersten, M. J., van der Holt, B., el Jarari, L., Mulligan, G., Goldschmidt, H., van Duin, M., and Sonneveld, P. (2010) Gene expression profiling for molecular classification of multiple myeloma in newly diagnosed patients. *Blood* **116**, 2543-2553

65. Akiyama, S., Dhavan, D., and Yi, T. (2010) PRL-2 increases Epo and IL-3 responses in hematopoietic cells. *Blood cells, molecules & diseases* **44**, 209-214

66. Yagi, T., Morimoto, A., Eguchi, M., Hibi, S., Sako, M., Ishii, E., Mizutani, S., Imashuku, S., Ohki, M., and Ichikawa, H. (2003) Identification of a gene expression signature associated with pediatric AML prognosis. *Blood* **102**, 1849-1856

67. Zhou, J. B., Bi, C. L., Chng, W. J., Cheong, L. L., Liu, S. C., Mahara, S., Tay, K. G., Zeng, Q., Li, J., Guo, K., Tan, C. P. B., Yu, H., Albert, D. H., and Chen, C. S. (2011) PRL-3, a Metastasis Associated Tyrosine Phosphatase, Is Involved in FLT3-ITD Signaling and Implicated in Anti-AML Therapy. *PloS one* **6**

68. Zhou, J. B., Cheong, L. L., Liu, S. C., Chong, P. S. Y., Mahara, S., Bi, C. L., Ong, K. O., Zeng, Q., and Chng, W. J. (2012) The pro-metastasis tyrosine phosphatase, PRL-3 (PTP4A3), is a novel mediator of oncogenic function of BCR-ABL in human chronic myeloid leukemia. *Mol Cancer* **11**

69. Wang, Q., Holmes, D. I., Powell, S. M., Lu, Q. L., and Waxman, J. (2002) Analysis of stromal-epithelial interactions in prostate cancer identifies PTPCAAX2 as a potential oncogene. *Cancer letters* **175**, 63-69

70. Stephens, B., Han, H., Hostetter, G., Demeure, M. J., and Von Hoff, D. D. (2008) Small interfering RNA-mediated knockdown of PRL phosphatases results in altered Akt phosphorylation and reduced clonogenicity of pancreatic cancer cells. *Molecular cancer therapeutics* **7**, 202-210

71. Wu, X., Zeng, H., Zhang, X., Zhao, Y., Sha, H., Ge, X., Zhang, M., Gao, X., and Xu, Q. (2004) Phosphatase of regenerating liver-3 promotes motility and metastasis of mouse melanoma cells. *The American journal of pathology* **164**, 2039-2054

72. Ming, J., Liu, N., Gu, Y., Qiu, X., and Wang, E. H. (2009) PRL-3 facilitates angiogenesis and metastasis by increasing ERK phosphorylation and up-regulating the levels and activities of Rho-A/C in lung cancer. *Pathology* **41**, 118-126

73. Guo, K., Li, J., Tang, J. P., Koh, V., Gan, B. Q., and Zeng, Q. (2004) Catalytic domain of PRL-3 plays an essential role in tumor metastasis: formation of PRL-3 tumors inside the blood vessels. *Cancer biology & therapy* **3**, 945-951
74. Qian, F., Li, Y. P., Sheng, X., Zhang, Z. C., Song, R., Dong, W., Cao, S. X., Hua, Z. C., and Xu, Q. (2007) PRL-3 siRNA inhibits the metastasis of B16-BL6 mouse melanoma cells in vitro and in vivo. *Molecular medicine* **13**, 151-159
75. St Croix, B., Rago, C., Velculescu, V., Traverso, G., Romans, K. E., Montgomery, E., Lal, A., Riggins, G. J., Lengauer, C., Vogelstein, B., and Kinzler, K. W. (2000) Genes expressed in human tumor endothelium. *Science* **289**, 1197-1202
76. Guo, K., Li, J., Wang, H., Osato, M., Tang, J. P., Quah, S. Y., Gan, B. Q., and Zeng, Q. (2006) PRL-3 initiates tumor angiogenesis by recruiting endothelial cells in vitro and in vivo. *Cancer research* **66**, 9625-9635
77. Rouleau, C., Roy, A., St Martin, T., Dufault, M. R., Boutin, P., Liu, D., Zhang, M., Puorro-Radzwill, K., Rulli, L., Reczek, D., Bagley, R., Byrne, A., Weber, W., Roberts, B., Klinger, K., Brondyk, W., Nacht, M., Madden, S., Burrier, R., Shankara, S., and Teicher, B. A. (2006) Protein tyrosine phosphatase PRL-3 in malignant cells and endothelial cells: expression and function. *Molecular cancer therapeutics* **5**, 219-229
78. Wang, Y., and Lazo, J. S. (2012) Metastasis-associated phosphatase PRL-2 regulates tumor cell migration and invasion. *Oncogene* **31**, 818-827
79. Wang, H., Quah, S. Y., Dong, J. M., Manser, E., Tang, J. P., and Zeng, Q. (2007) PRL-3 down-regulates PTEN expression and signals through PI3K to promote epithelial-mesenchymal transition. *Cancer research* **67**, 2922-2926
80. Dong, Y., Zhang, L., Zhang, S., Bai, Y., Chen, H., Sun, X., Yong, W., Li, W., Colvin, S. C., Rhodes, S. J., Shou, W., and Zhang, Z. Y. (2012) Phosphatase of regenerating liver 2 (PRL2) is essential for placental development by down-regulating PTEN (Phosphatase and Tensin Homologue Deleted on Chromosome 10) and activating Akt protein. *The Journal of biological chemistry* **287**, 32172-32179
81. Dong, Y., Zhang, L., Bai, Y., Zhou, H. M., Campbell, A. M., Chen, H., Yong, W., Zhang, W., Zeng, Q., Shou, W., and Zhang, Z. Y. (2013) Phosphatase of regenerating liver 2 (PRL2) deficiency impairs Kit signaling and spermatogenesis. *The Journal of biological chemistry*

82. Maehama, T., and Dixon, J. E. (1998) The tumor suppressor, PTEN/MMAC1, dephosphorylates the lipid second messenger, phosphatidylinositol 3,4,5-trisphosphate. *The Journal of biological chemistry* **273**, 13375-13378
83. Kobayashi, M., Bai, Y., Dong, Y., Yu, H., Chen, S., Gao, R., Zhang, L., Yoder, M. C., Kapur, R., and Zhang, Z. Y. (2014) PRL2/PTP4A2 phosphatase is important for hematopoietic stem cell self-renewal. *STEM CELLS*
84. Subauste, M. C., Nalbant, P., Adamson, E. D., and Hahn, K. M. (2005) Vinculin controls PTEN protein level by maintaining the interaction of the adherens junction protein beta-catenin with the scaffolding protein MAGI-2. *The Journal of biological chemistry* **280**, 5676-5681
85. Peng, L., Jin, G., Wang, L., Guo, J., Meng, L., and Shou, C. (2006) Identification of integrin alpha1 as an interacting protein of protein tyrosine phosphatase PRL-3. *Biochemical and biophysical research communications* **342**, 179-183
86. Liang, F., Liang, J., Wang, W. Q., Sun, J. P., Udho, E., and Zhang, Z. Y. (2007) PRL3 promotes cell invasion and proliferation by down-regulation of Csk leading to Src activation. *The Journal of biological chemistry* **282**, 5413-5419
87. Walls, C. D., Iliuk, A., Bai, Y., Wang, M., Tao, W. A., and Zhang, Z. Y. (2013) Phosphatase of Regenerating Liver 3 (PRL3) Provokes a Tyrosine Phosphoproteome to Drive Prometastatic Signal Transduction. *Molecular & cellular proteomics : MCP* **12**, 3759-3777
88. Luo, Y., Liang, F., and Zhang, Z. Y. (2009) PRL1 promotes cell migration and invasion by increasing MMP2 and MMP9 expression through Src and ERK1/2 pathways. *Biochemistry* **48**, 1838-1846
89. Okada, M., Nada, S., Yamanashi, Y., Yamamoto, T., and Nakagawa, H. (1991) CSK: a protein-tyrosine kinase involved in regulation of src family kinases. *The Journal of biological chemistry* **266**, 24249-24252
90. Liang, F., Luo, Y., Dong, Y., Walls, C. D., Liang, J., Jiang, H. Y., Sanford, J. R., Wek, R. C., and Zhang, Z. Y. (2008) Translational control of C-terminal Src kinase (Csk) expression by PRL3 phosphatase. *The Journal of biological chemistry* **283**, 10339-10346
91. Defilippi, P., Di Stefano, P., and Cabodi, S. (2006) p130Cas: a versatile scaffold in signaling networks. *Trends in cell biology* **16**, 257-263
92. Fiordalisi, J. J., Dewar, B. J., Graves, L. M., Madigan, J. P., and Cox, A. D. (2013) Src-mediated phosphorylation of the tyrosine phosphatase PRL-3 is required for PRL-3 promotion of Rho activation, motility and invasion. *PloS one* **8**, e64309

93. Vogt, D. L., Gray, C. D., Young, W. S., 3rd, Orellana, S. A., and Malouf, A. T. (2007) ARHGAP4 is a novel RhoGAP that mediates inhibition of cell motility and axon outgrowth. *Molecular and cellular neurosciences* **36**, 332-342
94. Christerson, L. B., Gallagher, E., Vanderbilt, C. A., Whitehurst, A. W., Wells, C., Kazempour, R., Sternweis, P. C., and Cobb, M. H. (2002) p115 Rho GTPase activating protein interacts with MEKK1. *Journal of cellular physiology* **192**, 200-208
95. Wang, J., Kirby, C. E., and Herbst, R. (2002) The tyrosine phosphatase PRL-1 localizes to the endoplasmic reticulum and the mitotic spindle and is required for normal mitosis. *The Journal of biological chemistry* **277**, 46659-46668
96. Werner, S. R., Lee, P. A., DeCamp, M. W., Crowell, D. N., Randall, S. K., and Crowell, P. L. (2003) Enhanced cell cycle progression and down regulation of p21(Cip1/Waf1) by PRL tyrosine phosphatases. *Cancer letters* **202**, 201-211
97. Basak, S., Jacobs, S. B., Krieg, A. J., Pathak, N., Zeng, Q., Kaldis, P., Giaccia, A. J., and Attardi, L. D. (2008) The metastasis-associated gene Prl-3 is a p53 target involved in cell-cycle regulation. *Molecular cell* **30**, 303-314
98. Min, S. H., Kim, D. M., Heo, Y. S., Kim, Y. I., Kim, H. M., Kim, J., Han, Y. M., Kim, I. C., and Yoo, O. J. (2009) New p53 target, phosphatase of regenerating liver 1 (PRL-1) downregulates p53. *Oncogene* **28**, 545-554
99. Min, S. H., Kim, D. M., Heo, Y. S., Kim, H. M., Kim, I. C., and Yoo, O. J. (2010) Downregulation of p53 by phosphatase of regenerating liver 3 is mediated by MDM2 and PIRH2. *Life sciences* **86**, 66-72
100. Oren, M. (1992) p53: the ultimate tumor suppressor gene? *FASEB journal : official publication of the Federation of American Societies for Experimental Biology* **6**, 3169-3176
101. Friend, S. (1994) p53: a glimpse at the puppet behind the shadow play. *Science* **265**, 334-335
102. Picksley, S. M., and Lane, D. P. (1994) p53 and Rb: their cellular roles. *Current opinion in cell biology* **6**, 853-858
103. Pathak, M. K., Dhawan, D., Lindner, D. J., Borden, E. C., Farver, C., and Yi, T. (2002) Pentamidine is an inhibitor of PRL phosphatases with anticancer activity. *Molecular cancer therapeutics* **1**, 1255-1264

104. Ahn, J. H., Kim, S. J., Park, W. S., Cho, S. Y., Ha, J. D., Kim, S. S., Kang, S. K., Jeong, D. G., Jung, S. K., Lee, S. H., Kim, H. M., Park, S. K., Lee, K. H., Lee, C. W., Ryu, S. E., and Choi, J. K. (2006) Synthesis and biological evaluation of rhodanine derivatives as PRL-3 inhibitors. *Bioorganic & medicinal chemistry letters* **16**, 2996-2999

105. Min, G., Lee, S. K., Kim, H. N., Han, Y. M., Lee, R. H., Jeong, D. G., Han, D. C., and Kwon, B. M. (2013) Rhodanine-based PRL-3 inhibitors blocked the migration and invasion of metastatic cancer cells. *Bioorganic & medicinal chemistry letters* **23**, 3769-3774

106. Daouti, S., Li, W. H., Qian, H., Huang, K. S., Holmgren, J., Levin, W., Reik, L., McGady, D. L., Gillespie, P., Perrotta, A., Bian, H., Reidhaar-Olson, J. F., Bliss, S. A., Olivier, A. R., Sergi, J. A., Fry, D., Danho, W., Ritland, S., Fotouhi, N., Heimbrook, D., and Niu, H. (2008) A selective phosphatase of regenerating liver phosphatase inhibitor suppresses tumor cell anchorage-independent growth by a novel mechanism involving p130Cas cleavage. *Cancer research* **68**, 1162-1169

107. Choi, S. K., Oh, H. M., Lee, S. K., Jeong, D. G., Ryu, S. E., Son, K. H., Han, D. C., Sung, N. D., Baek, N. I., and Kwon, B. M. (2006) Biflavonoids inhibited phosphatase of regenerating liver-3 (PRL-3). *Natural product research* **20**, 341-346

108. Park, H., Jung, S. K., Jeong, D. G., Ryu, S. E., and Kim, S. J. (2008) Discovery of novel PRL-3 inhibitors based on the structure-based virtual screening. *Bioorganic & medicinal chemistry letters* **18**, 2250-2255

109. Wang, L., Shen, Y., Song, R., Sun, Y., Xu, J., and Xu, Q. (2009) An anticancer effect of curcumin mediated by down-regulating phosphatase of regenerating liver-3 expression on highly metastatic melanoma cells. *Molecular pharmacology* **76**, 1238-1245

110. Guo, K., Li, J., Tang, J. P., Tan, C. P., Hong, C. W., Al-Aidaroos, A. Q., Varghese, L., Huang, C., and Zeng, Q. (2011) Targeting intracellular oncoproteins with antibody therapy or vaccination. *Science translational medicine* **3**, 99ra85

111. Zimmerman, M. W., McQueeney, K. E., Isenberg, J. S., Pitt, B. R., Wasserloos, K. A., Homanics, G. E., and Lazo, J. S. (2014) PTP4A3 phosphatase promotes VEGF signaling and enables endothelial cell motility. *The Journal of biological chemistry*

112. Pagarigan, K. T., Bunn, B. W., Goodchild, J., Rahe, T. K., Weis, J. F., and Saucedo, L. J. (2013) Drosophila PRL-1 is a growth inhibitor that counteracts the function of the Src oncogene. *PloS one* **8**, e61084
113. Nakashima, M., and Lazo, J. S. (2010) Phosphatase of regenerating liver-1 promotes cell migration and invasion and regulates filamentous actin dynamics. *The Journal of pharmacology and experimental therapeutics* **334**, 627-633
114. Roux, P. P., and Blenis, J. (2004) ERK and p38 MAPK-activated protein kinases: a family of protein kinases with diverse biological functions. *Microbiology and molecular biology reviews : MMBR* **68**, 320-344
115. Hall, A. (1998) G proteins and small GTPases: distant relatives keep in touch. *Science* **280**, 2074-2075
116. Bishop, A. L., and Hall, A. (2000) Rho GTPases and their effector proteins. *The Biochemical journal* **348 Pt 2**, 241-255
117. Bollag, G., and McCormick, F. (1995) Intrinsic and GTPase-activating protein-stimulated Ras GTPase assays. *Methods in enzymology* **255**, 161-170
118. Quilliam, L. A., Rebhun, J. F., Zong, H., and Castro, A. F. (2001) Analyses of M-Ras/R-Ras3 signaling and biology. *Methods in enzymology* **333**, 187-202
119. Wells, C. D., Gutowski, S., Bollag, G., and Sternweis, P. C. (2001) Identification of potential mechanisms for regulation of p115 RhoGEF through analysis of endogenous and mutant forms of the exchange factor. *The Journal of biological chemistry* **276**, 28897-28905
120. Otwinowski, Z., and Minor, W. (1997) Processing of X-ray diffraction data collected in oscillation mode. *Method Enzymol* **276**, 307-326
121. Navaza, J. (1994) Amore - an Automated Package for Molecular Replacement. *Acta Crystallogr A* **50**, 157-163
122. Brunger, A. T., Adams, P. D., Clore, G. M., DeLano, W. L., Gros, P., Grosse-Kunstleve, R. W., Jiang, J. S., Kuszewski, J., Nilges, M., Pannu, N. S., Read, R. J., Rice, L. M., Simonson, T., and Warren, G. L. (1998) Crystallography & NMR system: A new software suite for macromolecular structure determination. *Acta Crystallogr D* **54**, 905-921
123. Brunger, A. T. (1992) Free R value: a novel statistical quantity for assessing the accuracy of crystal structures. *Nature* **355**, 472-475
124. Jones, T. A., Zou, J. Y., Cowan, S. W., and Kjeldgaard, M. (1991) Improved methods for building protein models in electron density maps and the location of errors in these models. *Acta Crystallogr A* **47 ( Pt 2)**, 110-119

125. Tribioli, C., Droetto, S., Bione, S., Cesareni, G., Torrisi, M. R., Lotti, L. V., Lanfrancone, L., Toniolo, D., and Pelicci, P. (1996) An X chromosome-linked gene encoding a protein with characteristics of a rhoGAP predominantly expressed in hematopoietic cells. *Proceedings of the National Academy of Sciences of the United States of America* **93**, 695-699
126. Wong, K., Ren, X. R., Huang, Y. Z., Xie, Y., Liu, G., Saito, H., Tang, H., Wen, L., Brady-Kalnay, S. M., Mei, L., Wu, J. Y., Xiong, W. C., and Rao, Y. (2001) Signal transduction in neuronal migration: roles of GTPase activating proteins and the small GTPase Cdc42 in the Slit-Robo pathway. *Cell* **107**, 209-221
127. Tcherkezian, J., and Lamarche-Vane, N. (2007) Current knowledge of the large RhoGAP family of proteins. *Biology of the cell / under the auspices of the European Cell Biology Organization* **99**, 67-86
128. Li, X., Chen, Y., Liu, Y., Gao, J., Gao, F., Bartlam, M., Wu, J. Y., and Rao, Z. (2006) Structural basis of Robo proline-rich motif recognition by the srGAP1 Src homology 3 domain in the Slit-Robo signaling pathway. *The Journal of biological chemistry* **281**, 28430-28437
129. Forte, E., Orsatti, L., Talamo, F., Barbato, G., De Francesco, R., and Tomei, L. (2008) Ezrin is a specific and direct target of protein tyrosine phosphatase PRL-3. *Biochimica et biophysica acta* **1783**, 334-344
130. Mizuuchi, E., Semba, S., Kodama, Y., and Yokozaki, H. (2009) Down-modulation of keratin 8 phosphorylation levels by PRL-3 contributes to colorectal carcinoma progression. *International journal of cancer. Journal international du cancer* **124**, 1802-1810
131. Tian, W., Qu, L., Meng, L., Liu, C., Wu, J., and Shou, C. (2012) Phosphatase of regenerating liver-3 directly interacts with integrin beta1 and regulates its phosphorylation at tyrosine 783. *BMC biochemistry* **13**, 22
132. Zheng, P., Liu, Y. X., Chen, L., Liu, X. H., Xiao, Z. Q., Zhao, L., Li, G. Q., Zhou, J., Ding, Y. Q., and Li, J. M. (2010) Stathmin, a new target of PRL-3 identified by proteomic methods, plays a key role in progression and metastasis of colorectal cancer. *Journal of proteome research* **9**, 4897-4905
133. Schmidt, A., and Hall, A. (2002) Guanine nucleotide exchange factors for Rho GTPases: turning on the switch. *Genes & development* **16**, 1587-1609
134. Moon, S. Y., and Zheng, Y. (2003) Rho GTPase-activating proteins in cell regulation. *Trends in cell biology* **13**, 13-22

135. Lange-Carter, C. A., Pleiman, C. M., Gardner, A. M., Blumer, K. J., and Johnson, G. L. (1993) A divergence in the MAP kinase regulatory network defined by MEK kinase and Raf. *Science* **260**, 315-319

136. Johnson, N. L., Gardner, A. M., Diener, K. M., Lange-Carter, C. A., Gleavy, J., Jarpe, M. B., Minden, A., Karin, M., Zon, L. I., and Johnson, G. L. (1996) Signal transduction pathways regulated by mitogen-activated/extracellular response kinase kinase kinase induce cell death. *The Journal of biological chemistry* **271**, 3229-3237

137. Bai, Y., Luo, Y., Liu, S., Zhang, L., Shen, K., Dong, Y., Walls, C. D., Quilliam, L. A., Wells, C. D., Cao, Y., and Zhang, Z. Y. (2011) PRL-1 protein promotes ERK1/2 and RhoA protein activation through a non-canonical interaction with the Src homology 3 domain of p115 Rho GTPase-activating protein. *The Journal of biological chemistry* **286**, 42316-42324

138. Irwin, J. J., and Shoichet, B. K. (2005) ZINC--a free database of commercially available compounds for virtual screening. *Journal of chemical information and modeling* **45**, 177-182

139. Lang, P. T., Brozell, S. R., Mukherjee, S., Pettersen, E. F., Meng, E. C., Thomas, V., Rizzo, R. C., Case, D. A., James, T. L., and Kuntz, I. D. (2009) DOCK 6: combining techniques to model RNA-small molecule complexes. *Rna* **15**, 1219-1230

140. Moustakas, D. T., Lang, P. T., Pegg, S., Pettersen, E., Kuntz, I. D., Brooijmans, N., and Rizzo, R. C. (2006) Development and validation of a modular, extensible docking program: DOCK 5. *Journal of computer-aided molecular design* **20**, 601-619

141. Huey, R., Morris, G. M., Olson, A. J., and Goodsell, D. S. (2007) A semiempirical free energy force field with charge-based desolvation. *Journal of computational chemistry* **28**, 1145-1152

142. Morris, G. M., Goodsell, D. S., Halliday, R. S., Huey, R., Hart, W. E., Belew, R. K., and Olson, A. J. (1998) Automated docking using a Lamarckian genetic algorithm and an empirical binding free energy function. *Journal of computational chemistry* **19**, 1639-1662

143. Pettersen, E. F., Goddard, T. D., Huang, C. C., Couch, G. S., Greenblatt, D. M., Meng, E. C., and Ferrin, T. E. (2004) UCSF Chimera--a visualization system for exploratory research and analysis. *Journal of computational chemistry* **25**, 1605-1612

144. Minor, W., Cymborowski, M., Otwinowski, Z., and Chruszcz, M. (2006) HKL-3000: the integration of data reduction and structure solution--from diffraction images to an initial model in minutes. *Acta crystallographica. Section D, Biological crystallography* **62**, 859-866
145. Vagin, A., and Teplyakov, A. (1997) MOLREP: an automated program for molecular replacement. *J Appl Crystallogr* **30**, 1022-1025
146. Brunger, A. T., Adams, P. D., Clore, G. M., DeLano, W. L., Gros, P., Grosse-Kunstleve, R. W., Jiang, J. S., Kuszewski, J., Nilges, M., Pannu, N. S., Read, R. J., Rice, L. M., Simonson, T., and Warren, G. L. (1998) Crystallography & NMR system: A new software suite for macromolecular structure determination. *Acta crystallographica. Section D, Biological crystallography* **54**, 905-921
147. Emsley, P., Lohkamp, B., Scott, W. G., and Cowtan, K. (2010) Features and development of Coot. *Acta crystallographica. Section D, Biological crystallography* **66**, 486-501
148. Krissinel, E. (2010) Crystal Contacts as Nature's Docking Solutions. *Journal of computational chemistry* **31**, 133-143
149. Krissinel, E., and Henrick, K. (2005) Detection of protein assemblies in crystals. *Lect Notes Comput Sc* **3695**, 163-174
150. Krissinel, E., and Henrick, K. (2007) Inference of macromolecular assemblies from crystalline state. *Journal of molecular biology* **372**, 774-797
151. Li, J., Guo, K., and Zeng, Q. (2005) Generation of PRL-3 and PRL-1 specific monoclonal antibodies as potential diagnostic markers for cancer metastases. *Mech Develop* **122**, S106-S106
152. Stephens, B. J., Han, H., Gokhale, V., and Von Hoff, D. D. (2005) PRL phosphatases as potential molecular targets in cancer. *Molecular cancer therapeutics* **4**, 1653-1661
153. Bessette, D. C., Qiu, D., and Pallen, C. J. (2008) PRL PTPs: mediators and markers of cancer progression. *Cancer metastasis reviews* **27**, 231-252
154. Rossant, J., and Cross, J. C. (2001) Placental development: lessons from mouse mutants. *Nat Rev Genet* **2**, 538-548
155. Coan, P. M., Conroy, N., Burton, G. J., and Ferguson-Smith, A. C. (2006) Origin and characteristics of glycogen cells in the developing murine placenta. *Dev Dyn* **235**, 3280-3294
156. Watson, E. D., and Cross, J. C. (2005) Development of structures and transport functions in the mouse placenta. *Physiology* **20**, 180-193

157. Song, M. S., Salmena, L., and Pandolfi, P. P. (2012) The functions and regulation of the PTEN tumour suppressor. *Nature reviews. Molecular cell biology* **13**, 283-296
158. Hofmann, M. C., Narisawa, S., Hess, R. A., and Millan, J. L. (1992) Immortalization of Germ-Cells and Somatic Testicular Cells Using the Sv40 Large T-Antigen. *Exp Cell Res* **201**, 417-435
159. Torres, J., and Pulido, R. (2001) The tumor suppressor PTEN is phosphorylated by the protein kinase CK2 at its C terminus. Implications for PTEN stability to proteasome-mediated degradation. *The Journal of biological chemistry* **276**, 993-998
160. Griswold, M. D. (1995) Interactions between Germ-Cells and Sertoli Cells in the Testis. *Biology of reproduction* **52**, 211-216
161. Mruk, D. D., and Cheng, C. Y. (2004) Sertoli-Sertoli and Sertoli-germ cell interactions and their significance in germ cell movement in the seminiferous epithelium during spermatogenesis. *Endocr Rev* **25**, 747-806
162. Buaas, F. W., Kirsh, A. L., Sharma, M., McLean, D. J., Morris, J. L., Griswold, M. D., de Rooij, D. G., and Braun, R. E. (2004) Plzf is required in adult male germ cells for stem cell self-renewal. *Nature genetics* **36**, 647-652
163. Vincent, S., Segretain, D., Nishikawa, S., Nishikawa, S. I., Sage, J., Cuzin, F., and Rassoulzadegan, M. (1998) Stage-specific expression of the Kit receptor and its ligand (KL) during male gametogenesis in the mouse: a Kit-KL interaction critical for meiosis. *Development* **125**, 4585-4593
164. Zhao, Z., Lee, C. C., Monckton, D. G., Yazdani, A., Coolbaugh, M. I., Li, X., Bailey, J., Shen, Y., and Caskey, C. T. (1996) Characterization and genomic mapping of genes and pseudogenes of a new human protein tyrosine phosphatase. *Genomics* **35**, 172-181
165. Reith, A. D., Rottapel, R., Giddens, E., Brady, C., Forrester, L., and Bernstein, A. (1990) W mutant mice with mild or severe developmental defects contain distinct point mutations in the kinase domain of the c-kit receptor. *Genes & development* **4**, 390-400
166. Gilbert, D., Rapley, E., and Shipley, J. (2011) Testicular germ cell tumours: predisposition genes and the male germ cell niche. *Nature reviews. Cancer* **11**, 278-288

167. Nishikawa, S., Kusakabe, M., Yoshinaga, K., Ogawa, M., Hayashi, S., Kunisada, T., Era, T., Sakakura, T., and Nishikawa, S. (1991) In utero manipulation of coat color formation by a monoclonal anti-c-kit antibody: two distinct waves of c-kit-dependency during melanocyte development. *The EMBO journal* **10**, 2111-2118
168. Guerif, F., Cadoret, V., Rahal-Perola, V., Lansac, J., Bernex, F., Panthier, J. J., Hochereau-de Reviers, M. T., and Royere, D. (2002) Apoptosis, onset and maintenance of spermatogenesis: evidence for the involvement of Kit in Kit-haplodeficient mice. *Biology of reproduction* **67**, 70-79
169. Blume-Jensen, P., Jiang, G., Hyman, R., Lee, K. F., O'Gorman, S., and Hunter, T. (2000) Kit/stem cell factor receptor-induced activation of phosphatidylinositol 3'-kinase is essential for male fertility. *Nature genetics* **24**, 157-162
170. Kissel, H., Timokhina, I., Hardy, M. P., Rothschild, G., Tajima, Y., Soares, V., Angeles, M., Whitlow, S. R., Manova, K., and Besmer, P. (2000) Point mutation in kit receptor tyrosine kinase reveals essential roles for kit signaling in spermatogenesis and oogenesis without affecting other kit responses. *The EMBO journal* **19**, 1312-1326
171. Ciraolo, E., Morello, F., Hobbs, R. M., Wolf, F., Marone, R., Iezzi, M., Lu, X., Mengozzi, G., Altruda, F., Sorba, G., Guan, K., Pandolfi, P. P., Wymann, M. P., and Hirsch, E. (2010) Essential role of the p110beta subunit of phosphoinositide 3-OH kinase in male fertility. *Molecular biology of the cell* **21**, 704-711
172. Chen, W. S., Xu, P. Z., Gottlob, K., Chen, M. L., Sokol, K., Shiyanova, T., Roninson, I., Weng, W., Suzuki, R., Tobe, K., Kadowaki, T., and Hay, N. (2001) Growth retardation and increased apoptosis in mice with homozygous disruption of the Akt1 gene. *Genes & development* **15**, 2203-2208
173. Kim, S. T., Omurtag, K., and Moley, K. H. (2012) Decreased spermatogenesis, fertility, and altered Slc2A expression in Akt1-/- and Akt2-/- testes and sperm. *Reprod Sci* **19**, 31-42
174. Rasoulpour, T., DiPalma, K., Kolvek, B., and Hixon, M. (2006) Akt1 suppresses radiation-induced germ cell apoptosis in vivo. *Endocrinology* **147**, 4213-4221
175. Suzuki, A., de la Pompa, J. L., Stambolic, V., Elia, A. J., Sasaki, T., del Barco Barrantes, I., Ho, A., Wakeham, A., Itie, A., Khoo, W., Fukumoto, M., and Mak, T. W. (1998) High cancer susceptibility and embryonic lethality associated with mutation of the PTEN tumor suppressor gene in mice. *Curr Biol* **8**, 1169-1178
176. Salmena, L., Carracedo, A., and Pandolfi, P. P. (2008) Tenets of PTEN tumor suppression. *Cell* **133**, 403-414

177. Alimonti, A., Carracedo, A., Clohessy, J. G., Trotman, L. C., Nardella, C., Egia, A., Salmena, L., Sampieri, K., Haveman, W. J., Brogi, E., Richardson, A. L., Zhang, J., and Pandolfi, P. P. (2010) Subtle variations in Pten dose determine cancer susceptibility. *Nature genetics* **42**, 454-458
178. Frese, K. K., and Tuveson, D. A. (2007) Maximizing mouse cancer models. *Nature reviews. Cancer* **7**, 645-658
179. Cheon, D. J., and Orsulic, S. (2011) Mouse models of cancer. *Annual review of pathology* **6**, 95-119
180. Di Cristofano, A., Pesce, B., Cordon-Cardo, C., and Pandolfi, P. P. (1998) Pten is essential for embryonic development and tumour suppression. *Nature genetics* **19**, 348-355
181. Donehower, L. A., Harvey, M., Slagle, B. L., McArthur, M. J., Montgomery, C. A., Jr., Butel, J. S., and Bradley, A. (1992) Mice deficient for p53 are developmentally normal but susceptible to spontaneous tumours. *Nature* **356**, 215-221
182. Anai, S., Goodison, S., Shiverick, K., Iczkowski, K., Tanaka, M., and Rosser, C. J. (2006) Combination of PTEN gene therapy and radiation inhibits the growth of human prostate cancer xenografts. *Hum Gene Ther* **17**, 975-984
183. Saito, Y., Swanson, X., Mhashilkar, A. M., Oida, Y., Schrock, R., Branch, C. D., Chada, S., Zumstein, L., and Ramesh, R. (2003) Adenovirus-mediated transfer of the PTEN gene inhibits human colorectal cancer growth in vitro and in vivo. *Gene Ther* **10**, 1961-1969
184. Stewart, A. L., Mhashilkar, A. M., Yang, X. H., Ekmekcioglu, S., Saito, Y., Sieger, K., Schrock, R., Onishi, E., Swanson, X., Mumm, J. B., Zumstein, L., Watson, G. J., Snary, D., Roth, J. A., Grimm, E. A., Ramesh, R., and Chada, S. (2002) PI3 kinase blockade by Ad-PTEN inhibits invasion and induces apoptosis in RGP and metastatic melanoma cells. *Molecular medicine* **8**, 451-461
185. Liu, Z., Li, J., Huang, J., Ke, F., Qi, Q., Jiang, X., and Zhong, Z. (2012) Mannan-modified Ad5-PTEN treatment combined with docetaxel improves the therapeutic effect in H22 tumor-bearing mice. *Int J Nanomedicine* **7**, 5039-5049

# CURRICULUM VITAE

## Yunpeng Bai

## EDUCATION

2008-2014 Ph.D. in Biochemistry and Molecular Biology
Indiana University, Indianapolis, Indiana, USA
Advisor: Zhong-Yin Zhang, Ph. D.

2005-2008 M.S. in Biochemistry and Molecular Biology
Nankai University, Tianjin, China
Advisor: Youjia Cao, Ph. D.

2001-2005 B.S. in Bioscience
Nankai University, Tianjin, China

## AWARDS

2010 First place poster presentation at FASEB Summer Research Conference on Protein Phosphatases, Steamboat Springs, Colorado

2011 Honorable mention for poster presentation at IU Simon Cancer Center Cancer Research Day, Indianapolis, Indiana

## CONFERENCES ATTENDED

2010 FASEB Summer Research Conference on Protein Phosphatases, Steamboat Springs, Colorado

2012 FASEB Summer Research Conference on Protein Phosphatases, Snowmass, Colorado

## PUBLICATIONS

1. Hydroxyindole Carboxylic Acid-Based Inhibitors for Receptor-Type Protein Tyrosine Protein Phosphatase Beta. *Antioxidants & redox signaling, In press.*
2. Dong, Y., Zhang, L., **Bai, Y.**, Zhou, H. M., Campbell, A. M., Chen, H., Yong, W., Zhang, W., Zeng, Q., Shou, W., and Zhang, Z. Y. (2014) Phosphatase of Regenerating Liver 2 (PRL2) Deficiency Impairs Kit Signaling and Spermatogenesis. *The Journal of biological chemistry* **289**, 3799-3810
3. Walls, C. D., Iliuk, A., **Bai, Y.**, Wang, M., Tao, W. A., and Zhang, Z. Y. (2013) Phosphatase of Regenerating Liver 3 (PRL3) Provokes a Tyrosine Phosphoproteome to Drive Prometastatic Signal Transduction. *Molecular & cellular proteomics* **12**, 3759-3777
4. Dong, Y., Zhang, L., Zhang, S., **Bai, Y.**, Chen, H., Sun, X., Yong, W., Li, W., Colvin, S. C., Rhodes, S. J., Shou, W., and Zhang, Z. Y. (2012) Phosphatase of regenerating liver 2 (PRL2) is essential for placental development by down-regulating PTEN

(Phosphatase and Tensin Homologue Deleted on Chromosome 10) and activating Akt protein. *The Journal of biological chemistry* **287**, 32172-32179

5. **Bai, Y.**, Luo, Y., Liu, S., Zhang, L., Shen, K., Dong, Y., Walls, C. D., Quilliam, L. A., Wells, C. D., Cao, Y., and Zhang, Z. Y. (2011) PRL-1 protein promotes ERK1/2 and RhoA protein activation through a non-canonical interaction with the Src homology 3 domain of p115 Rho GTPase-activating protein. *The Journal of biological chemistry* **286**, 42316-42324
6. Zhang, H., Li, X., **Bai, Y.**, Niu, R., Jia, Y., Zhang, C., Zhang, L., Feng, X., and Cao, Y. (2009) Metastatic cell detection using a phage-peptide-modified light-addressable potentiometric sensor. *Biotechnol Appl Bioc* **53**, 185-192
7. Jia, Y., Qin, M., Zhang, H., Niu, W., Li, X., Wang, L., Li, X., **Bai, Y.**, Cao, Y., and Feng, X. (2007) Label-free biosensor: a novel phage-modified Light Addressable Potentiometric Sensor system for cancer cell monitoring. *Biosensors & bioelectronics* **22**, 3261-3266